공학석사 학위논문

Seismic Performance of RC Moment Frames Retrofitted with Internal or External Steel Frames

끼움강재골조 및 외부강재골조로 보강된 철근콘크리트 골조의 내진 성능

2019년 8월

서울대학교 대학원

건축학과

이 해 빈

Abstract

Seismic Performance of RC Moment Frames Retrofitted with Internal or External Steel Frames

Lee, Hae bin
Department of Architecture and Architectural Engineering
College of Engineering
Seoul National University

As the awareness of the possibility of earthquake in Korea increases, interest in the seismic retrofit design of existing reinforced concrete structures with non - seismic details is increasing. Various seismic retrofitting methods have been developed for school buildings which have non-seismic details. In the case of old school buildings, however, it is difficult to find an appropriate retrofitting method for the existing structure because it is very poor in concrete strength and construction quality as well as having non-seismic details.

The retrofitting methods of the school building to increase the strength and stiffness of the structure are commonly used lately. Retrofitting RC frame with external steel moment frame and internal steel moment frame are widely used, which are constructed in longitudinal direction of school building. Since the

existing RC columns are not continuously reinforced with the internal steel moment frame, however, the steel frame changes the load transfer mechanism and increases the total load acting on the structure.

In this study, to verify the seismic performance of the retrofitting method, five two-story frame specimens were tested under cyclic lateral loading. To verify the test results, a frame analysis model was proposed and the predicted strength and failure modes according to the elastic analysis were compared with test results. In addition, shear connection methods were developed and verified by shear test.

The test results showed that the proposed retrofit method significantly increase the stiffness and strength of the RC moment frame. In the internal steel frame specimen, the maximum strength was reached due to the shear failure of the 1st story column and it was three times greater than that of RC frame without steel frame. The ductility capacity decreased slightly compared to the non - retrofitted frame but showed good energy dissipation due to yielding of retrofitted steel frame. The maximum load of external steel frame specimens decreased due to flexural crushing at the bottom of the 1st-story column. The deformation capacity was better but the energy dissipation was smaller than that of internal steel frame specimens.

An analytical model consisting of line elements was proposed for the retrofitting structure design in practice and the analysis results were compared with the test results. Connection elements of analytical models were considered for shear and compressive behavior for internal-retrofitting and tensile, compressive and shear behavior for external-retrofitting. In the linear structure

analysis result, the ordinary RC moment frame showed flexural failure of the 2nd-story beam while the result did not match the actual failure mode due to poor anchorage of rebars in beam-column joints. In case of internal-retrofitting, the analytical model showed shear failure of the 1st-story tensile column and it was consistent with the test result. The external-retrofitting model also showed failure of the 1st-story columns due to the crushing of concrete.

In this study, experiments on two story and one bay RC moment frames retrofitted with internal or external steel frame were carried out to verify the seismic performance of the retrofitting methods to RC frames with non-seismic details. Based on the results of the experiment, the analytical model for RC frame was proposed. The results of the elastic analysis were compared to the test results to confirm the suitability of the design for the proposed model, and the design concept for the steel-retrofitted frame system was proposed.

Keywords : Seismic retrofit; non-seismic RC school buildings; Internal steel frame; External steel frame; Connection; Elastic analysis; Response modification coefficient; Pushover

Student Number : 2017-23408

Contents

List of Tables

List of Figures

Chapter 1. Introduction

1.1 Motivation of Research

As awareness of the possibility of earthquakes occurring in Korea after the Gyeongju earthquake (2016) and Pohang earthquake (2017) increases, interest in the design of seismic retrofitting of existing reinforced concrete structures with non-seismic details is also increasing(Figure 1-1). In particular, various methods have been developed for school buildings with non-seismic details, but in the case of old school buildings, it is very difficult to find suitable reinforcement methods as the existing structures are not only of non-seismic details, but also of concrete strength and construction quality. o that end, the Education Ministry and the Korean Association of Architects supplied earthquake-resistant design standards and performance evaluation and reinforcement manuals for school facilities.

Recently, there have been many studies on retrofitting of school facilities such as shear wall installation, column cross section expansion, internal steel frame construction, fitting wall, steel frame construction, and damper construction method as shown in Figure 1-2. Among them, a number of school buildings with non-seismic details have been used to secure seismic performance by increasing the strength and stiffness of existing structures. In particular, the external steel frame construction method and the internal steel frame construction method are widely used considering the characteristics of school buildings that are vulnerable in the long direction (Figure 1-3). These

two methods are preferred in Korea over the diagonal bracing method, which is commonly used for the seismic retrofitting method in other countries because they have the advantage of maintaining the architectural appearance without damaging windows and other openings.

However, in the case of internal steel frame construction, since the columns of the existing frame are not continuously reinforced, the destruction of the existing frame is often preceded and the intended reinforcement effect cannot be obtained because it changes the existing load carrying path and distribution and increases the overall load acting on the structure. Therefore, it is required to verify the seismic performance of the internal steel frame method through experiment, but the study on the reinforcement effect of internal steel frame without diagonal braces is not yet preceded.

Figure 1-1 Damages of the school buildings with non-seismic details (Pohang earthquake, 2017)

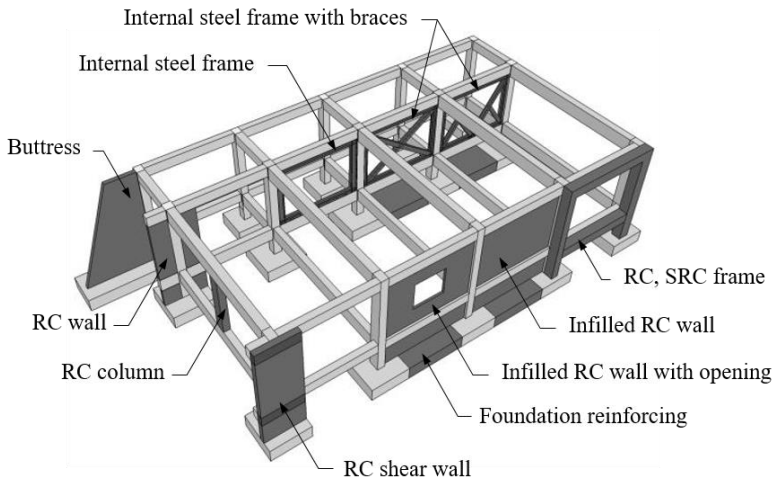

Figure 1-2 Seismic retrofitting methods for school building

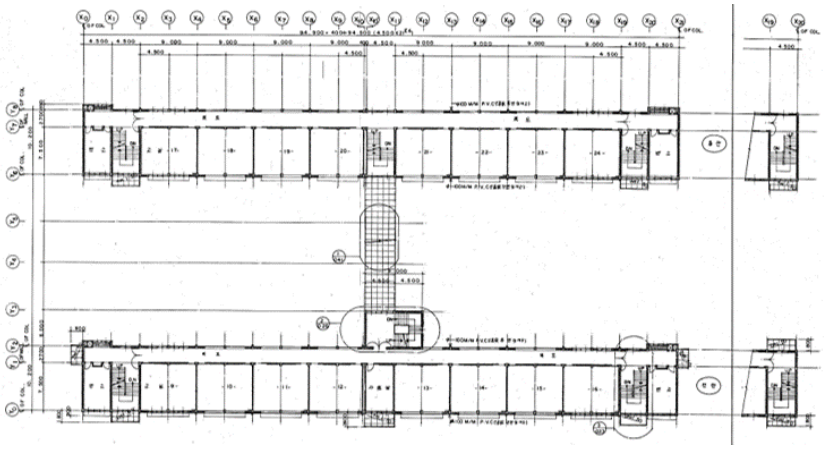

Figure 1-3 Typical floor plan of school building

1.2 Objective and Scope Research

In this study, the construction method and details were presented to ensure the seismic performance and constructability of internal steel frame and external steel frame installation. Also their seismic performance was verified through cyclic test. In addition, a shear test of new connecting method which connect retrofitting steel frames to existing structures was preceded. Based on the test results of retrofitting and connecting method, the structural analysis model and design method for the retrofitting frame were proposed.

1.3 Outline of Thesis

The research manuscript is organized in five chapters. Chaper 3 ~ Chapter 5 deal with experimental and analytical studies on each research topic. A flow chart of experimental and analytical studies in Chapter 3 ~ Chapter 5 is illustrated in Figure 1-4.

In Chapter 3, experimental studies were conducted to evaluate seismic performance of proposed RC-steel connection, comparing with traditional indirect connection in current design manual. The shear strength and stiffness of connection module and effects of connection method type and clearance of anchor hole were mainly investigated by a shear cyclic test.

In Chapter 4, two-story and one-bay frame tests were performed to verify the seismic performance and failure mode of retrofitting RC frame with steel frame. The overall seismic behavior of non-seismic school building was investigated in system level. The interaction between RC and steel column were also

examined.

Chapter 5 deal with analytical studies on elastic design of frame, using proposed line element model to apply the actual behavior of retrofitted RC frame. In the numerical model, connection element between RC and steel frame which has properties derived from Chapter 3 was used.

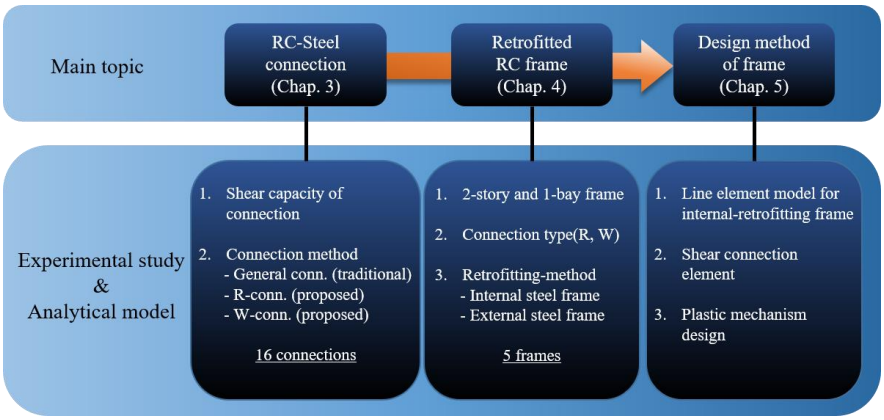

Figure 1-4 Flow chart of experimental study and analytical model

Chapter 2. Literature Review

2.1 Code Review

2.1.1 General methods connecting RC frame with steel frame

The seismic performance evaluation and reinforcement manual for school facilities defines traditional direct and indirect connection methods as general methods used to connect existing reinforced concrete frame to steel frame. The traditional direct-connection is used in general structural retrofitting construction, where flanges of steel member and existing RC member are connected using post-installed anchors as shown in Figure 2-1. The traditional indirect-connection method is pouring mortar between anchors and studs welded to the steel web for the unification of steel and RC frame as shown in Figure 2-2. The details are the same as those required in the Japanese earthquake-resistant design guidelines and descriptions. For the direct connection method, it is assumed that the interfacial shear force between the steel section and the RC section is transmitted only by the steel anchor, and the connection design follows the same criteria as the ACI 318 post-installed anchor design. However, direct connection method is difficult to drill anchor holes in existing frame and install anchors. Therefore, sufficient safety factor and thorough quality control are required for anchor design.

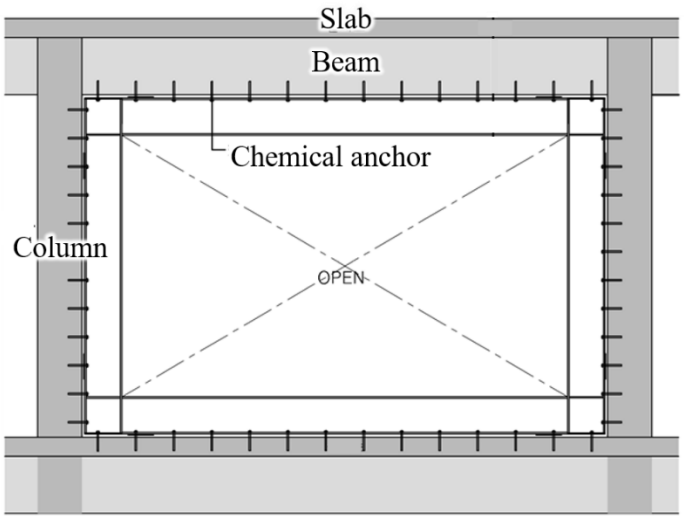

(a) Example of connection with internal steel frame

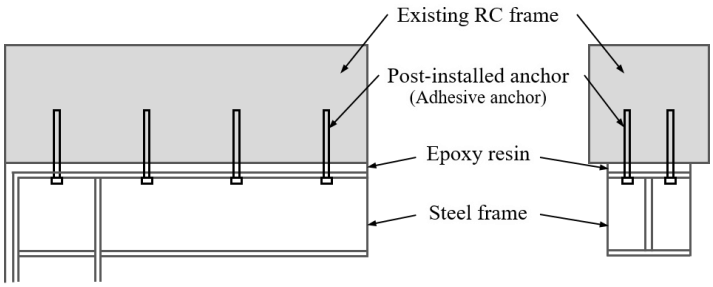

(b) Details of connection

Figure 2-1 General direct connection (flange connection)

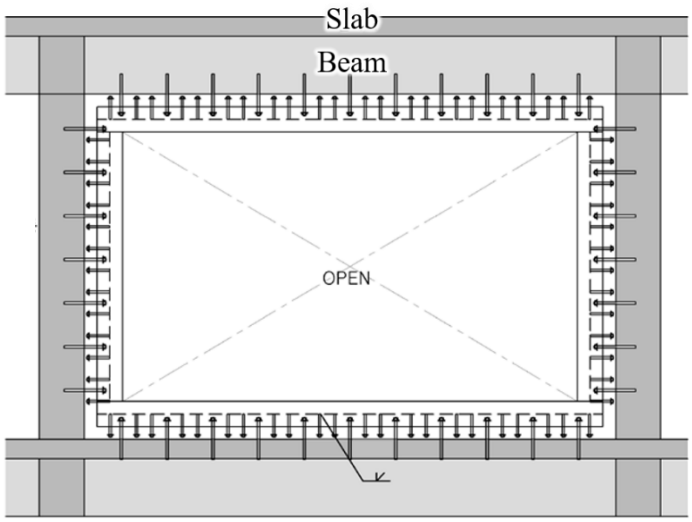

(a) Example of connection with internal steel frame

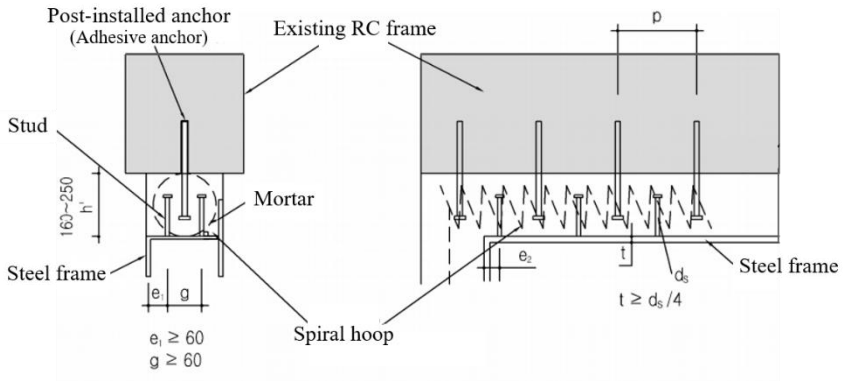

(b) Details of connection

Figure 2-2 General indirect connection (web connection)

Chapter 3. Shear Capacity of Anchor Connections

3.1 Introduction

3.1.1 Research needs

Retrofitting method using steel frame is most commonly used because of its excellent reinforcing performance, light weight and short construction period. The retrofitting guidelines for existing RC frames in Korea and Japan are presented as a typical construction method using a steel framing method. The part of the retrofitting frame is composed of steel frame and braces as shown in Figure 3-1 (a). At this time, only the lateral resistance of the braces is considered in the strength of the reinforced part, and the steel frame is installed with a weak axis in consideration of the constructability(Figure 3-1 (a)).

The connections between the steel frame and the existing frame are generally utilized for indirect connections consisting of studs and post-installed anchors, spiral hoop and mortar. However, for such general indirect connection details, the difficulty of installing spiral hoop significantly reduces the construction efficiency and makes it difficult to secure the performance of the connection. In addition, diagonal bracing structures are not preferred in Korea due to restrictions on the appearance, view, lighting, and access of buildings.

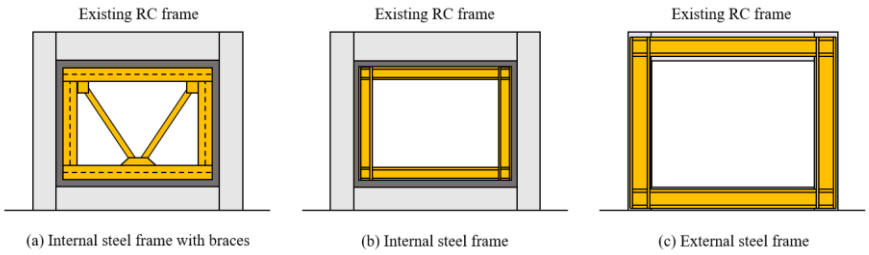

Figure 3-1 Retrofitting RC frame with steel frame

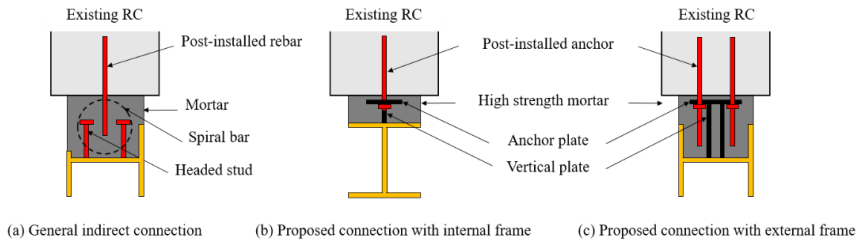

Figure 3-2 Connection methods between RC and steel frame

Two steel-encased connection methods have been proposed to improve the constructability of the general indirect connections, and to utilize the strong axes of inserted and externally attached steel frames without using diagonal braces. These are modular connections developed for connecting RC-steel frame for seismic retrofitting(Figure 3-1 (b), (c)), which are divided into internal connections that connect with flanges of retrofitting steel and external connections that connect with web(Figure 3-2 (b), (c)) within each construction method. Connections made by the two proposed methods require verification of structural performance. In this chapter, the following studies have been conducted.

1) Seismic performance of proposed connections, such as strength, deformation capability, and failure modes, is evaluated through a cyclic lateral load test.

2) Ensure that the experimental strength of the proposed connections meets the strength design values specified in Seismic Performance Evaluation and Reinforcement Manual for school facilities (2019, Korea).

3.1.2 Properties of connection methods

The proposed R-connection and W-connection consist of a vertical plate, post-installed anchors, an anchor plate, studs, and high-strength mortar as shown in Figure 3-3 and Figure 3-4. Depending on how stiffening steel frames are connected to the vertical plate, the two methods can be distinguished. R-connection and W-connection are connected by welding and bolting respectively. These two joints, consisting of one module, can be modified by moving only the vertical plate when responding to rebar interference of existing RC frame. In addition, the connection of vertical plate and stiffening steel enables the steel frame to be tightened without any additional support even before mortar is placed, providing the better constructability than that of general indirect connections. For convenience, R-Connection and W-Connection are labeled Type 1 and Type 2, respectively.

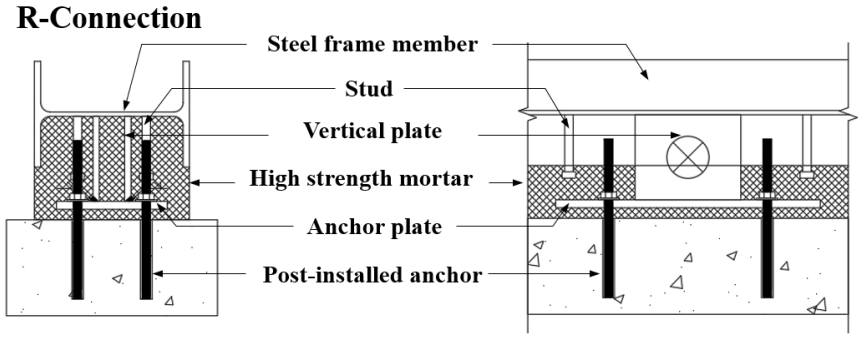

(a) Connection between concrete and web

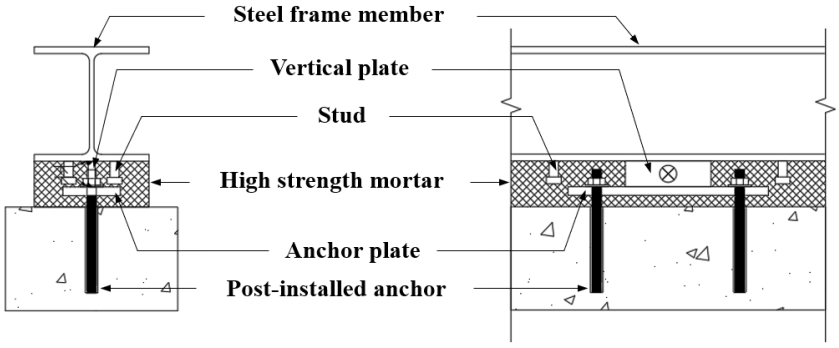

(b) Connection between concrete and flange

Figure 3-3 Details of R-Connections (Type 1)

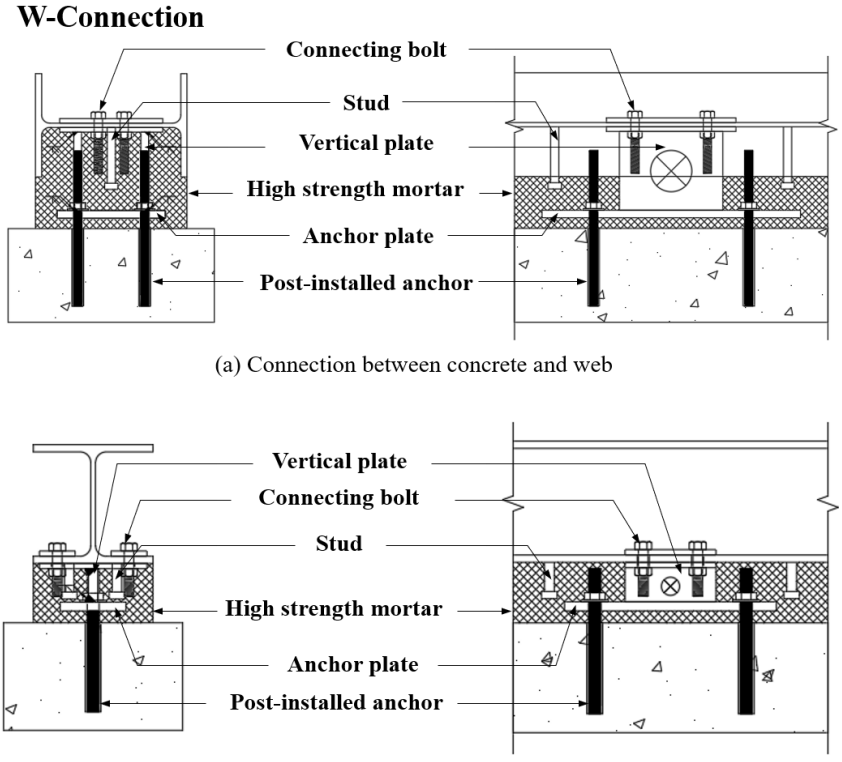

(a) Connection between concrete and web

(b) Connection between concrete and flange

Figure 3-4 Details of W-Connections (Type 2)

3.2 Test Program of Various Connection Methods

3.2.1 Major design parameters and specimen details

Four major design parameters were planned for RC-steel frame connection tests. Table 3-1 presents design parameters of connection tests. As the major test parameters, three types of connections, retrofitting position of each specimen, the number of connection modules, and the clearance between anchor plate hole and anchor were considered.

The general indirect connection specimen(**IND**) was designed according to the standards of Seismic performance evaluation and retrofitting manual of school facilities 2019, which referenced the standards of The Japan Building Disaster Prevention Association. Figure 3-6 Shows the details of indirect connection specimen. Steel bar D6 was used for spiral hoop and two post-installed rebar D16 were used for web connection.

Type 1 and Type 2 specimens(**R-I1**, **R-I2**, **R-E1**, **W-I1**, **W-E1**) were designed in the same dimensions and scale as those applied in the actual field without reduction. The details of specimens are presented in Figure 3-7 and Figure 3-8. Two and four post-install anchors M16 were used for flange and web connection respectively. The thickness of the vertical plate was 12 mm, and the thickness of the anchor plate was 15 mm. High strength mortar was infilled between steel and base concrete. The design strength of this mortar is 60 MPa. Table 3-2 shows the main materials used in the connection specimens.

In order to verify the shear performance of the connections, the cross section of RC members similar to actual school building was reflected in the base

concrete design. Figure 3-5 shows the details of base concrete specimen.

Table 3-1 Test parameters of anchor connection specimens

Specimens[1)]	Type of connection	Connecting position[2)]	Number of modules	Anchor hole clearance[3)]	Number of specimens
IND	General indirect	Web	-	-	1
R-I1-1	Type 1 (R-Conn.)	Flange	1	2 mm	2
R-I1-2					
R-I1-3				4 mm	1
R-I2-1	Type 1 (R-Conn.)	Flange	2	2 mm	2
R-I2-2					
R-I2-3				4 mm	1
R-E1-1	Type 1 (R-Conn.)	Web	1	2 mm	2
R-E1-2					
R-E1-3				4 mm	1
W-I1-1	Type 2 (W-Conn.)	Flange	1	2 mm	2
W-I1-2					
W-I1-3				4 mm	1
W-E1-1	Type 2 (W-Conn.)	Web	1	2 mm	2
W-E1-2					
W-E1-3				4 mm	1

1) Connection method – connecting position with # of modules - # of specimens

2) I : Connecting with flange of H-beam,
E : Connecting with web of H-beam

3) Clearance of anchor plate hole

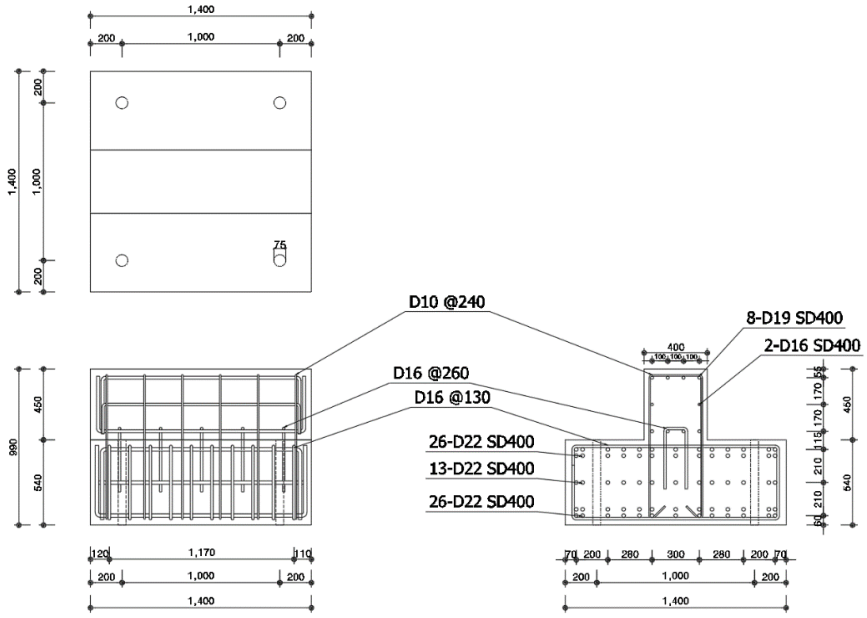

Figure 3-5 Reinforcement details of base concrete specimen

Table 3-2 Main materials of connection specimens

Specimen		IND	R-I1	R-I2	R-E1	W-I1	W-E1
Post-install		Steel rebar (D16)	Anchor (M16)				
Mortar		Portland cement (Type 1)	High strength				
Stud		-	M16				
Spiral hoop		D6	-				
Steel plate		-	Vertical plate (12T)				
			Anchor plate (15T)				
H-beam	Flange conn.	-	H-294×200×8×12				
	Web conn.	H-400×200×8×13	H-400×200×8×13				

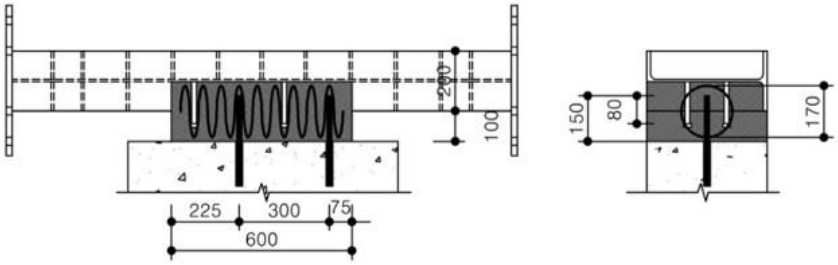

Figure 3-6 Dimensions and details of specimen with indirect connection (**IND**)

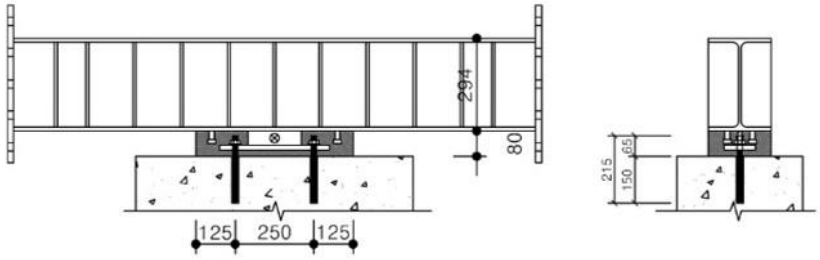

(a) Flange connection (1 module)

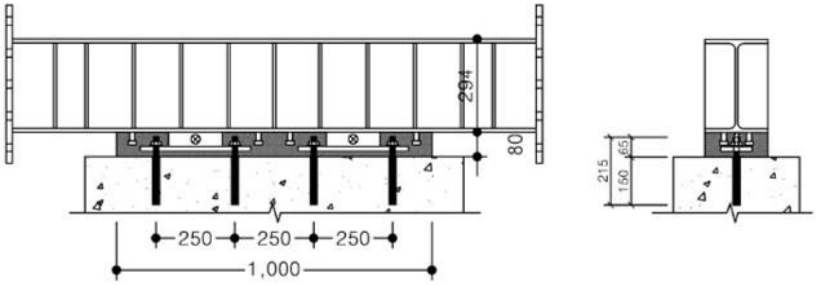

(b) Flange connection (2 modules)

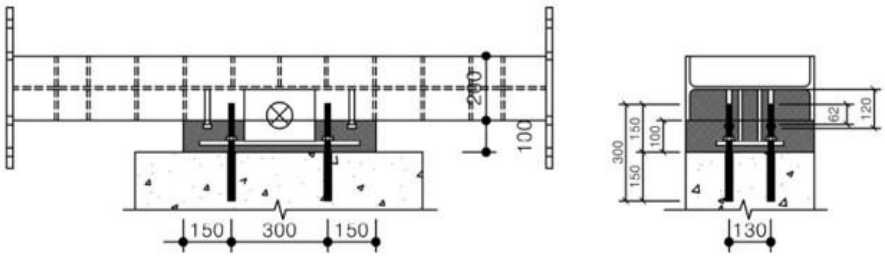

(c) Web connection

Figure 3-7 Dimensions and details of specimen with Type 1 (**R-I1**, **R-I2**, **R-E1**)

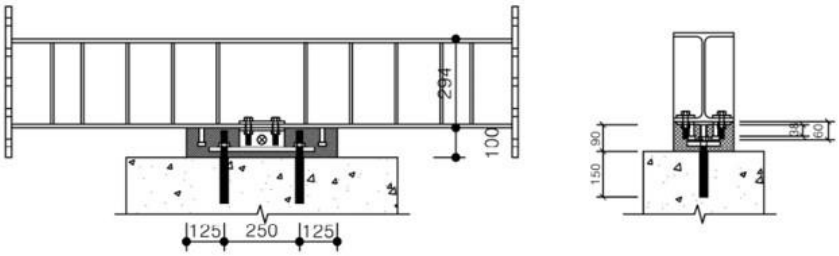

(a) Flange connection

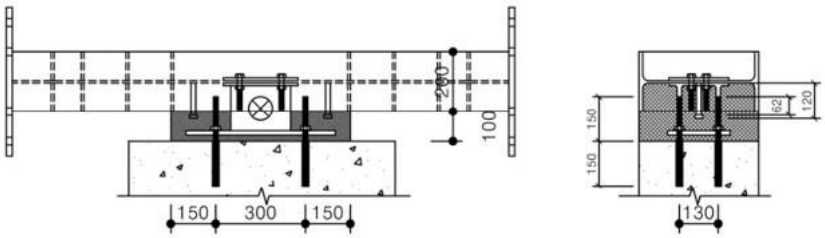

(b) Web connection

Figure 3-8 Dimensions and details of specimen with Type 2 (**W-I1**, **W-E1**)

3.2.2 Construction process of anchor connection specimens

To confirm the maximum performance of the connection itself, the strength of the base concrete was designed to be higher than the strength of the existing school building to prevent premature failure of base concrete. All of the connection specimens were constructed by the same procedure as the actual construction after the base concrete was sufficiently cured. Figure 3-9 shows the construction process of the base reinforced concrete.

The construction procedures of general indirect connection and connection with flange and web are presented in Figure 3-10 ~ Figure 3-12. The construction of connection was carried out in the order of rebar detection, boring concrete, and anchor installation(Figure 3-10 (a) ~ (b), Figure 3-11 (a) ~ (c), Figure 3-12 (a) ~ (c)). After installing anchors, the anchor plate and the anchor were fixed with nuts(Figure 3-11 (d), Figure 3-12 (d)). The vertical plate which was welded or bolted(Type 1 or Type 2) with H-beam was welded to the anchor plate to fasten the H-beam(Figure 3-11 (e), Figure 3-12 (e)). After the vertical plate was welded, formwork was installed and mortar was poured.

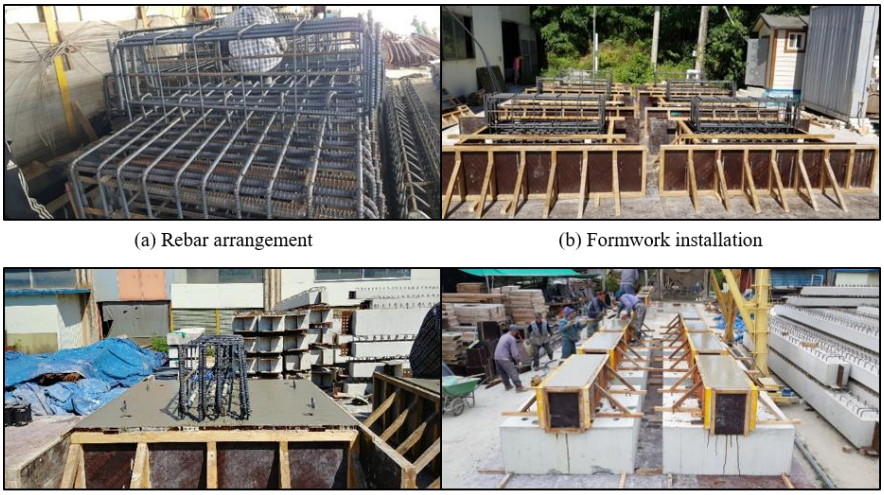

(a) Rebar arrangement (b) Formwork installation

(c) Concrete pouring in bottom (d) Concrete pouring in top

Figure 3-9 Construction process of base reinforced concrete

(a) Rebar detection (b) Boring and chipping concrete and installing chemical anchors

(c) Inserting spiral rebar to steel frame (f) Formwork installation and mortar pouring

Figure 3-10 Construction process of indirect connection specimen (**IND**)

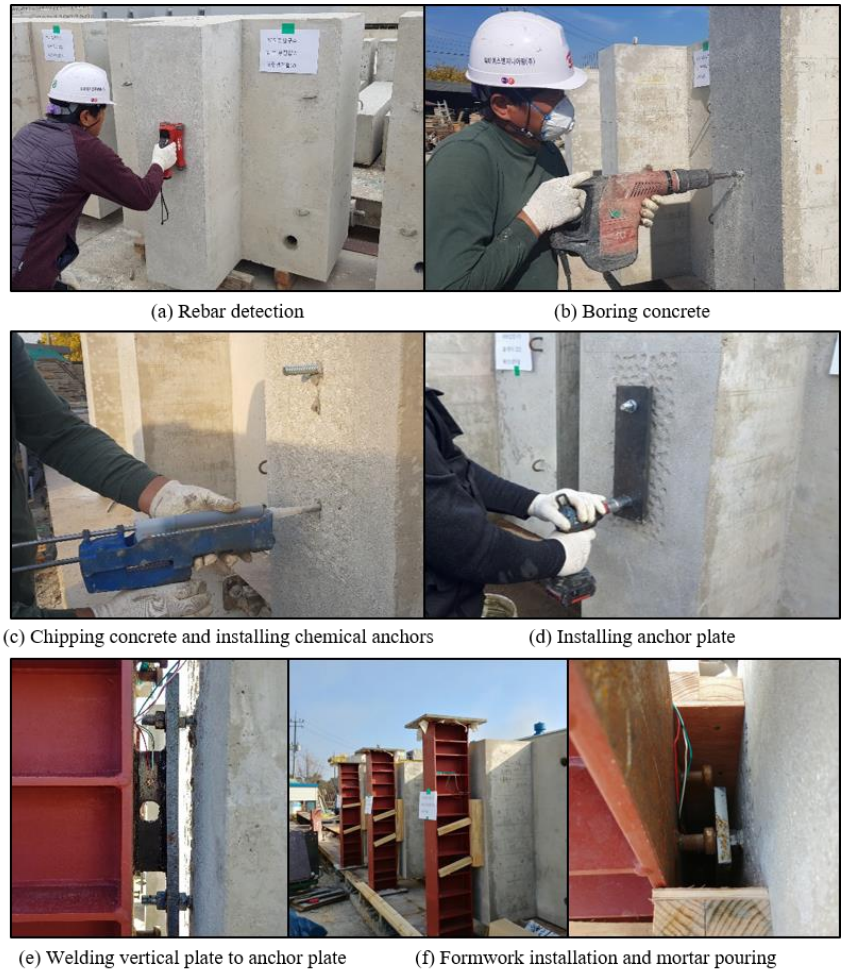

(a) Rebar detection (b) Boring concrete

(c) Chipping concrete and installing chemical anchors (d) Installing anchor plate

(e) Welding vertical plate to anchor plate (f) Formwork installation and mortar pouring

Figure 3-11 Construction process of specimens (**R-I1**, **R-I2**, **W-I1**)

(a) Rebar detection (b) Boring concrete

(c) Chipping concrete and installing chemical anchors (d) Installing anchor plate

(e) Welding vertical plate to anchor plate (f) Formwork installation and mortar pouring

Figure 3-12 Construction process of specimens (**R-E1**, **W-E1**)

3.2.3 Material strength

The main materials of anchor connection specimens and their strength are presented in Table 3-3. The compressive strength test of mortar cubes were performed on the day of the cyclic test. Three concrete cylinders were made from the top of base concrete.

Table 3-3 Strength of steel rebars, anchors, plates, mortar, and concrete

Materials		f_y (MPa)	f_u (MPa)	f'_c (MPa)
Post-install anchor (gvz 8.8)[1)]	M16	739	851	-
Post-install rebar (SD400)	D16	490	611	-
Steel plate (SM355)	Vertical plate (12T)	355[2)]	490[2)]	-
	Anchor plate (15T)	355[2)]	490[2)]	-
Mortar	Portland cement Type 1	-	-	29
	High strength [3)]	-	-	55
Base concrete		-	-	31

1) Tensile strength of anchor = 800 MPa

2) Yield strength of SM355

3) High strength mortar, f'_c = 60 MPa

3.2.4 Estimation of test strength

The nominal shear strength of connection specimen is determined by the smaller value of the shear strength of anchor and the concrete failure strength. The design shear strength of post-installed anchors in concrete is specified in ACI 318 (USA). In the code, nominal strength of an anchor in shear shall not exceed (a) and (b).

(a) In ACI 318, the nominal strength of group anchors in shear is as follows.

$$V_{sa} = n(0.6)A_{se}f_{uta} \qquad 3\text{-}1$$

where n is the number of anchors in the group, A_{se} is the effective cross-sectional area of an anchor in shear, mm^2 and f_{uta} shall not be taken greater than the smaller of $1.9f_{ya}$ and 860 MPa.

(b) In ACI 318, the concrete breakout strength of anchor in shear is as follows.

$$V_{cbg} = \frac{A_{Vc}}{A_{Vco}}\Psi_{ec,V}\Psi_{ed,V}\Psi_{c,V}\Psi_{h,V}V_b \qquad 3\text{-}2$$

where V_b is the basic concrete breakout strength value for a single anchor. A_{Vco} is the projected area for a single anchor in a deep member as shown in Figure 3-14. $\Psi_{ec,V}$, $\Psi_{ed,V}$, $\Psi_{c,V}$, and $\Psi_{h,V}$ are the modification factor of eccentric load, edge effect, reinforcement of concrete, and depth ratio between concrete and anchor respectively. Since the calculation process of V_{cbg} has complex conditions and very conservative value, it its difficult to judge the concrete breakout strength of the specimens.

For more reliable and simple prediction of the concrete breakout strength of anchor connection specimens, the concrete strength of steel headed stud anchors of composite beams specified in AISC 360 was applied to prediction of concrete breakout.

(c) In AISC 360, the concrete pryout strength per an stud anchor embedded in a solid concrete slab shall be determined as follows.

$$Q_c = 0.5A_{sa}\sqrt{f_c' E_c} \qquad 3\text{-}3$$

where A_{sa} is the cross-sectional area of an anchor, mm^2.

Table 3-4 shows the results of strength evaluation of test specimens.

Table 3-4 Prediction of nominal strengths depending on failure modes

Specimen	Connection Type	# of modules	# of anchors	Strength evaluation		
				Anchor failure	Concrete failure	
				V_{sa} [1] (kN)	V_{cbg} [2] (kN)	Q_c [3] (kN)
IND	General indirect	-	2	114	76	138
R-I1	Type 1 (Flange)	1	2	125	38	138
R-I2		2	4	250	76	276
R-E1	Type 1 (Web)	1	4	250	72	276
W-I1	Type 2 (Flange)	1	2	125	38	138
W-E1	Type 2 (Web)	1	4	250	72	276

1) An anchor shear capacity $v_{sa} = 0.8(0.6A_{se}f_{uta})$ = 62.5kN (ACI 318, a factor 0.8 multiplied addressing the effect of built-up grout pads), where f_u = 851 MPa

2) Concrete breakout capacity of a group V_{cbg} = 102.5kN

3) Concrete pryout capacity per anchor $q_c = 0.5A_{ae}\sqrt{(E_c f'_c)}$ = 68.9kN, where A_{ae} = 153 mm^2, $E_c = 4{,}700\sqrt{f'_c}$ = 26,168 MPa, and f'_c = 31 MPa

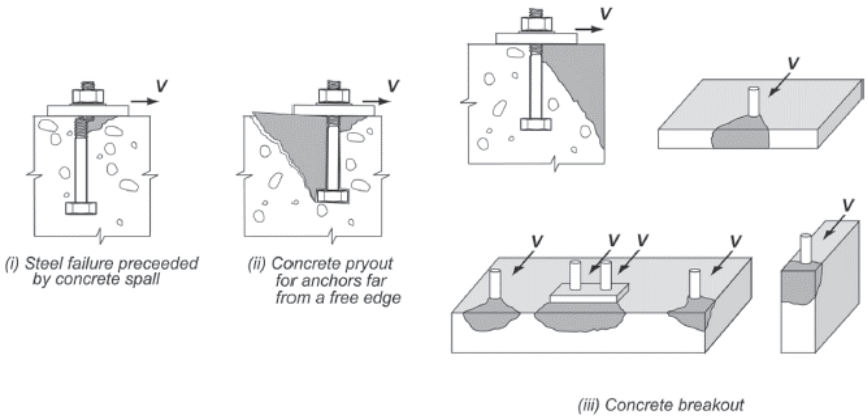

Figure 3-13 Failure modes of anchor in shear (ACI318)

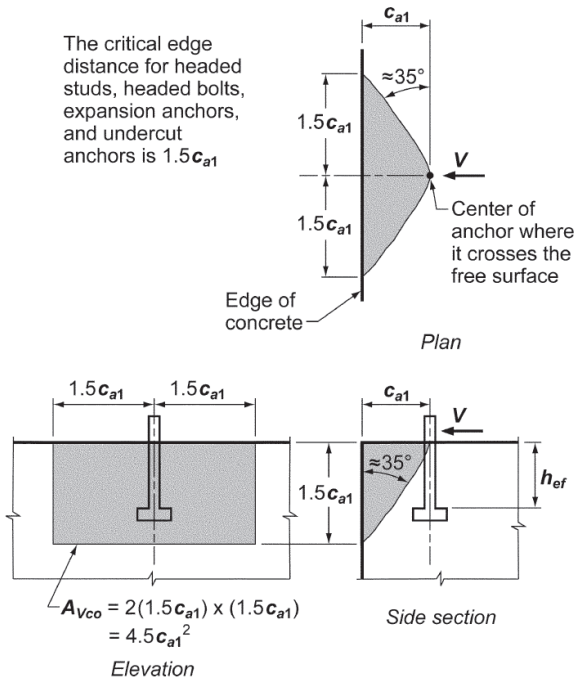

Figure 3-14 Calculation of A_{Vco} (ACI 318)

3.2.5 Test setup and loading plan

For the pure shear test, a hinge type steel jigs were installed at both ends of the specimen to eliminate moment effects due to eccentricity (Figure 3-15 (a)). Connections are installed on the frame and receive the same history of force, so basically the same history(Chapter 4.2.3) of force as the frame test was used. In the connection shear test, the displacement corresponding to the load of $0.25V_n$(V_n is the predicted shear strength of specimen **R-I1**, 138kN) was set as the target displacement in the first loading step in order to prevent sudden fracture of specimen. The displacement corresponding to $0.25V_n$ derived from the first specimen **R-I1** was 0.25 mm, and the loading plan was applied to all specimens in the same way(Figure 3-15 (b)).

According to ACI 374.1, the drift ratio for each loading step was increased from 0.25% to 1.3 times of the previous load drift ratio. The load cycles were repeated three times for each loading step.

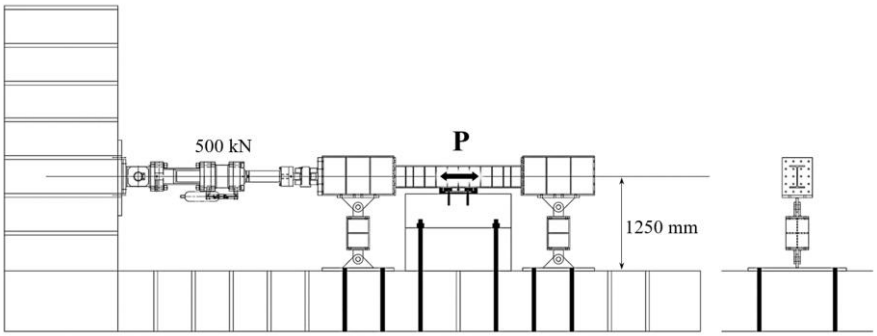

(a) Test setup for anchor connection specimen

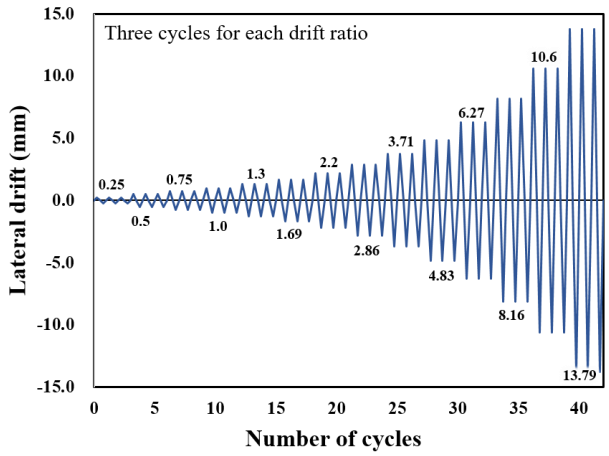

(b) Loading protocol for cyclic loading (ACI 374.1)

Figure 3-15 Loading plan for anchor connection specimen

3.2.6 Displacement measuring plan

As shown in Figure 3-16, the installation of LVDTs was planned to measure lateral displacement and vertical displacement of anchor connection.

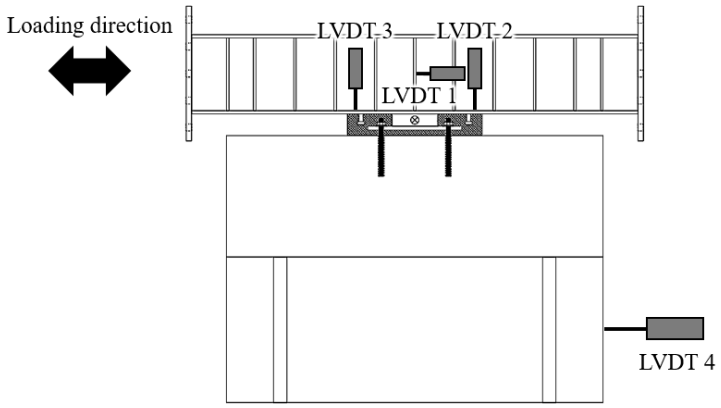

Figure 3-16 Displacement measuring plan of test specimens

3.3 Test Results and Observations

3.3.1 Load-displacement relations

The test results of general indirect connection and proposed anchor connection Type1 and Type2 are presented in Table 3-5. The load-displacement relationships and predicted strength of each specimen are presented in Figure 3-17 and Figure 3-18. The drift in load-displacement relationship represents the slip between the base concrete and steel member.

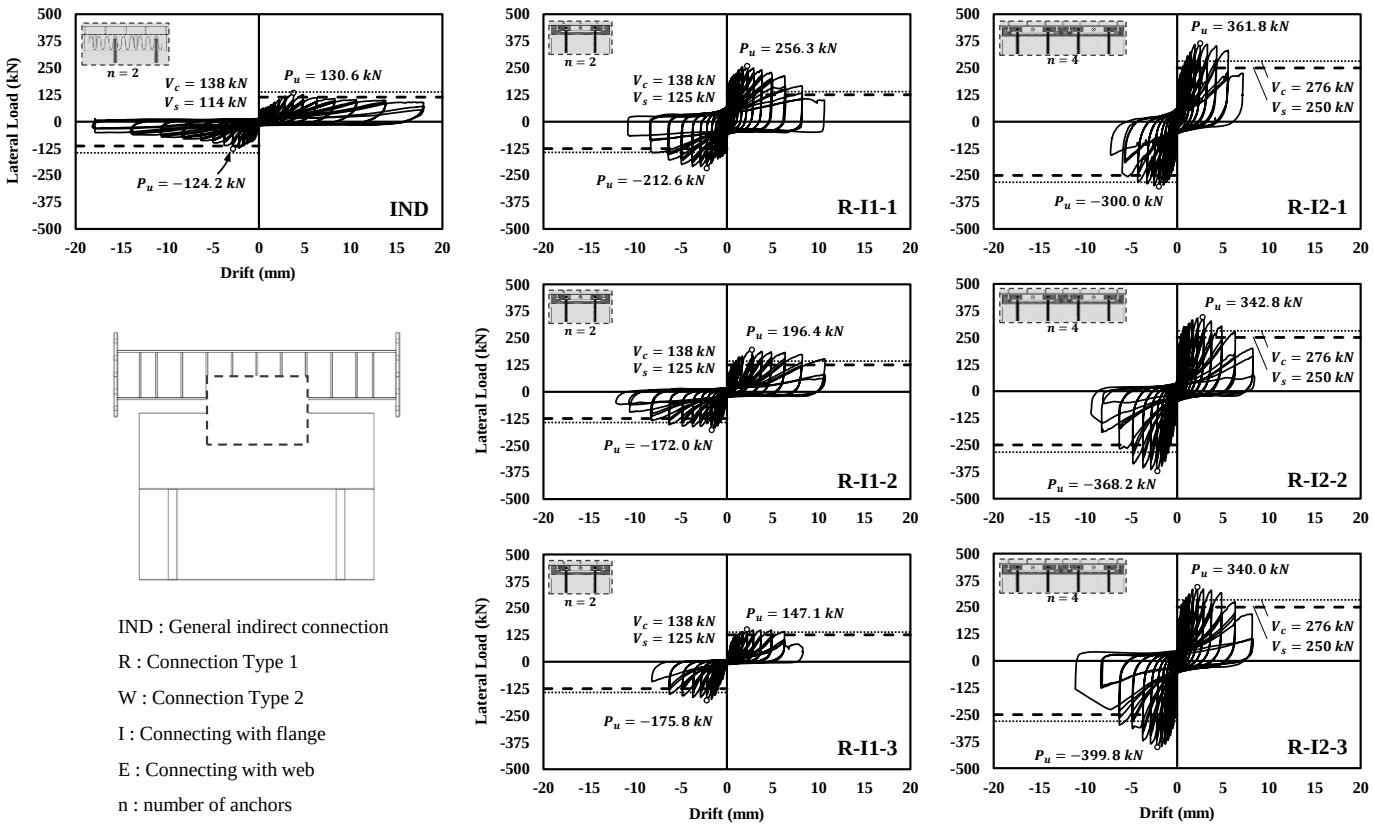

Figure 3-17 Lateral load and drift relationship of specimen **IND**, **R-I1**, and **R-I2**

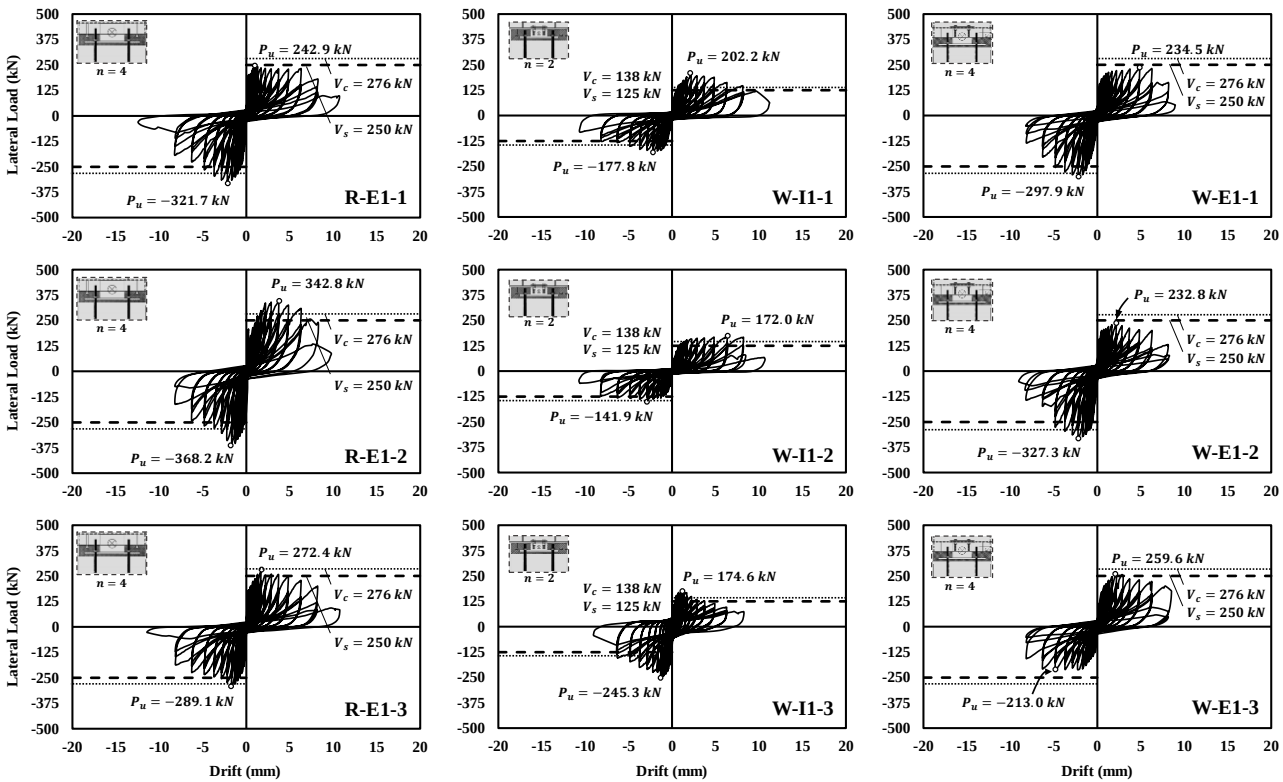

Figure 3-18 Lateral load and drift relationship of specimen **R-E1**, **W-I1**, and **W-E1**

Table 3-5 Test results of anchor connection specimens

Specimen	Connection Type	# of modules	# of anchors	Anchor hole clearance (mm)	Test results			Strength evaluation		
					P_u [1] (kN)	D_u (mm)	D_{max} [2] (mm)	V_c [3] (kN)	V_s [4] (kN)	P_u / V_s
IND	General indirect	-	2	-	124	2.81	-	138	114	1.09
R-I1-1	Type 1 (Flange)	1	2	2	213	2.19	6.27	138	125	1.70
R-I1-2					172	1.68	10.60			1.38
R-I1-3				4	147	2.85	8.16			1.18
R-I2-1		2	4	2	300	1.93	7.19	276	250	1.20
R-I2-2					343	2.89	8.16			1.37
R-I2-3				4	341	2.22	8.16			1.36
R-E1-1	Type 1 (Web)	1	4	2	243	0.99	6.27	276	250	0.97
R-E1-2					346	3.74	8.16			1.38
R-E1-3				4	272	1.67	8.16			1.09
W-I1-1	Type 2 (Flange)	1	2	2	178	2.20	10.6	138	125	1.42
W-I1-2					142	2.85	8.16			1.14
W-I1-3				4	175	1.29	8.16			1.40
W-E1-1	Type 2 (Web)	1	4	2	235	4.87	8.16	276	250	0.94
W-E1-2					233	2.19	6.27			0.93
W-E1-3				4	213	4.83	8.16			0.85

1) Smaller of peak loads in positive and negative loading
2) Displacement when first anchor failure occurs
3) V_c : Concrete bearing capacity of specimens
4) V_s : Anchor shear capacity of specimens

3.3.2 Failure mode of connection specimens

The cracks of mortar showed general diagonal cracks which usually occur in lateral cyclic loading as shown in Figure 3-19.

In the indirect connection specimen **IND**, the vertical cracking of mortar occurred with ultimate strength. After the ultimate strength, the shear strength of connection gradually decreased as the mortar cracks increased. The post-installed rebars, studs, and spiral hoop were hardly damaged and the spiral hoop provided the effect of confimement for the mortar.

In the proposed connection specimen **R-I1**, **I2**, **R-E1**, **W-I1**, and **W-E1** (Type 1 and Type 2), the diagonal cracks at both ends of high strength mortar occurred with ultimate strength. The diagonal cracks of mortar were developed by studs located at both ends of connection module(Figure 3-7, Figure 3-8, Figure 3-21 (b) ~ (f)). Unlike the indirect connection **IND**, after the ultimate strength, the post-installed anchors fractured due to repeated sliding between the concrete and mortar interface resulting in a sudden drop in strength at drift 6.3~10.6 mm(Figure 3-20). The center zone of the high strength mortar where the vertical plate, the anchor plate, and anchors were located was hardly damaged until the end of the test.

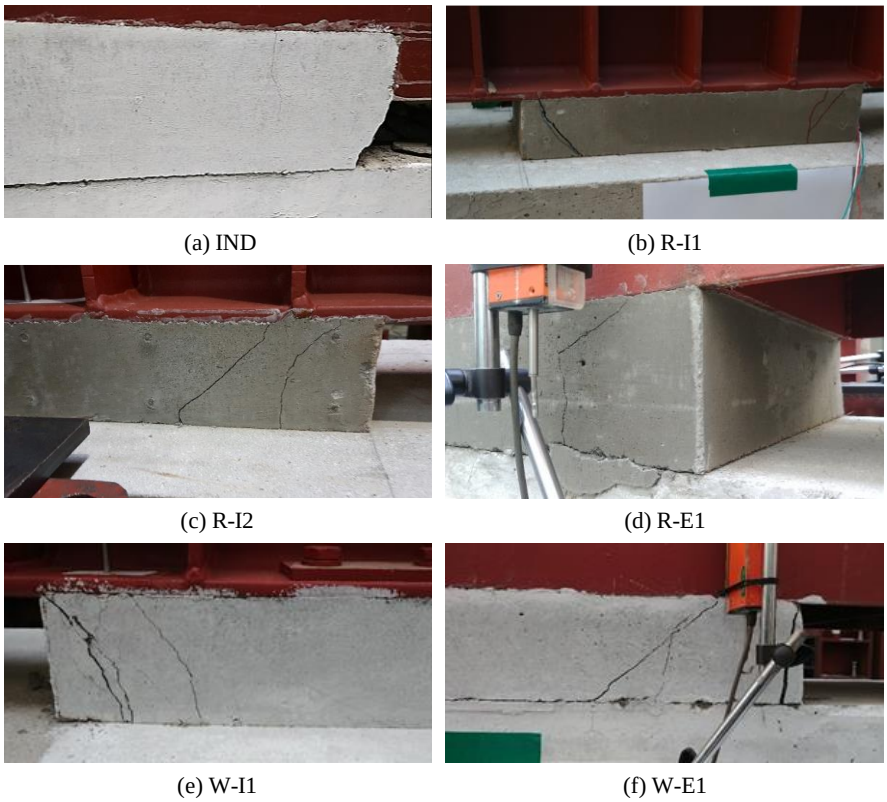

(a) IND (b) R-I1

(c) R-I2 (d) R-E1

(e) W-I1 (f) W-E1

Figure 3-19 Cracks of each connection type at ultimate load

Figure 3-20 Final failure mode after removing the mortar (**W-I1**)

(a) IND

(b) R-I1

(c) R-I2

(d) R-E1

(e) W-I1

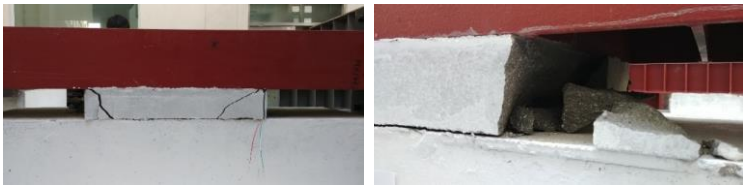

(f) W-E1

Figure 3-21 Failure modes of anchor connection specimens

3.3.3 Effects of design parameters

In the case of two anchors, specimen **IND**, **R-I1**, and **W-I1**(Figure 3-22 (a)), both specimens **R-I1** and **W-I1** met the expected strength V_s, and the failure mode was also consistent with the expected failure of the post-installed anchors due to the repeated load. Specimen **IND**, on the other hand, showed the mortar failure by repeated load without significant damage to the post-installed rebars, studs, and spiral hoop, and was not satisfied with the expected strength Vc corresponding to the failure mode. Average experimental strength was 143% and 133% higher than **R-I1** and **W-I1** compared to general indirect connections, respectively.

In the case of **R-I2**, **R-E1**, **W-E1** (Figure 3-22 (b)), specimen **R-I2** all met the predicted strength Vs and, for specimen **R-E1** and **W-E1**, displayed values similar to the same predicted strength Vs, but not most of them. The average maximum strength of **R-E1** and **W-E1**, which are equally connected to web, was 231% and 183% higher than the general indirect connection, respectively..

The web connection(**R-E1**, **W-E1**) strength per anchor tended to be smaller than that of flange connection(**R-I2**). In the case of four anchors, the average maximum strength of the web connection was 86% and 69% respectively, compared to that of the method of flange connection.

In specimen **R-I1** and **R-I2**, the maximum strength increased as the number of connection modules increased, but the average of maximum strength per module decreased to 93%.

Considering construction errors, two kinds of connection specimens were

made according to the clearance of the anchor plate hole. Figure 3-23 shows the maximum strength of the connection according to the clearance of anchor hole, and no significant effect on the strength of the connection with the clearance was shown within 4 mm.

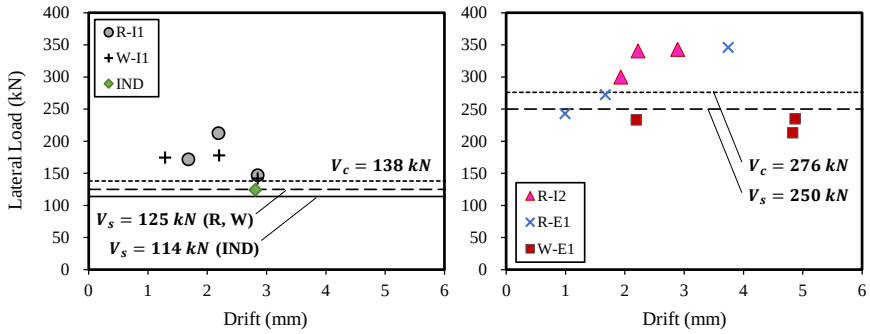

(a) Connection with two anchors (b) Connection with four anchors

Figure 3-22 Comparison of shear strength according to connecting methods

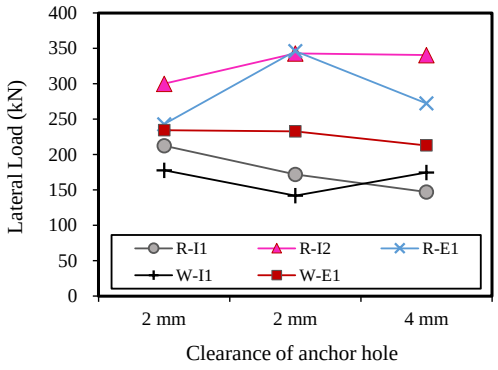

Figure 3-23 Comparison of shear strength according to anchor hole clearance

3.4 Discussion

1) Two methods of anchor connection are proposed to improve the constructability of the existing general indirect connection for constructing spiral hoop and to utilize the strong axis of retrofitted steel frame. Thus, cyclic loading test was performed to verify structural performance of the proposed connections.

2) In general indirect connection, the mortar failure occurred without damage to the post-installed rebars and studs.

2) On the other hand, the shear failure of the post-installed anchors occurred after repeated slip of the concrete-high strength mortar interface without damaging the welded vertical plate and the anchor plate in the proposed connection Type 1 and Type 2.

3) The anchor hole clearance (2mm, 4mm) of the anchor plate considering construction error did not significantly affect the maximum strength and deformation of the connection.

4) In the proposed connections(Type 1 and Type 2), the load was transferred directly to the post-installed anchor through welded vertical plate and anchor plate, which inhibited the mortar destruction in the center of the connection.

Chapter 4. Seismic Performance of Retrofitted RC Frames

4.1 Introduction

4.1.1 Research needs

Recently, there have been many studies on retrofitting of school facilities such as shear wall installation, column cross section expansion, internal steel frame construction, fitting wall, steel frame construction, and damper construction method. Among them, a number of school buildings with non-seismic details have been used to secure seismic performance by increasing the strength and stiffness of existing structures. In particular, the external steel frame construction method and the internal steel frame construction method are widely used considering the characteristics of school buildings that are vulnerable in the long direction. These two methods are preferred in Korea over the diagonal bracing method, which is commonly used for the seismic retrofitting method in other countries because they have the advantage of maintaining the architectural appearance without damaging windows and other openings.

However, in the case of internal steel frame construction, since the columns of the existing frame are not continuously reinforced, the destruction of the existing frame is often preceded and the intended reinforcement effect cannot be obtained because it changes the existing load carrying path and distribution and increases the overall load acting on the structure. Therefore, it is required

to verify the seismic performance of the internal steel frame method through experiment, but the study on the reinforcement effect of internal steel frame without diagonal braces is not yet preceded.

4.2 Test Program

4.2.1 Major design parameters and specimen details

Five specimens were planned for RC frame tests (Ordinary moment frame without strengthening, Moment frame with internal steel frames using connections Type1 and Type2, Moment frame with external steel frames using connections Type1 and Type2, respectively). Table 4-1 presents design criteria and test parameters of RC frame specimens. As the major test parameters, retrofitting position of each frame and two types of connections were considered.

Table 4-1 Test parameters of moment frame specimens

Specimens	**RC-0**	**IN-1**	**IN-2**	**EX-1**	**EX-2**
Existing RC frame	Column: 500×350 (mm) Beam: 250×450 (mm) Design concrete strength: 21MPa				
Retrofitting position		Internal steel frame		External steel frame	
Connection details	-	Type 1 (R-Conn.)	Type 2 (W-Conn.)	Type 1 (R-Conn.)	Type 2 (W-Conn.)
Retrofitting steel frame	-	Column: H-200×200×8×12 Beam: H-200×200×8×12 Steel grade: SM355		Column: H-294×200×8×12 Beam: H-294×200×8×12 Steel grade: SM355	
Other properties	-	-	-	Stiffening plate (9T)	-

The design of the test specimen was based on school building prototype with non-seismic reinforcement details. The school building prototype was characterized with span length of 4,500 mm and story height of 3,300 mm, in which the cross-sectional dimensions of columns and beams are $b_c \times h_c = 500 \times 350$ mm and $b_b \times d = 250 \times 450$ mm, respectively. In all specimens, an identical RC moment frame was used.

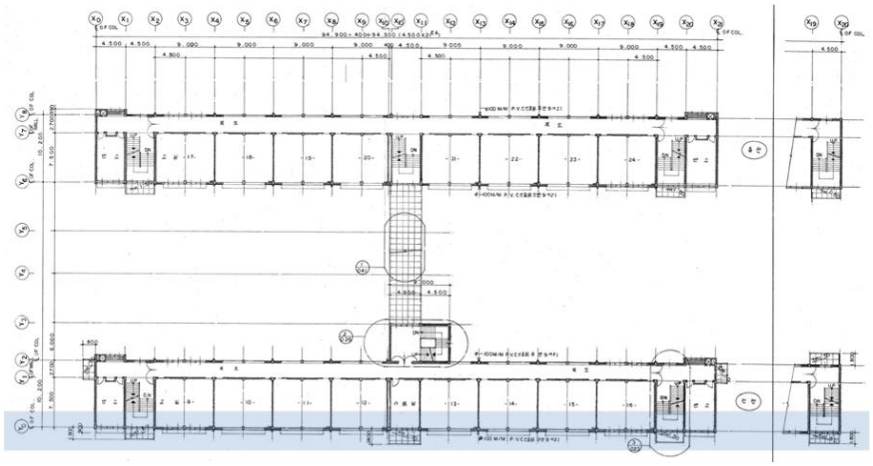

(a) Typical floor plan

(b) Structural section

Figure 4-1 School building with non-seismic reinforcement details (문교부 80)

In the internal retrofitted specimen **IN-1** and **IN-2**, built-up section of H-200×200×8×12 was used for both steel beams and columns. **IN-1** and **IN-2** were constructed using R-Connection(Type 1) and W-Connection(Type 2) respectively, which were described in Chapter 3.

In the external retrofitted specimen **EX-1** and **EX-2**, built-up section of H-294×200×8×12 was used for both steel beams and columns. **EX-1** and **EX-2** were also constructed using R-Connection(Type 1) and W-Connection(Type 2) respectively.

Member dimensions and section details of each member were presented in Figure 4-2 ~ Figure 4-6. A two-story RC moment frame with 71% scale of prototype span length and 83% scale of prototype story height was designed considering the experimental environment of the test center to carry out the RC frame test.

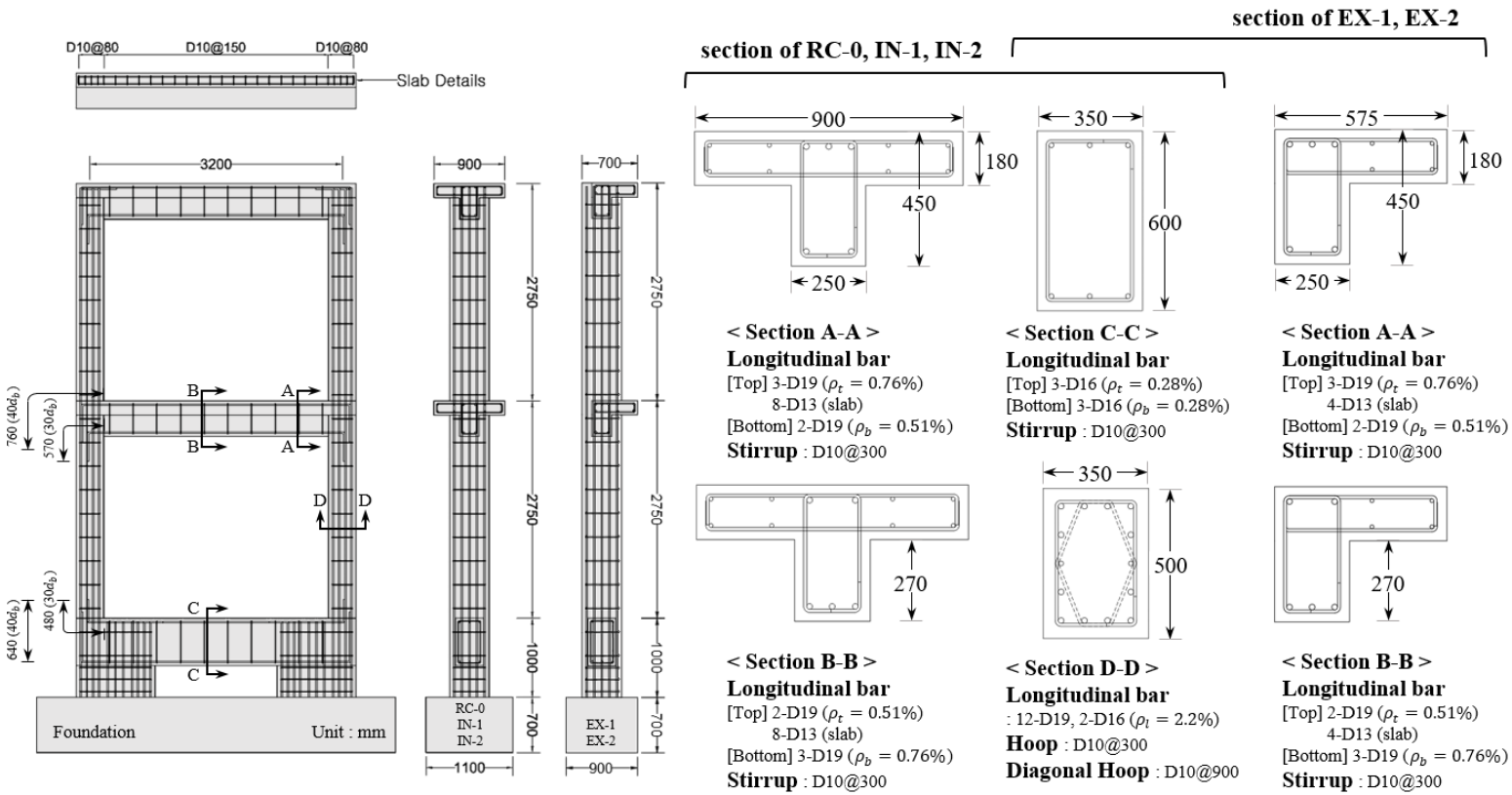

Figure 4-2 Dimensions and reinforcement details of the RC moment frame specimens for retrofitting

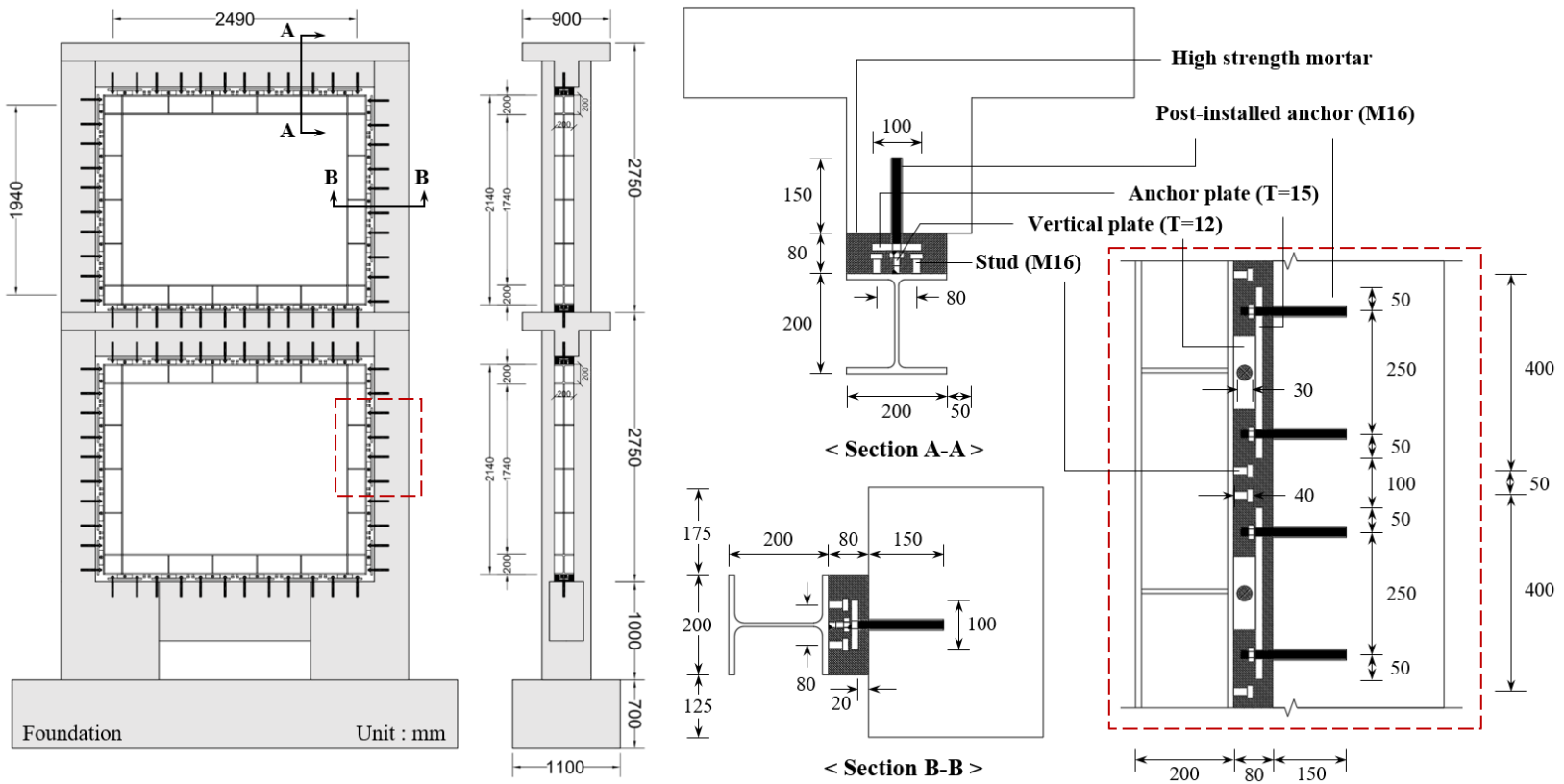

Figure 4-3 Dimensions and connection details of specimen retrofitted with internal steel moment frame (**IN-1**)

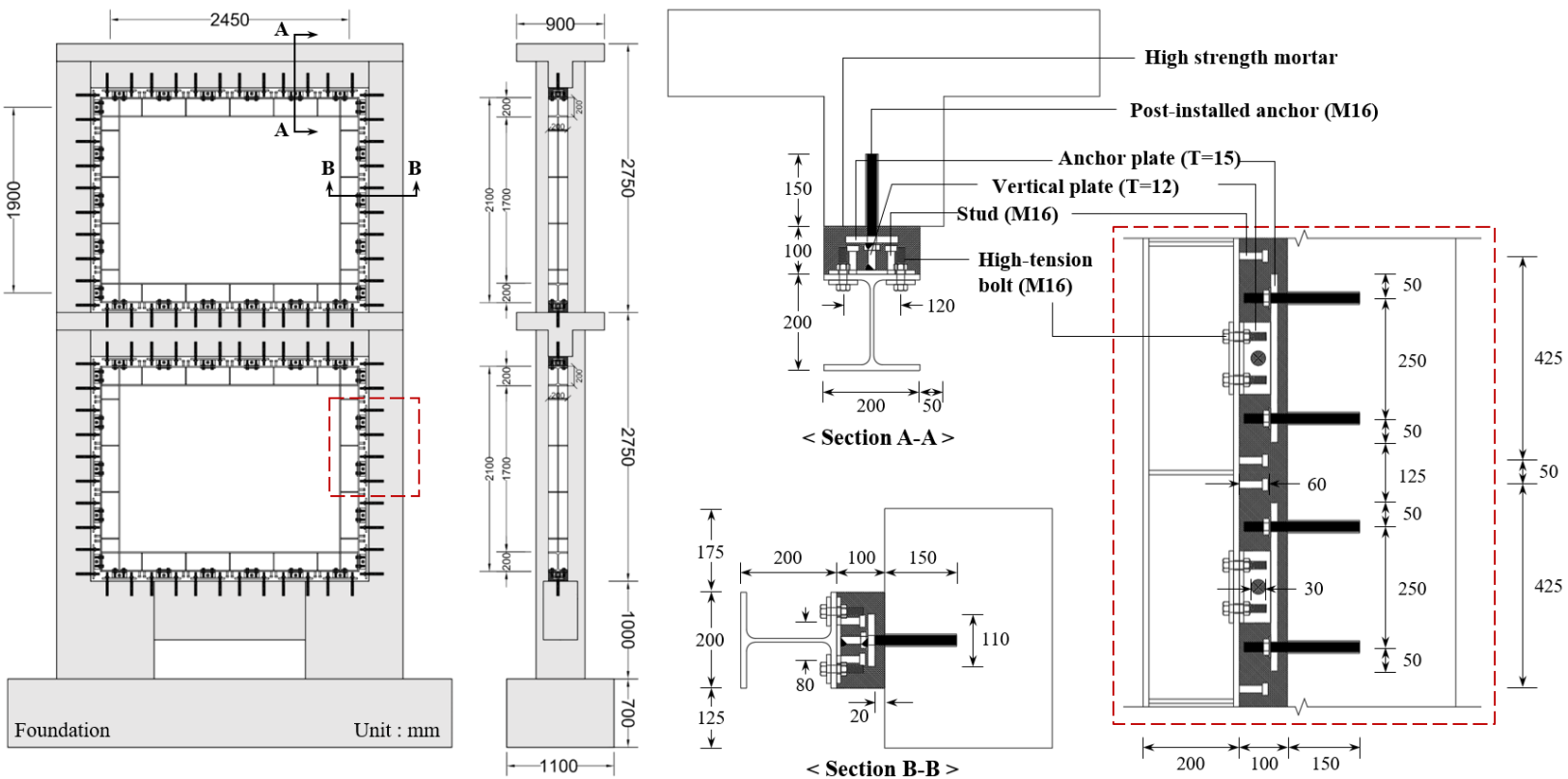

Figure 4-4 Dimensions and connection details of specimen retrofitted with internal steel moment frame (**IN-2**)

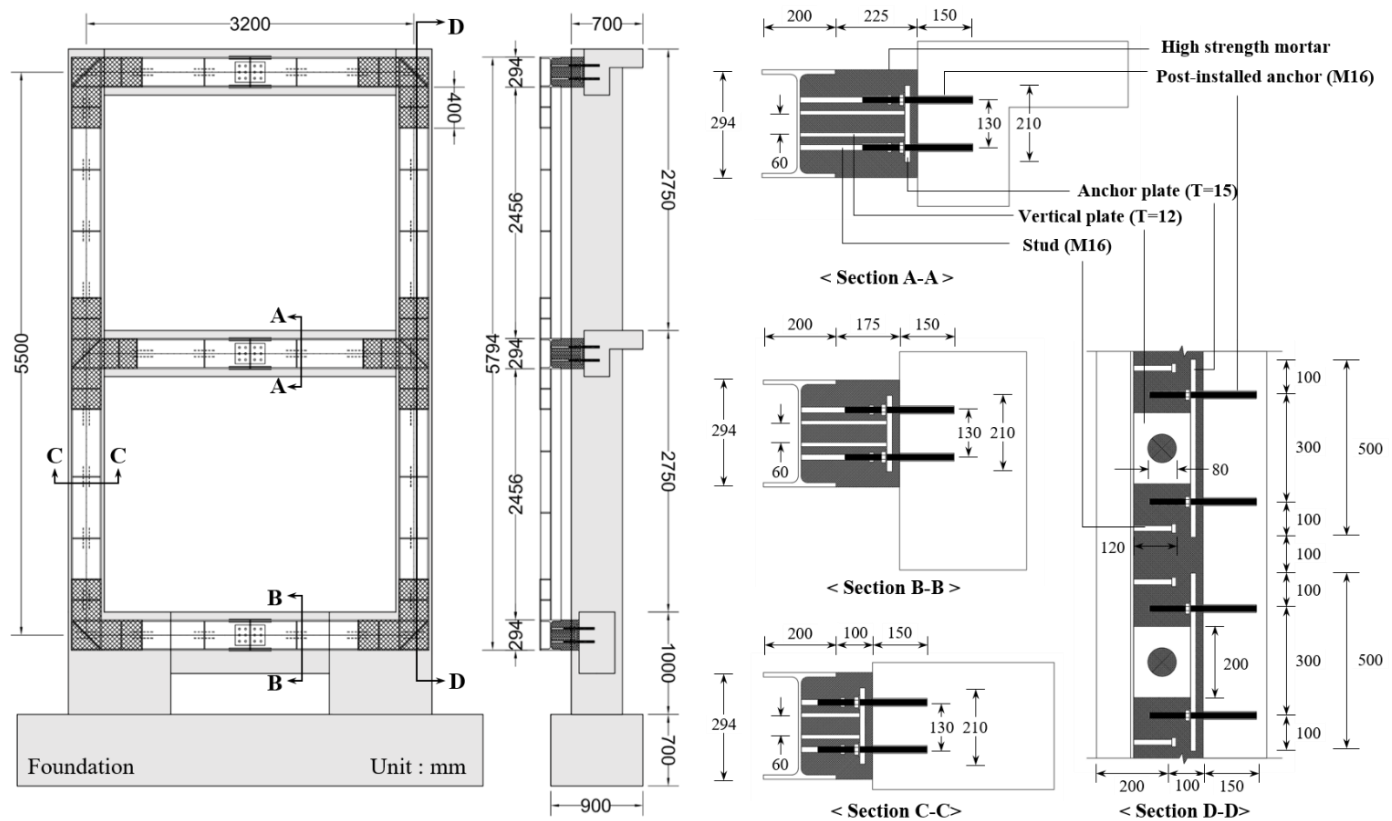

Figure 4-5 Dimensions and connection details of specimen retrofitted with external steel moment frame (**EX-1**)

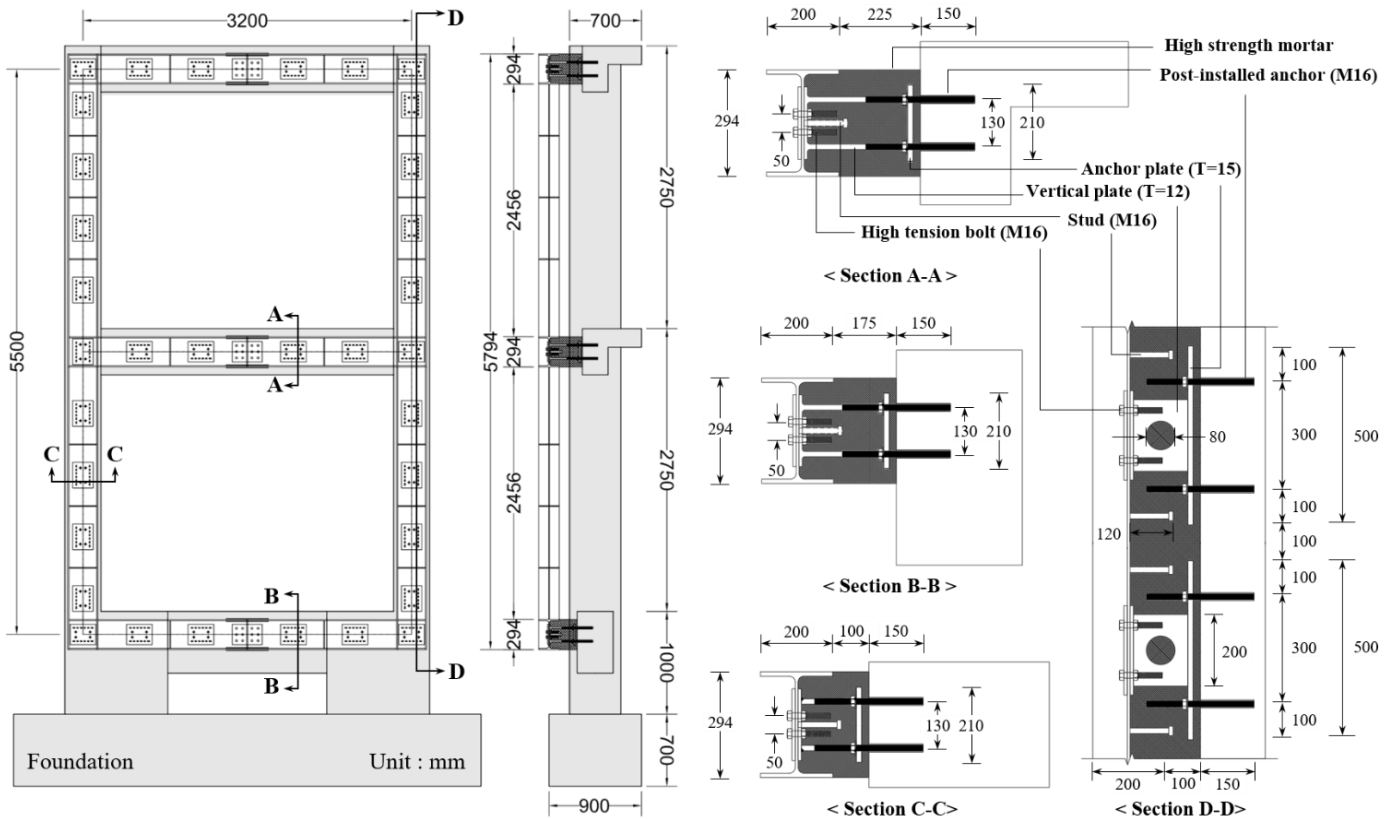

Figure 4-6 Dimensions and connection details of specimen retrofitted with external steel moment frame (**EX-2**)

4.2.2 Test setup for RC frames

To investigate ultimate capacity and behavior of retrofitted frames subjected to earthquake, pseudo-static lateral loading was applied. In order to apply lateral loads to two-story frame, the actuator was installed so that the load ratio between second-story and first-story slabs were 2:1, as assumed in seismic design for the 1st mode. Figure 4-7 shows the test setup for applying lateral loading. In detail of the loading point as shown in Figure 4-7, two hinges were provided for each floor to facilitate the distribution of lateral loads. Load cells were installed to measure two different loads applied on each floor. The lateral loads were transferred through slabs rather than beams to prevent exterior beam-column joints from being affected by the effect of confinement of jigs. Although actual thickness of slab was 130 mm, the thickness in the test specimens was increased to 180 mm to avoid the longitudinal shear failure during the load transfer. In the test setup, jigs were attached to the back faces of beam-column joints and fastened by steel bars passing above and below the slab as shown in Figure 4-7

In the test of ordinary moment frame without strengthening and moment frame with internal steel frames using connections Type1 and Type2 (**RC-0**, **IN-1**, **IN-2**), steel plates of which thickness is 30 mm were inserted between the slab back faces and jigs, blocking contact between beam-column joints and jigs as shown in Figure 4-8.

In the test of ordinary moment frame with external steel frames using connections Type1 and Type2 (**EX-1**, **EX-2**), RC beam-column joints were already affected by the effect of confinement of external steel frame, so there

was no need to block contact between joints and jigs. Instead blocking contact of joints, as shown in Figure 4-9, the jig was directly touching the outside of the beam-column joint and the steel bars were tightened to secure it. In addition, the actuator position was moved horizontally 200 mm from the center of the existing frame to the steel moment frame direction in order to minimize twisting effects due to the out of plane retrofitting.

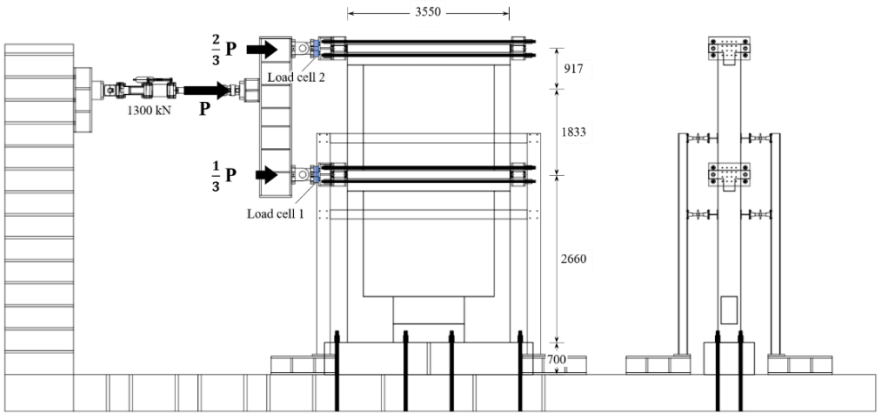

Figure 4-7 Test setup for cyclic test of two-story moment frame specimen

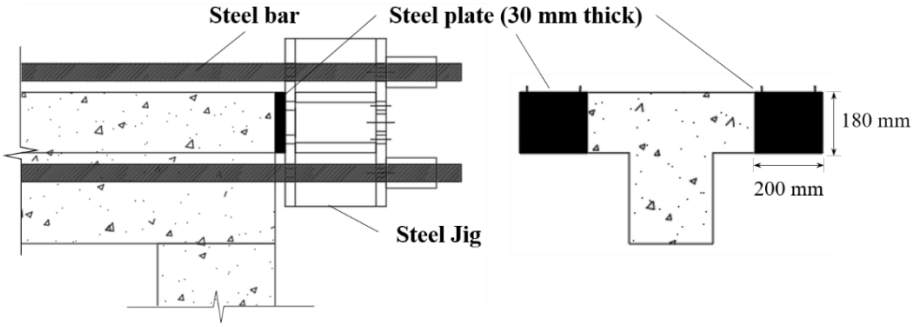

Figure 4-8 Contact detail between loading point and specimen (**RC-0**, **IN-1**, **IN-2**)

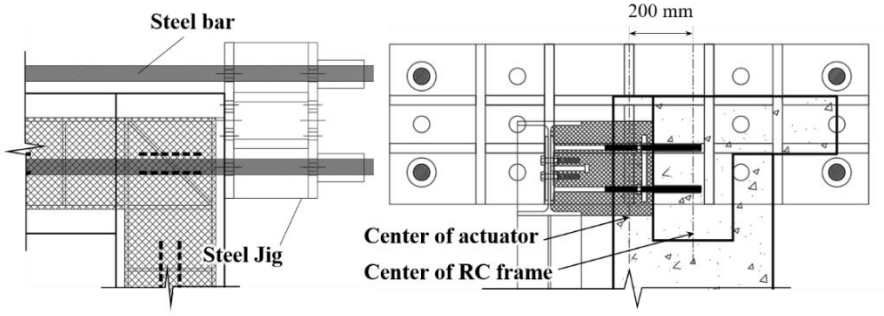

Figure 4-9 Contact detail between loading point and specimen (**EX-1**, **EX-2**)

4.2.3 Loading plan

Figure 4-10 shows the test setup for the cyclic loading of frame specimen and the drift history of the actuator for cyclic loading(h = the height of second floor, displacement controlled test). According to ACI 374.1, the drift ratio for each loading step was increased from 0.25% to 1.3 times of the previous load drift ratio. The load cycles were repeated three times for each loading step.

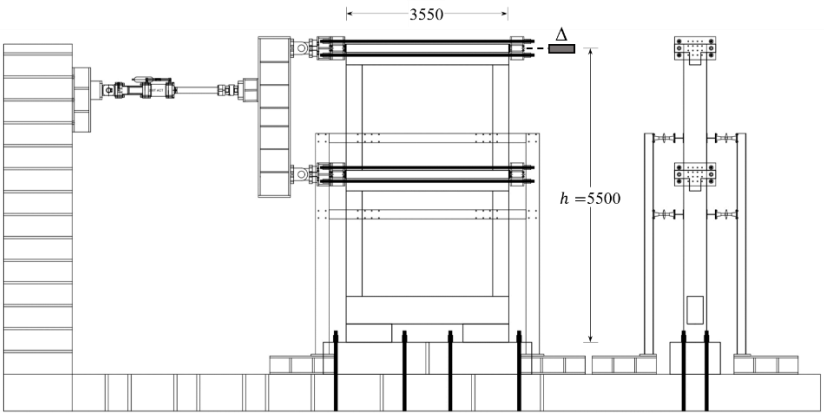

(a) Test setup for two-story moment frame specimen

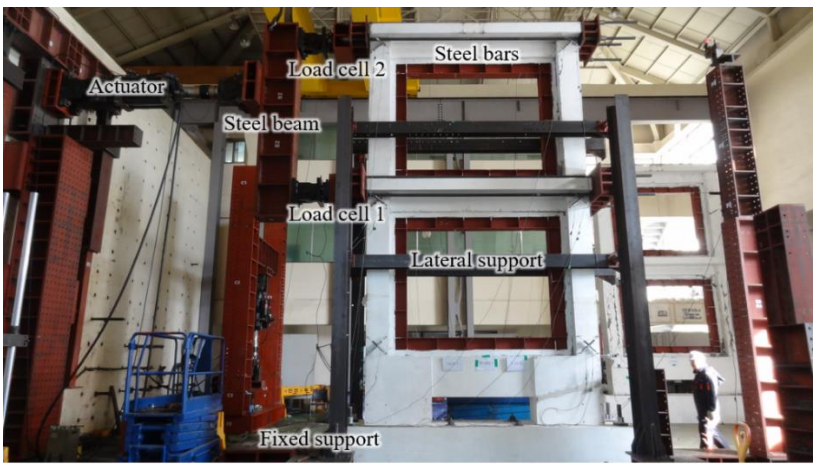

(b) Photograph of test setup for two-story moment frame specimen

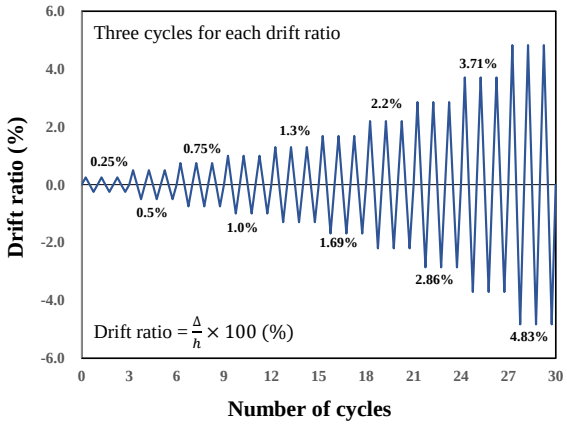

(c) Loading protocol for cyclic loading (ACI 374.1)

Figure 4-10 Loading plan for two-story frame specimen

4.2.4 Displacement and strain measuring plan

As shown in Figure 4-11, the installation of LVDTs was planned to measure lateral displacement and shear deformation (diagonal displacement) of beam-column joints.

In order to evaluate strengthening effect according to the steel moment frame, steel gauges were attached to both first and second story columns, beams, and RC beam-column joints. Gauges were attached to flexural bars and shear reinforcing bars to determine the flexural yielding of columns, beams, and the role of the shear bars. Figure 4-12 and Figure 4-13 show the location of steel gauges in test specimens.

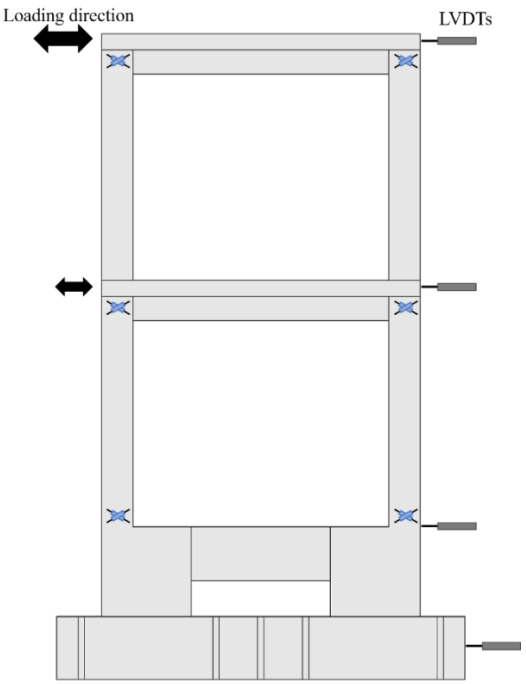

Figure 4-11 Displacement measuring plan of test specimens

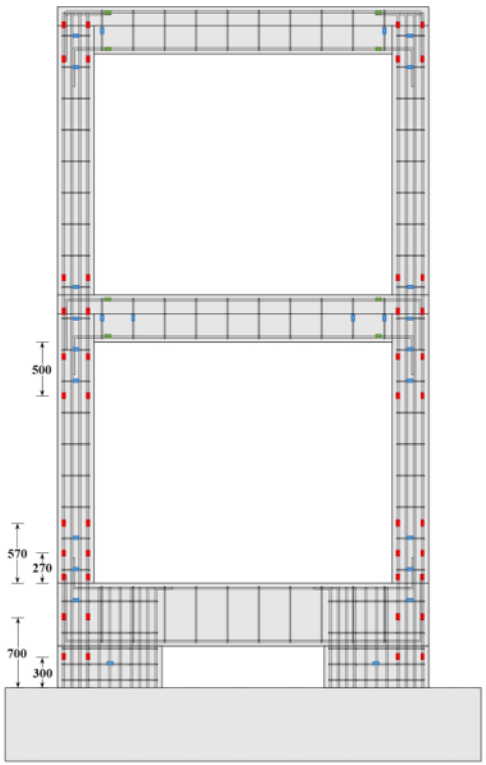

(a) Specimens **RC-0**, **IN-1**, **IN-2**, **EX-1**, and **EX-2**

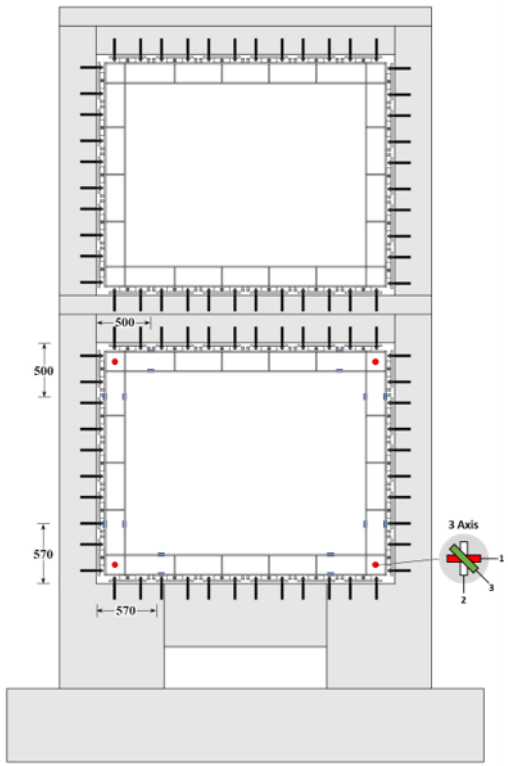

(b) Specimen **IN-1** and **IN-2**

Figure 4-12 Strain measuring plan of test specimens (Continued)

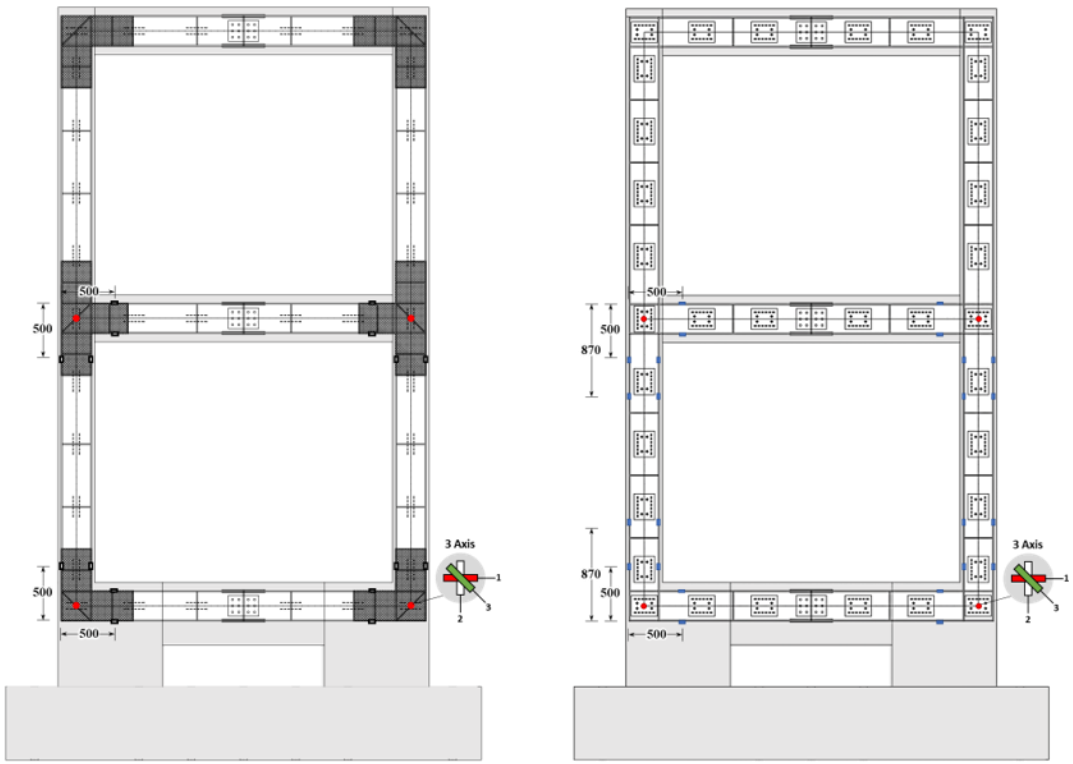

(c) Specimens **EX-1** (d) Specimen **EX-2**

Figure 4-13 Strain measuring plan of test specimens

4.2.5 Construction process of RC frame specimens

To construction procedures of frame specimens are presented in Figure 4-14 ~ Figure 4-15 and the concrete was poured at once. The construction of steel frames began after 80% or more of the design strength of concrete (0.8×21 = 16.8 MPa) was expressed. The construction process of internal steel frame and external steel frame is shown in Figure 4-16(**IN-1**, **IN-2**) and Figure 4-17(**EX-1**, **EX-2**). After drilling and chipping into RC frame after the surface treatment, anchors were installed (Figure 4-16 (a) ~ (c), Figure 4-17 (a) ~ (c)). As shown in Figure 4-16 (d) and Figure 4-17 (d), the anchor plate and the vertical plate were welded to secure the steel frame. Connect the vertical plate and the steel frame to the Type 1 connection by welding and the Type 2 connection by tightening the high-strength bolt. After removing steel frame, the formworks were installed and high-strength mortar was poured (Figure 4-16 (e) and (f), Figure 4-17 (e) and (f)). Since the temperature was below zero at the time of the concrete pouring of the frame specimens, steam curing and warming was carried out for more than 24 hours after the pouring.

(a) Joints (b) Columns (c) Slab

(d) Second story (e) Pedestal and foundation

Figure 4-14 Formwork installation and rebar arrangement of RC frame specimen

Figure 4-15 Concrete pouring in a whole frame at one time

(a) Rebar detection (b) Boring concrete

(c) Chipping concrete and installing chemical anchors (d) Welding vertical plate to steel frame

(e) Formwork installation and mortar pouring (f) Curing

Figure 4-16 Internal steel moment frame specimen construction process

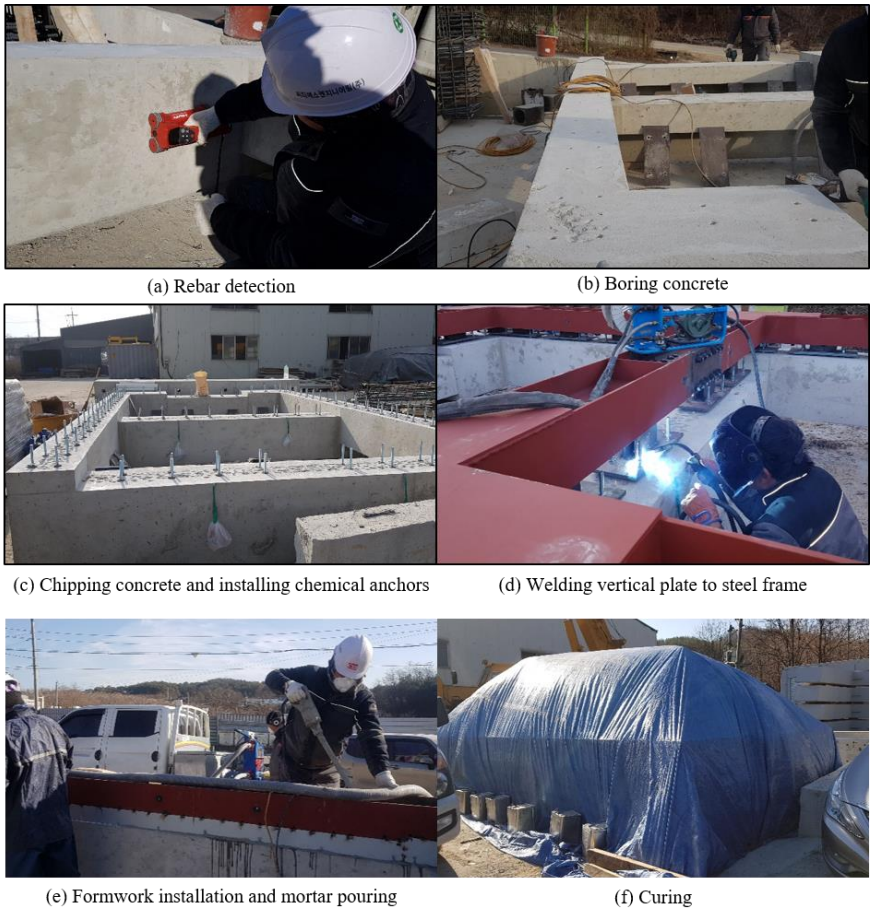

Figure 4-17 External steel moment frame specimen construction process

4.3 Test Results and Observations

4.3.1 Material Strength

Because one frame was poured at a time, concrete cylinders were made for each specimen. High-strength mortar was poured and grouped by internal-retrofitting specimen(**IN-1**, **IN-2**) and external- experiment (**EX-1**, **EX-2**), respectively, and the mortar cubes was also grouped. The compression test results of concrete cylinders and mortar cubes were presented in Table 4-2 and Figure 4-18. The curing period in Table 4-2 is the period from the day of concrete or mortar pouring to the day of the test. Concrete cylinders of all specimens showed compressive strength of 21 MPa or higher, and high strength mortar also expressed design strength of 60 MPa or higher except specimen EX-2.

The reinforcing bars used in the test specimens were D10, D13, D16, D19 and D22 with nominal strength of 400 MPa for flexure and shear reinforcement. Stiffener plate of panel zone in specimen **EX-1** and steel frame used for internal and external retrofitting specimens were used with SM355. Table 4-3 and Figure 4-19 show the yield strength and tensile strength of rebars used in the test specimens.

Table 4-2 Average compressive strengths of concrete and mortar

Specimen	Test No.	**RC-0**	**IN-1**	**IN-2**	**EX-1**	**EX-2**
Concrete Strength (Curing period)	Test 1	22	23	26	25	21
	Test 2	23	23	25	27	26
	Average	22.5 (23 days)	23 (25 days)	25.5 (26 days)	26 (28 days)	23.5 (22 days)
Mortar strength (Curing period)	Test 1	-	69	74	82	43
	Test 2	-	70	68	85	40
	Test 3	-	59	75	80	40
	Average	-	66 (7 days)	72.3 (5 days)	82.3 (10 days)	41 (12 days)

(a) Concrete cylinder

(b) Mortar cube (50×50×50 mm)

Figure 4-18 Test of compressive strength

Table 4-3 Average tensile strengths of steel rebars, anchors, and plates

Specimen		Location	A_s[1)] (mm^2)	f_y (MPa)	f_u (MPa)
Rebar (SD400)	D10	B/C/S shear	71.3	526	667.7
	D13	Slab flexure	126.7	456	620.7
	D16	Column flexure	198.6	490	611
	D19	B/C flexure	286.7	487	597.7
Anchor (gvz 8.8)	M16	Connection Type 1, 2	153.3	739	850.9
Steel plate (SM355)	Flange 12T	IN flange	300	386	543
		EX flange	300	380	541
	Web 8T	IN web	200	423	577
		EX web	200	424	578
	Stiffener 9T	EX-1 panel zone	225	419	527

1) Effective cross-sectional area of anchor

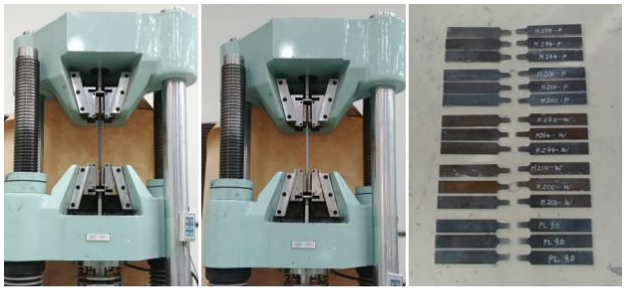

(a) Rebar (b) Anchor (c) Plate

Figure 4-19 Test of tensile strength

4.3.2 RC frame without strengthening (RC-0)

The test results of RC moment frame are summarized in Table 4-4. In this test, displacement did not increase more than 3.7% story drift ratio due to safety problem.

Table 4-4 Test results of RC frame specimens

Specimen		Peak load P_u (kN)	Drift ratio at P_u (%)	Ductility			Yield stiffness
				Δ_y [1] (%)	Δ_u [2] (%)	Δ_u/Δ_y	P_u/Δ_y (kN/mm)
RC-0	(+)	233.6	2.22	0.91	3.77	4.13	4.7
	(-)	-204.2	-2.17	-1.12	-3.65	3.25	3.3
IN-1	(+)	721.2	1.30	0.68	1.96	2.89	16.9
	(-)	-735.3	-1.30	-0.65	-2.04	3.12	18.0
IN-2	(+)	725.8	1.68	0.80	2.42	3.03	19.7
	(-)	-731.2	-1.71	-0.75	-2.19	2.93	20.8
EX-1	(+)	710.6	2.78	1.61	3.47	2.16	8.1
	(-)	-744.2	-2.23	-1.67	-3.50	2.10	8.2
EX-2	(+)	649.9	2.82	1.55	3.75	2.43	7.6
	(-)	-672.2	-2.84	-1.46	-3.41	2.33	8.3

1) Yield drift ratio = P_u/K_y where K_y is the secant stiffness, connecting the origin and the prepeak point of $0.75P_u$

2) Ultimate drift ratio defined as the post peak drift ratio corresponding to $0.9P_u$

The specimen **RC-0** attained the peak load P_u = 233.6 and -204.2 kN at 2.2% drift ratio, and the maximum drift ratio was 3.71% (Figure 4-20). As shown in Figure 4-21, as the drift increased, in the flexural cracks at the end of the 1st-story column and the shear cracks at the 2nd and 3rd-story beam-column joints increased gradually. The specimen failed due to shear failure at the beam-column joints as shown in Figure 4-22.

In addition, the column below the joint region was severely damaged, which was attributed to anchorage details of beam rebars. In all specimens, following rebar details of the prototype school buildings, beam bottom rebars (2-D19) were embedded only 200 mm inside the joint and the hook was anchored to the top of the column as shown in Figure 4-23.

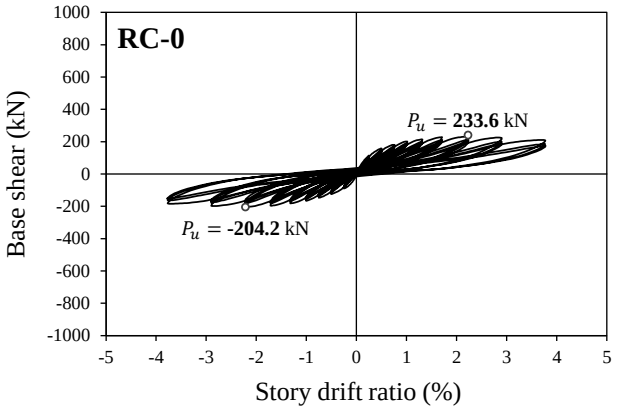

Figure 4-20 Lateral load and drift ratio relationship of **RC-0**

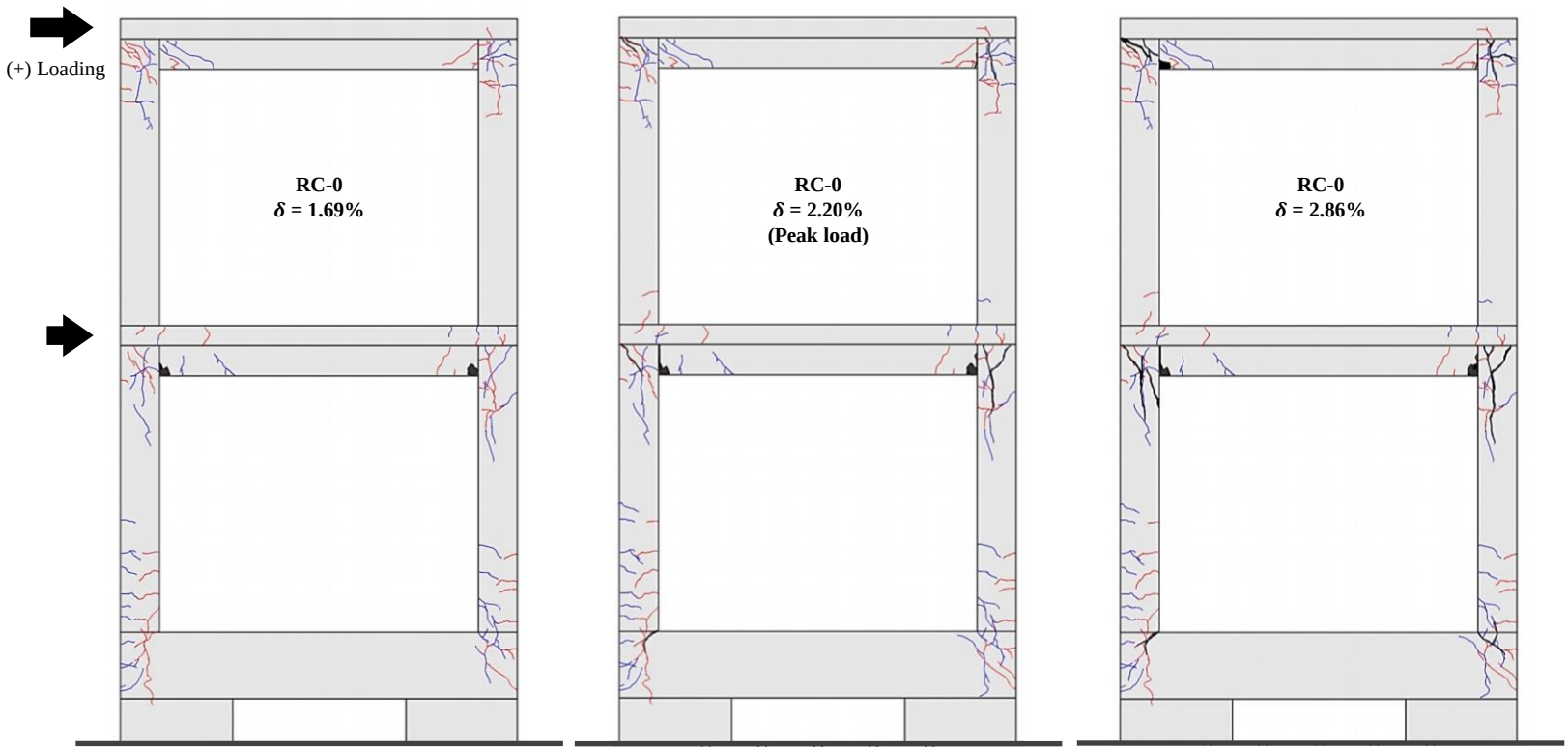

Figure 4-21 Failure sequence and crack patterns of specimen **RC-0**

(a) 3rd-story

(b) 2nd-story

Figure 4-22 Final failure mode of specimen **RC-0**

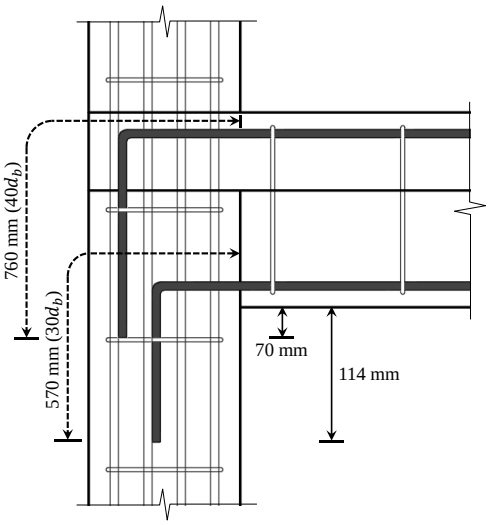

Figure 4-23 Joint reinforcement anchoring details of RC frame

4.3.3 RC frame with internal steel moment frame (IN-1)

In the retrofitted with internal steel moment frame specimen **IN-1**(Type 1, flange connection), the peak load was P_u = 721.2 and -735.3 kN at 1.3% drift ratio, which was 3.1 times greater than that of **RC-0** (Figure 4-24).

The crack patterns of **IN-1** were described in Figure 4-25 and Figure 4-26. After flexural yielding of the 1st-story RC columns at 1.3% drift ratio, **IN-I** ultimately failed by shear mechanism of the 1st-story RC columns as shown in Figure 4-27. At 1.3% drift ratio, when the peak load was attained, several diagonal cracks were distributed along the 1st-strory RC column mid-span. At 1.69% drift ratio, the cracks extended and were connected longitudinally. At 2.2% drift ratio, in the 1st-story steel frame, fracture of steel beam flange first occurred at the heat-affected region of weld joint between the beam and colum flanges(Figure 4-28). On the other hand, unlike **RC-0**, damages at RC beam-column joints were not significant until the end of the test (2.86% drift ratio).

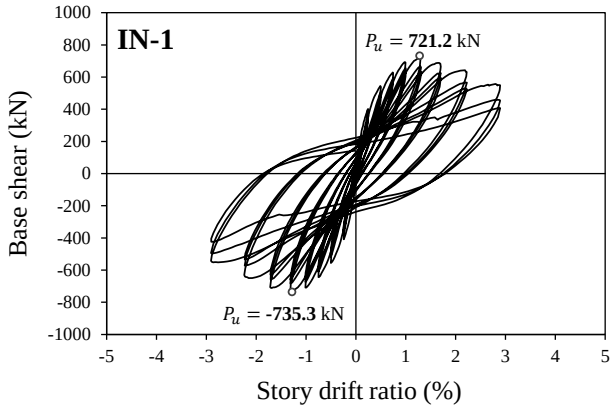

Figure 4-24 Lateral load and drift ratio relationship of **IN-1**

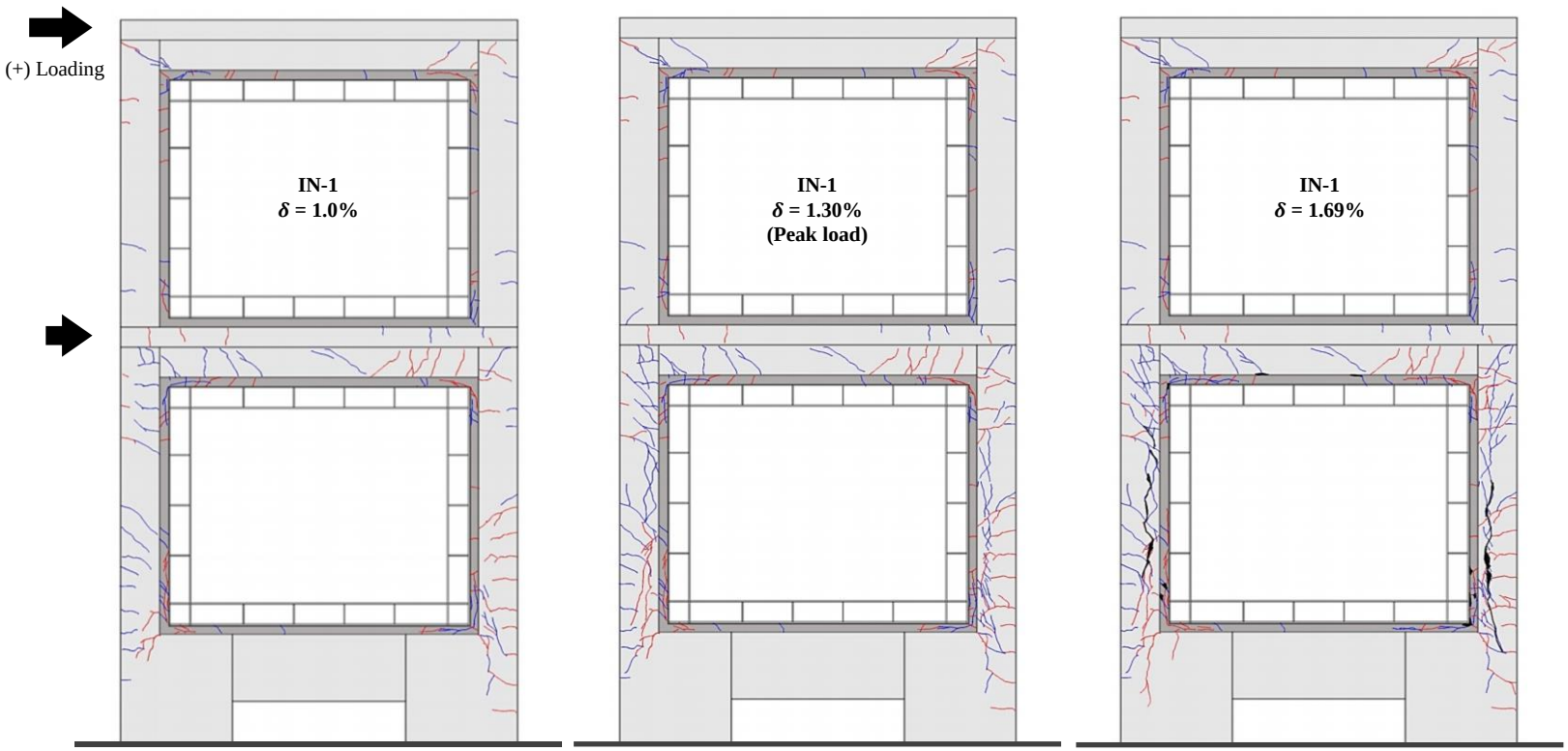

Figure 4-25 Failure sequence and crack patterns of specimen **IN-1** (Continued)

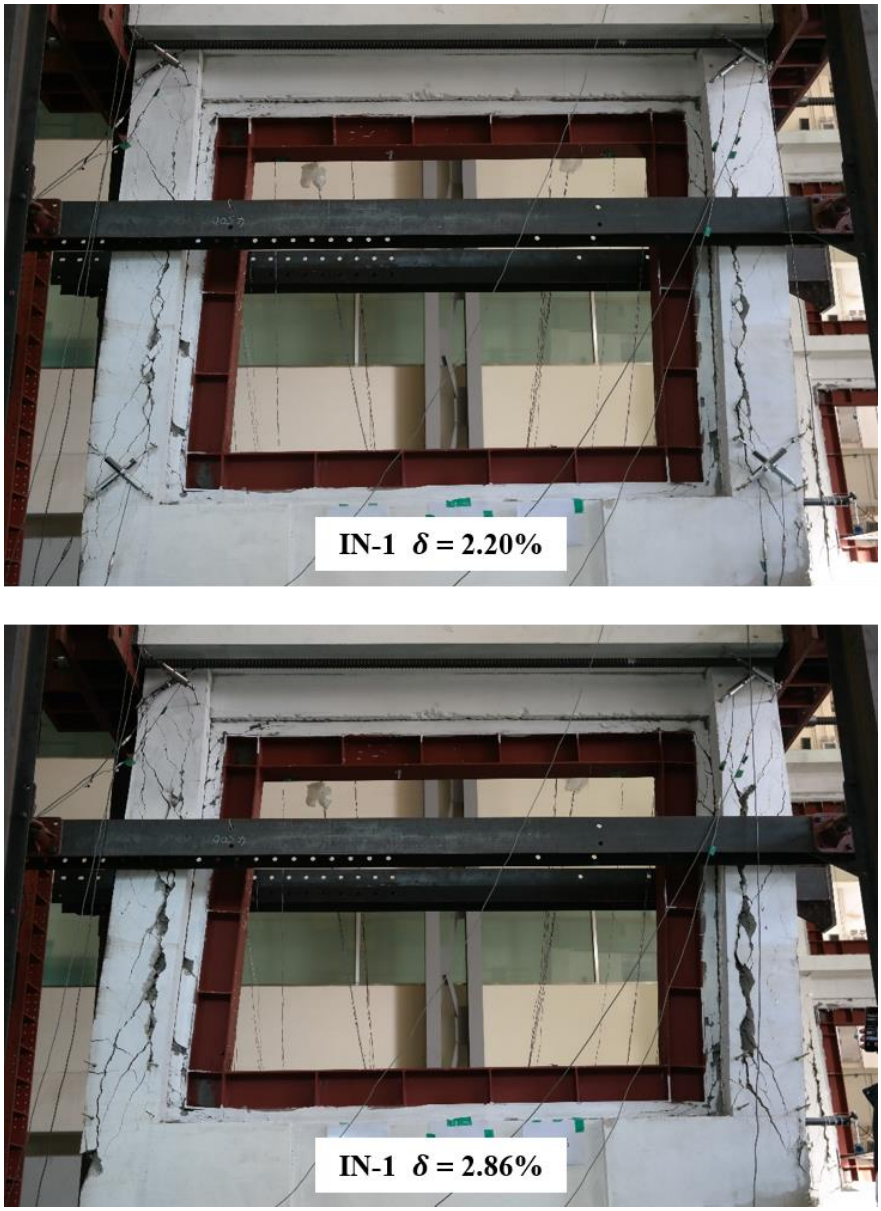

Figure 4-26 Failure sequence and crack patterns of specimen **IN-1**

Figure 4-27 Final failure mode of specimen **IN-1**

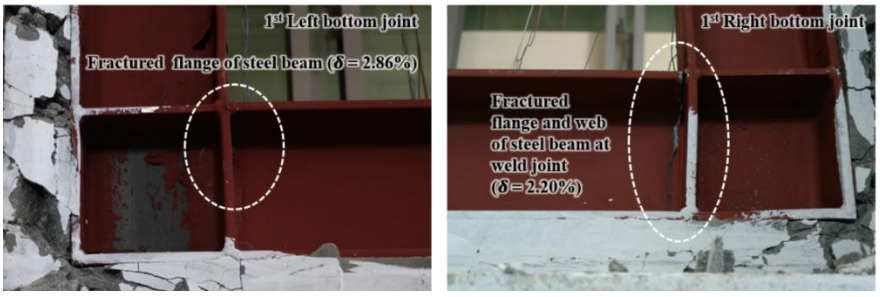

Figure 4-28 Failure mode of steel moment frame (**IN-1**)

4.3.4 RC frame with internal steel moment frame (IN-2)

The behavior of **IN-2**(Type 2, flange connection) was similar to that of **IN-1** and it is noted that the material strengths of concrete and mortar in **IN-2** were greater than those in **IN-1**(Table 4-2). The peak load was P_u= 725.8 and -731.2 kN at 1.69% drift ratio, which was 3.1 times greater than that of **RC-0** (Figure 4-29).

The crack patterns of **IN-2** were described in Figure 4-30 and Figure 4-31. After flexural yielding of the 1st-story RC columns at 1.3% drift ratio, **IN-2** ultimately failed by shear mechanism of the 1st-story RC columns as the specimen **IN-1** did(Figure 4-32). At 1.69% drift ratio, when the peak load was attained, several diagonal cracks were distributed and connected longitudinally along the 1st-story RC column mid-span. At 2.86% drift ratio, in the 1st-story steel frame, fracture of steel beam flange occurred at the heat-affected region of weld joint between the beam and column flanges(Figure 4-33). Unlike **RC-0**, damages at RC beam-column joints were not significant until the end of test (2.86% drift ratio) as **IN-1** did.

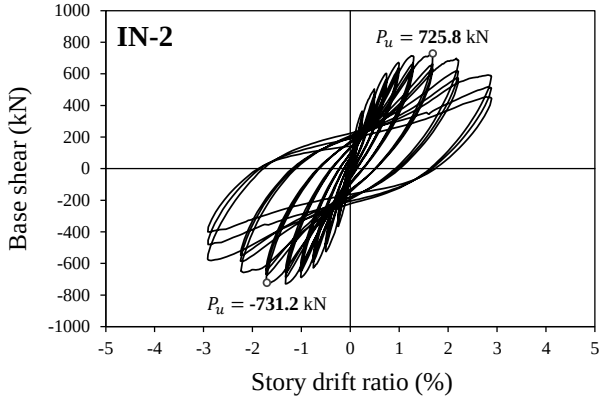

Figure 4-29 Lateral load and drift ratio relationship of **IN-2**

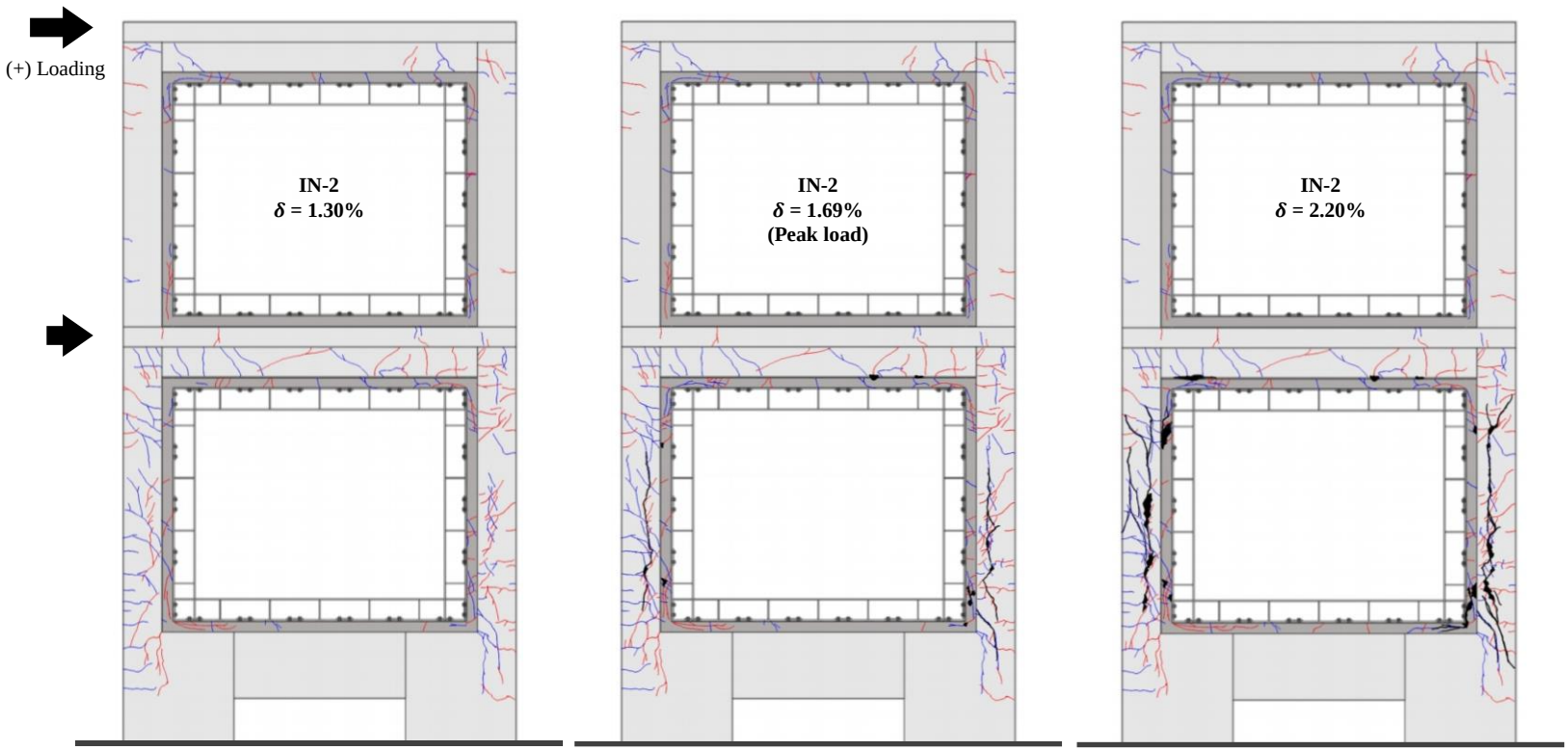

Figure 4-30 Failure sequence and crack patterns of specimen **IN-2** (Continued)

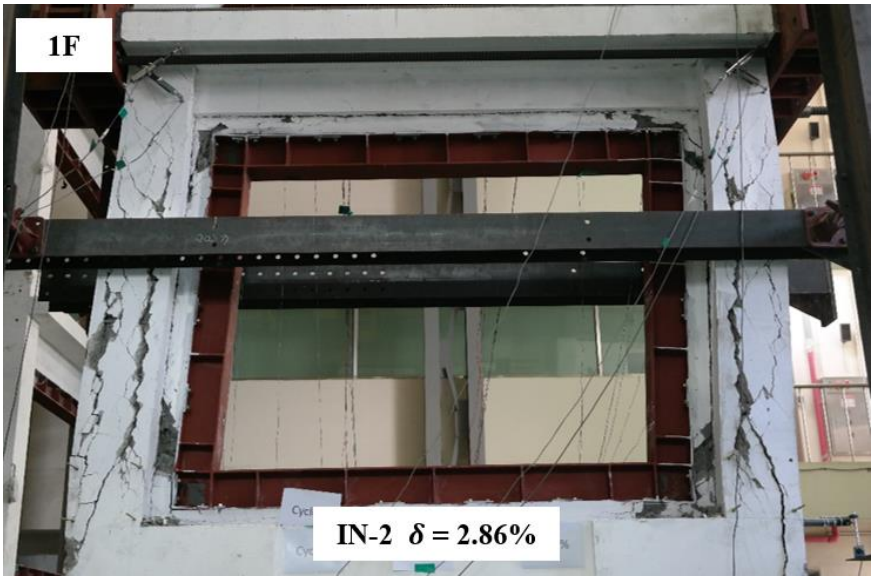

Figure 4-31 Failure sequence and crack patterns of specimen **IN-2**

Figure 4-32 Final failure mode of specimen **IN-2**

Figure 4-33 Failure mode of steel moment frame (**IN-2**)

4.3.5 RC frame with external steel moment frame (EX-1)

In the retrofitted with external steel moment frame specimen **EX-1**(Type 1, web connection), the peak load was P_u = 710.6 and -744.2 kN at 2.86% and 2.2% drift ratio respectively in

Figure 4-34, which was 3 times greater than that of **RC-0**.

The crack patterns of **EX-1** were described in Figure 4-35. After the peak load at 2.86% drift ratio, **EX-I** ultimately failed by flexural mechanism of the 1st-story RC columns as shown in Figure 4-36.

At 2.86% drift ratio, when the peak load was attained, splitting cracks and spalling of concrete cover and mortar occurred at the bottom of the 1st-story RC column as shown in Figure 4-35. At 3.71% drift ratio, longitudinal bars of the 1st-story column buckled significantly, decreasing the load carrying capacity(Figure 4-37).

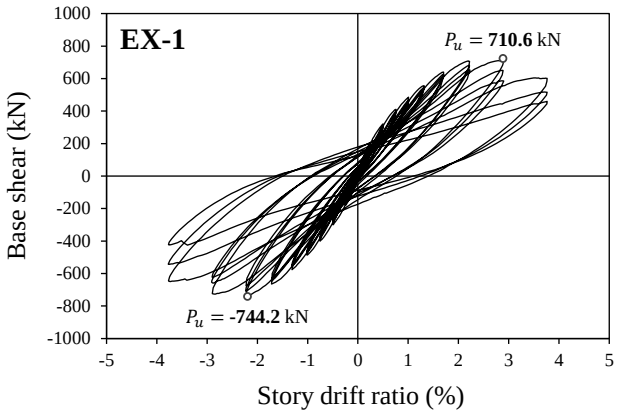

Figure 4-34 Lateral load and drift ratio relationship of **EX-1**

After the buckling of longitudinal bars, fracture of steel beam flange and stiffening plate in panel zone occurred at the heat-affected region of weld joint between the beam and column flanges(Figure 4-39). Unlike **IN-1** and **IN-2**, final damages at RC beam-column joints were more similar to **RC-0**, but the beam-column joints were also affected by the effect of confinement of external steel frame as the internal steel frame did.

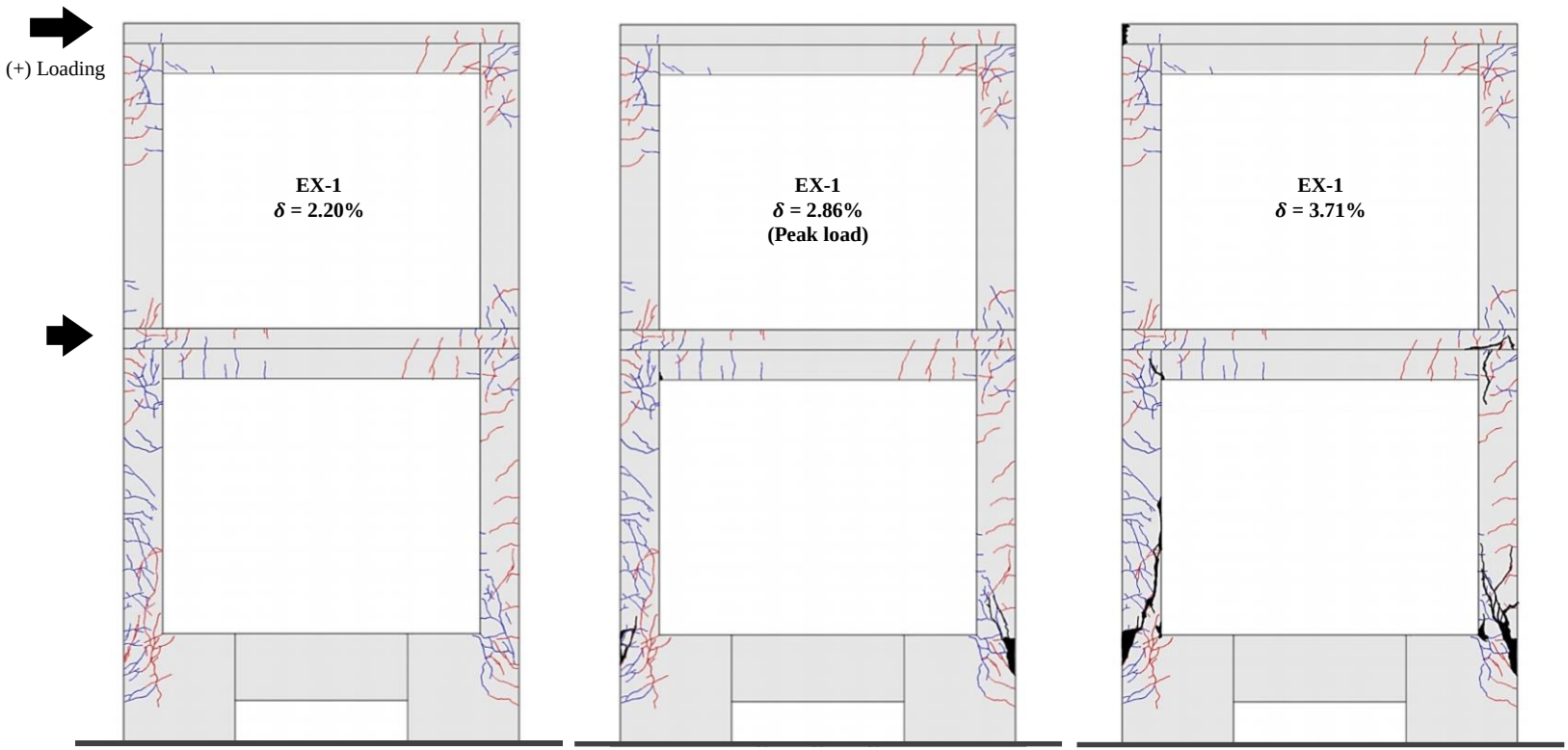

Figure 4-35 Failure sequence and crack patterns of specimen **EX-1**

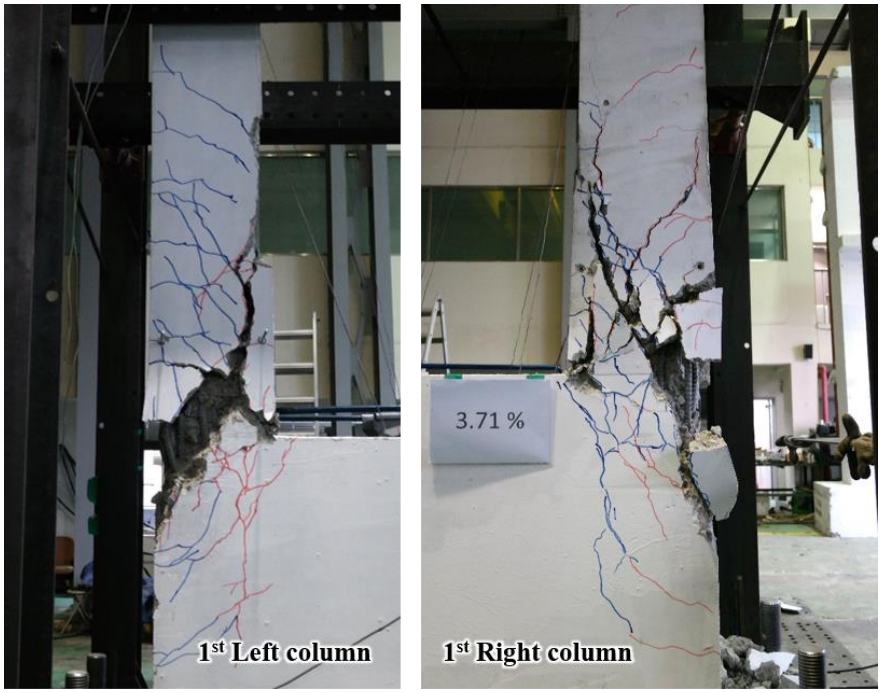

Figure 4-36 Final failure mode of specimen **EX-1** (Continued)

Figure 4-37 Final failure mode of specimen **EX-1** (Continued)

(a) 1st story (b) 2nd story

Figure 4-38 Final failure mode of specimen **EX-1**

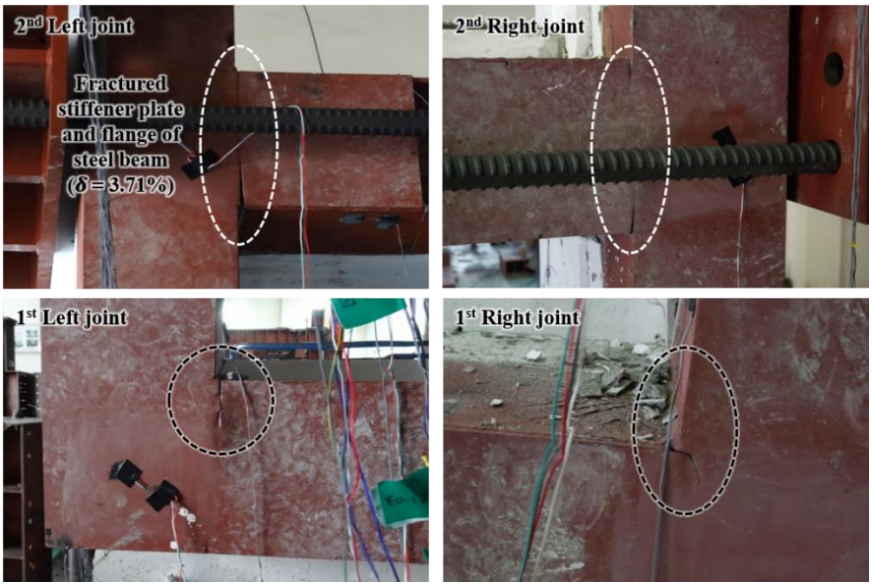

Figure 4-39 Failure mode of steel moment frame (**EX-1**)

4.3.6 RC frame with external steel moment frame (EX-2)

In the retrofitted with external steel moment frame specimen **EX-2**(Type 2, web connection), the peak load was P_u = 649.9 and -672.2 kN at 2.86% in

Figure 4-34 Figure 4-40, which was 2.8 times greater than that of **RC-0**.

The crack patterns of **EX-2** were described in Figure 4-41. After the peak load at 2.86% drift ratio, **EX-2** ultimately failed by flexural mechanism of the 1st-story RC columns as shown in Figure 4-42.

At 2.86% drift ratio, when the peak load was attained, splitting cracks and spalling of concrete cover and mortar occurred at the bottom of the 1st-story RC column as **EX-1** did(Figure 4-41Figure 4-43). At 3.71% drift ratio, longitudinal bars of 1st-story column buckled significantly, decreasing the load carrying capacity as shown in Figure 4-43.

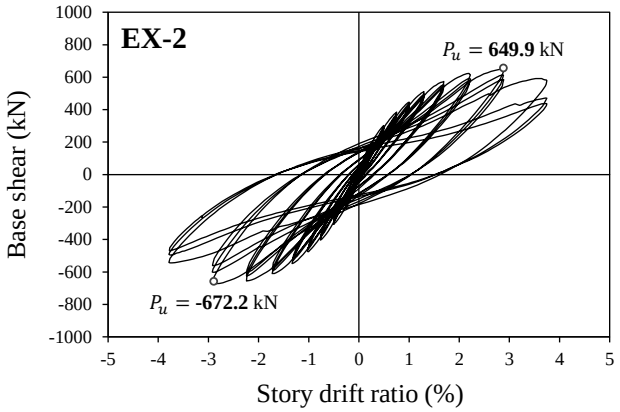

Figure 4-40 Lateral load and drift ratio relationship of **EX-2**

After the buckling of longitudinal bars, fracture of steel beam flange occurred at the heat-affected region of weld joint between the beam and column flanges(Figure 4-45). Similar to **EX-1**, final damages of RC beam-column joints were more significant than **IN-1** and **IN-2** but less than **RC-0**.

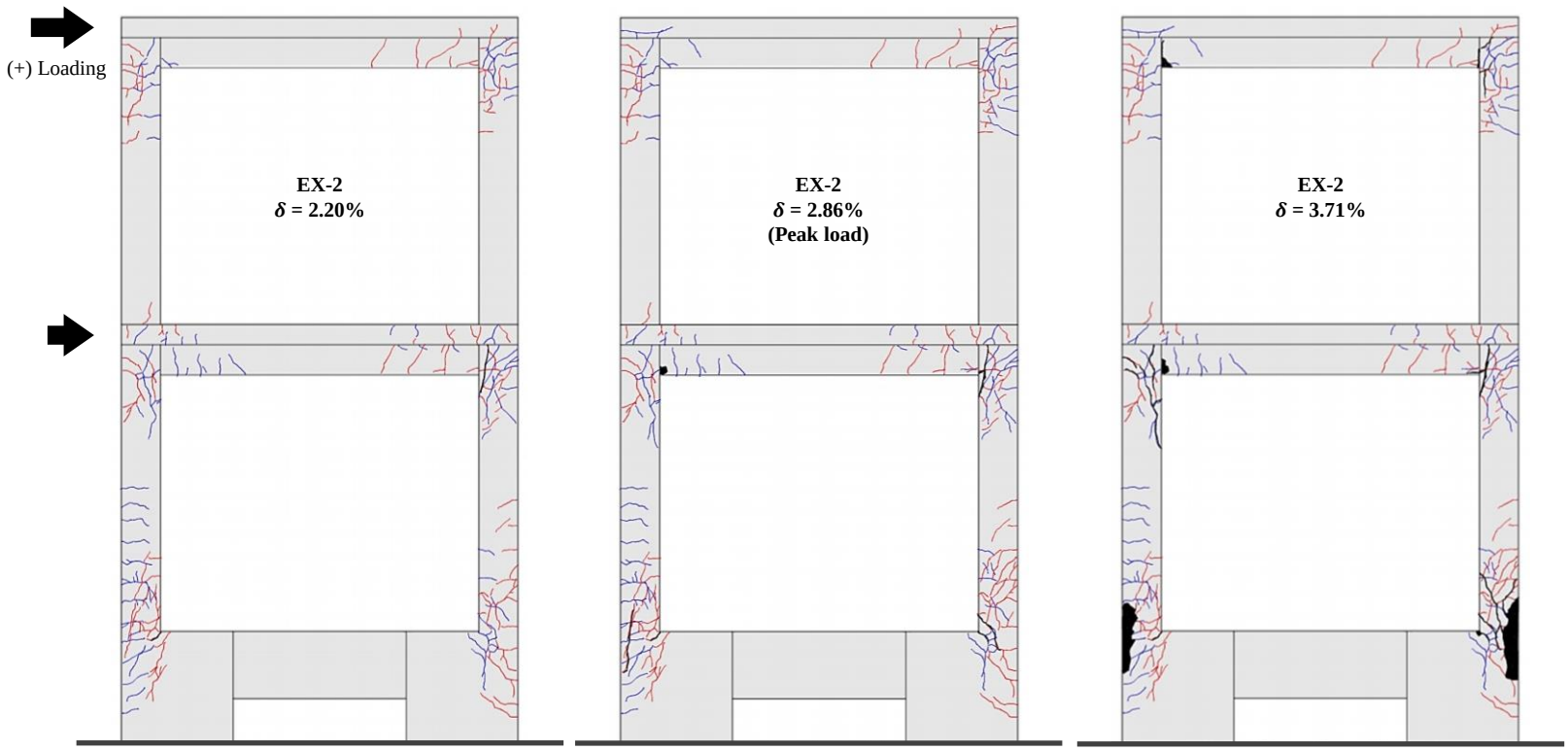

Figure 4-41 Failure sequence and crack patterns of specimen **EX-2**

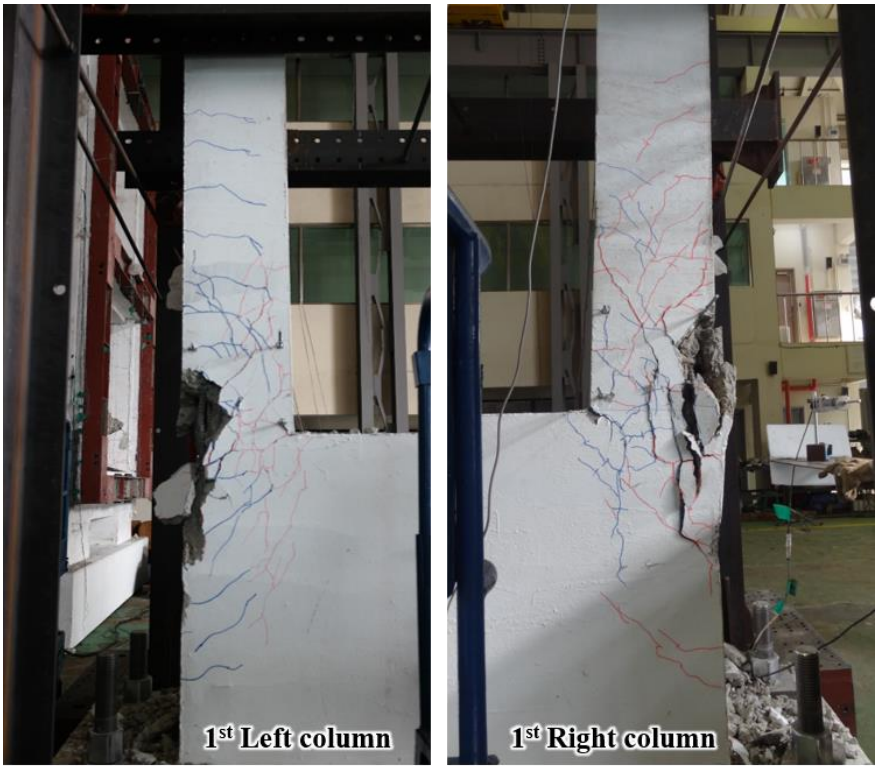

Figure 4-42 Final failure mode of specimen **EX-2** (Continued)

Figure 4-43 Final failure mode of specimen **EX-2** (Continued)

(a) 1st story (b) 2nd story

Figure 4-44 Final failure mode of specimen **EX-2**

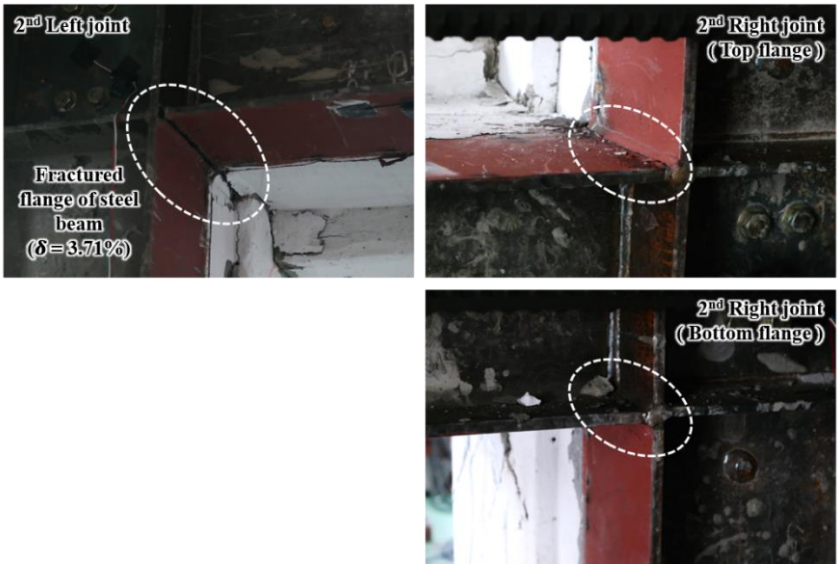

Figure 4-45 Failure mode of steel moment frame (**EX-2**)

4.4 Test Analysis

4.4.1 Comparison of load-drift ratio envelope curves

Figure 4-46 shows the envelope curves for each specimen in order to compare the load and drift ratio relationship. The envelope curve is a multiple straight line connecting maximum loads of first cycles at each drift ratio according to ACI 374.1.

The initial stiffness of the specimens was greatly influenced by frame retrofitting methods. The internal-retrofitting specimens(**IN-1** and **IN-2**) and the external-retrofitting specimens(**EX-1** and **EX-2**) showed similar stiffness up to 1.3% and 1.0% drift ratio respectively. Specimen **IN-1** and **IN-2**, retrofitted with internal steel frames, exhibited initial stiffness 4 times larger than that of **RC-0** and 2 times larger than that of **EX-1** and **EX-2**.

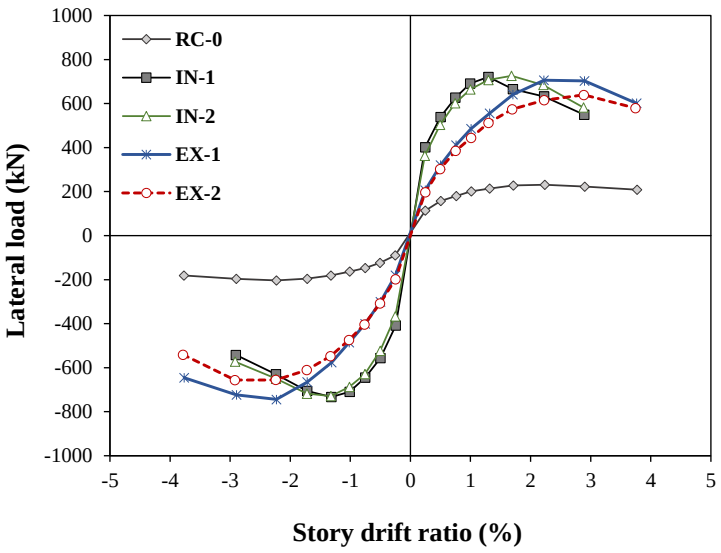

Figure 4-46 Comparison of load-drift ratio envelope curves

The maximum strength of the specimen was also affected by frame retrofitting methods, not by connecting methods. Even though the internal steel frame were smaller in size than external steel frame, the specimen **IN-1** and **IN-2**(H-200×200×8×12) showed 2~12% greater strength and 2.3 times greater yield stiffness than that of specimen **EX-1** and **EX-2**(H-294×200×8×12). This is because the bending strength of the composite members of internal-retrofitting specimens are greatly increased more than that of external-retrofitting specimens. Due to the effect of stiffneing plate in panel zone, the maximum strength of the specimen **EX-1** was 10% greater than that of **EX-2**.

Though all retrofitted specimens(**IN-1**, **IN-2**, **EX-1** and **EX-2**) exhibited lower ductility than **RC-0**, the internal and external retrofitting specimens showed 3.1 and 2.9 times greater strength and 4.7 and 2 times greater yield stiffness than that of **RC-0**, respectively.

4.4.2 Comparison of energy dissipation capacity

The energy dissipation capacity is the ability of a structure to absorb energy during cyclic loading, which is expressed as the area (E_d) enclosed by the load and displacement hysteresis curves as shown in Figure 4-47. The amount of energy dissipation during cyclic loading is an important factor to evaluate seismic performance of structures. Figure 4-47 and Figure 4-48 shows cumulative energy dissipation capacity and energy dissipation ratio for each specimen, respectively.

The cumulative energy dissipation capacity was influenced by the maximum deformation capacity and load carrying capacity of test specimens. Specimen **RC-0** showed poor energy dissipation mainly due to the shear failure in beam-column joints. The energy dissipation ratio of prototype RC frame was 11.9% which was less than 12.5% recommended by acceptance criteria of ACI 374.1-05. Specimen **IN-1** and **IN-2** with highest load carrying capacity showed the highest energy dissipation capacity with the drift ratio of 2.86%, which was 6.8 times greater than that of **RC-0**. Specimen **EX-1** and **EX-2** showed 4.2 times greater energy dissipation capacity than **RC-0**. The energy dissipation ratio of all retrofitted specimens was greater than 12.5% recommended by ACI 374.1-05.

Specimen **IN-1** and **IN-2**, retrofitted with internal steel frame with connection Type1 and Type2 ,respectively, showed the similar cumulative energy dissipation capacity. Specimen **EX-2** showed 8% greater energy dissipation capacity with the drift ratio 3.71% than that of **EX-1** This indicates that the connection types did not significantly affect the structural performance

of the test specimens. The energy dissipation capacity of test specimens varied greatly depending on the retrofitting method(internal and external). Thought the specimens with internal steel frame(**IN-1** and **IN-2**) showed the maximum deformation capacity 39% less than that of external-retrofitting specimens(**EX-1** and **EX-2**), **IN-1** and **IN-2** showed energy dissipation capacity with the drift ratio 2.86%, which was 1.7 times greater than that of **EX-1** and **EX-2**.

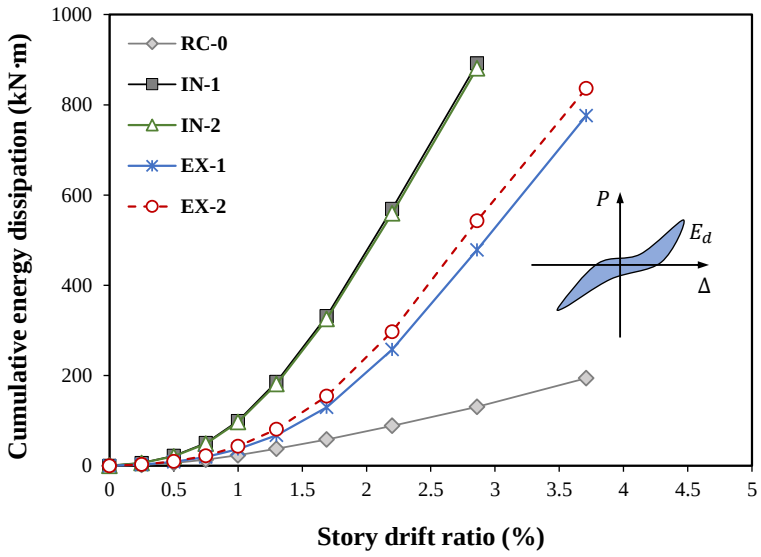

Figure 4-47 Comparison of cumulative energy dissipation capacity

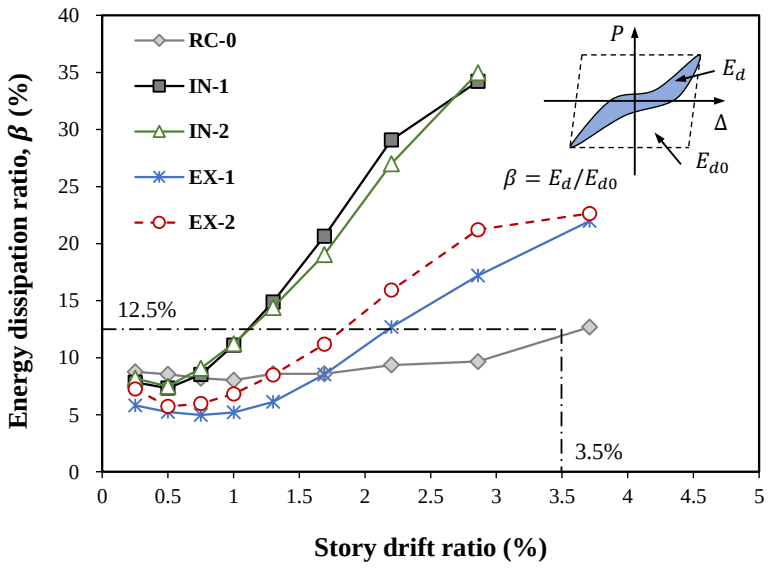

Figure 4-48 Comparison of energy dissipation ratio (3rd cycle)

4.4.3 Deformation contributions of rebar flexure and shear

Most major cracks were concentrated on the columns compared with beams and joints in the frame specimens, except specimen **RC-0** whose beam-column joints were damaged severely. In particular, vertical splitting cracks and diagonal shear cracks were concentrated on the 1st-story columns. The behavior of each RC member(columns, beams, joints etc.) in the specimens was important to verify the effect of retrofitting RC frame.

The strains measured from longitudinal bars in plastic hinge regions of columns and beams and transverse bars of beam-column joint regions were examined. The plastic mechanism of frames was verified by measured strains from longitudinal bars and transverse bars in plastic hinge regions(Figure 4-49 ~ Figure 4-61).

The test result of specimen **RC-0** showed that the shear failure occurred in beam-column joints before the longitudinal bars of the 1st-story columns yield as shown in (d). Because of the weakly anchored hook of beam bottom rebars(2-D19), the diagonal shear cracks and vertical splitting cracks were developed before the yielding of longitudinal bars in the 1st-story columns. In addition, the transverse bars in the beam-column joints did not yield until the specimen destroyed as shown in Figure 4-59 and Figure 4-60.

The internal-retrofitting specimens(**IN-1** and **IN-2**) showed that the strain of longitudinal bars in plastic hinge regions of the 1st-story columns had values close to or exceeding the yield strain near the maximum strength of the frames as shown in Figure 4-51 (d) and Figure 4-53 (d). The sequence of plastic hinge mechanism in frames was described in Figure 4-52 and Figure 4-54.

The external-retrofitting specimens(**EX-1** and **EX-2**) showed that the yielding of longitudinal bars in plastic hinge regions of the 1st-story columns occurred before the maximum strength of the frames as shown in Figure 4-55 and Figure 4-57. After the yielding of the 1st-story columns, concrete cover spalling occurred by crushing at the bottom of columns. This resulted in load degradation due to the buckling of the column reinforcement. Figure 4-56 and Figure 4-58 described the sequence of plastic hinge mechanism in external-retrofitting specimens.

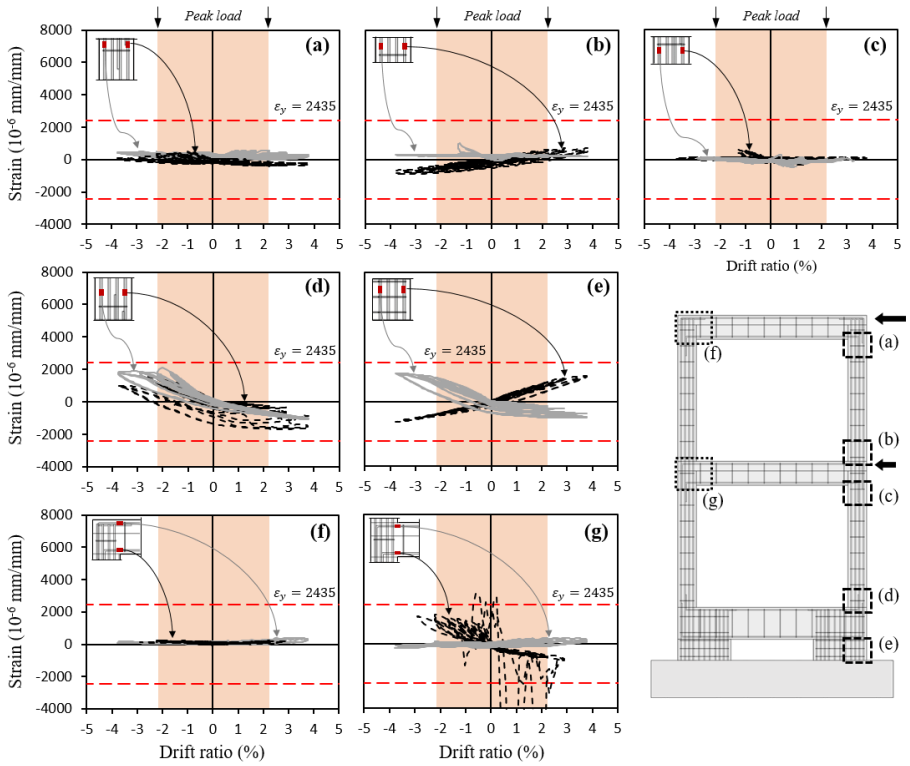

Figure 4-49 Strains of longitudinal bars in specimen **RC-0**

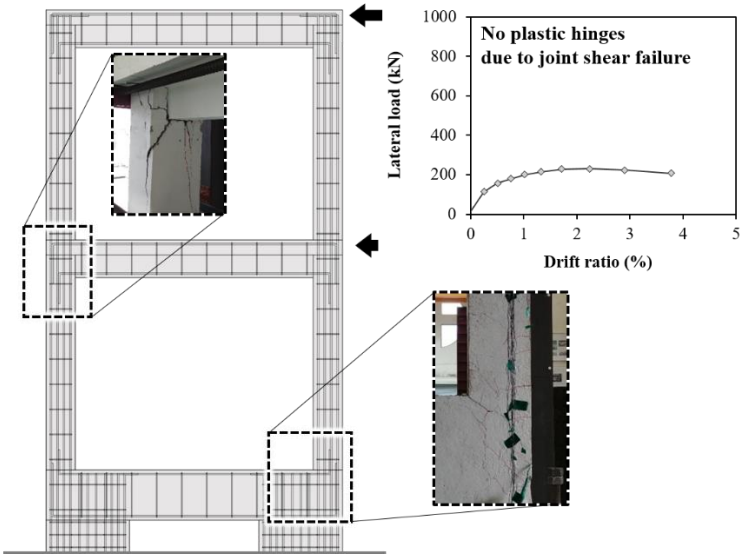

Figure 4-50 Sequence of plastic hinge mechanism in specimen **RC-0**

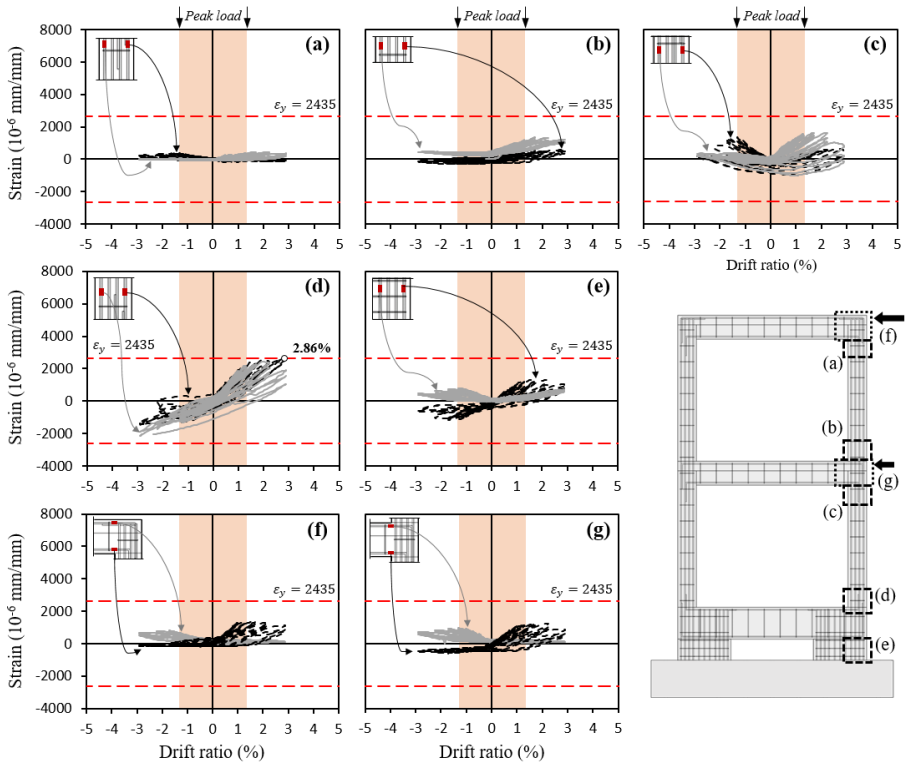

Figure 4-51 Strains of longitudinal bars in specimen **IN-1**

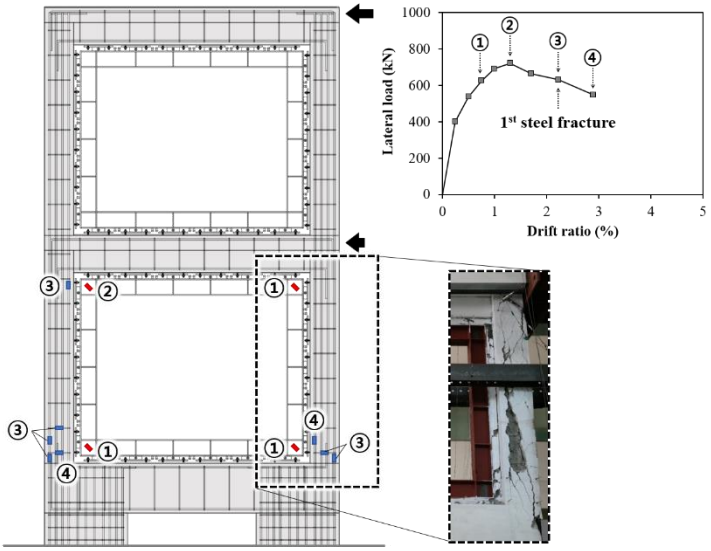

Figure 4-52 Sequence of plastic hinge mechanism in specimen **IN-1**

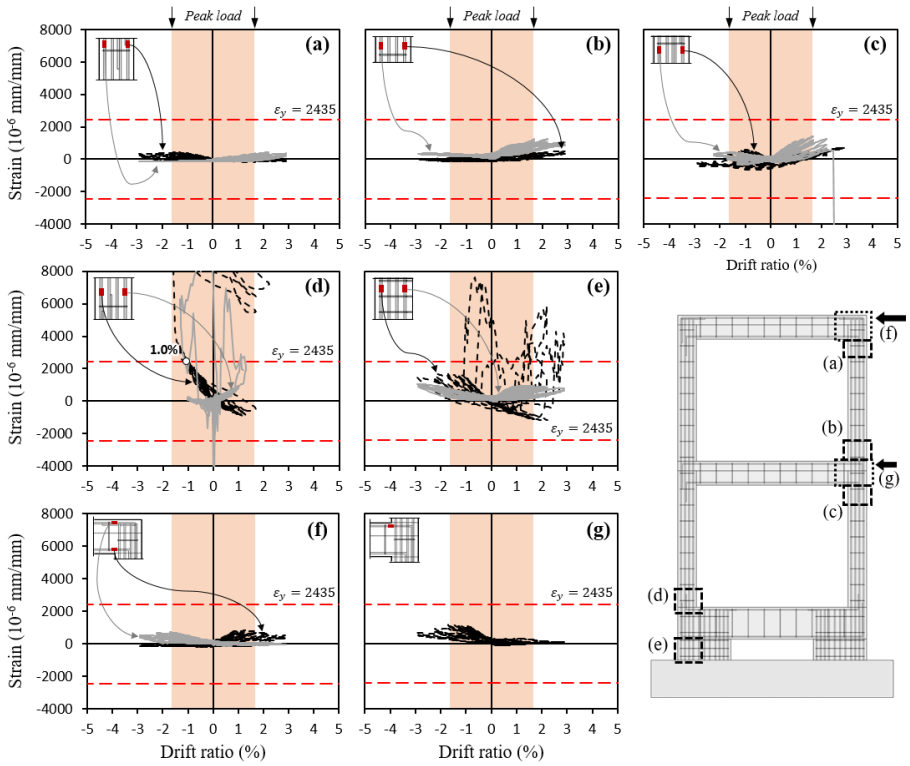

Figure 4-53 Strains of longitudinal bars in specimen **IN-2**

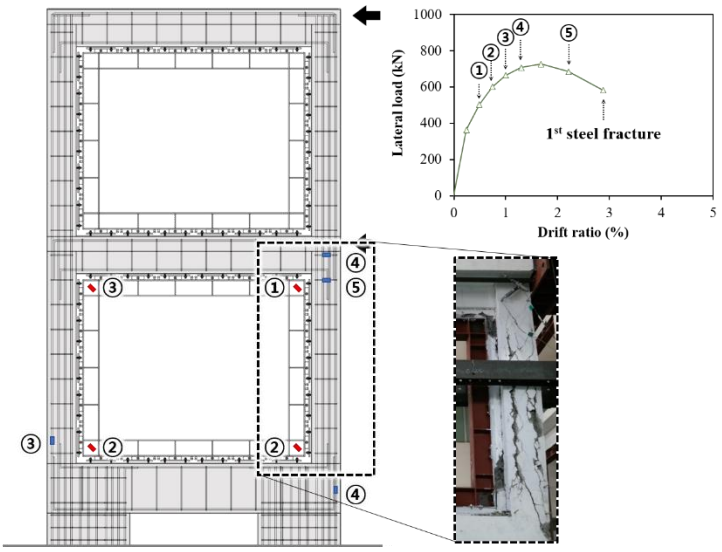

Figure 4-54 Sequence of plastic hinge mechanism in specimen **IN-2**

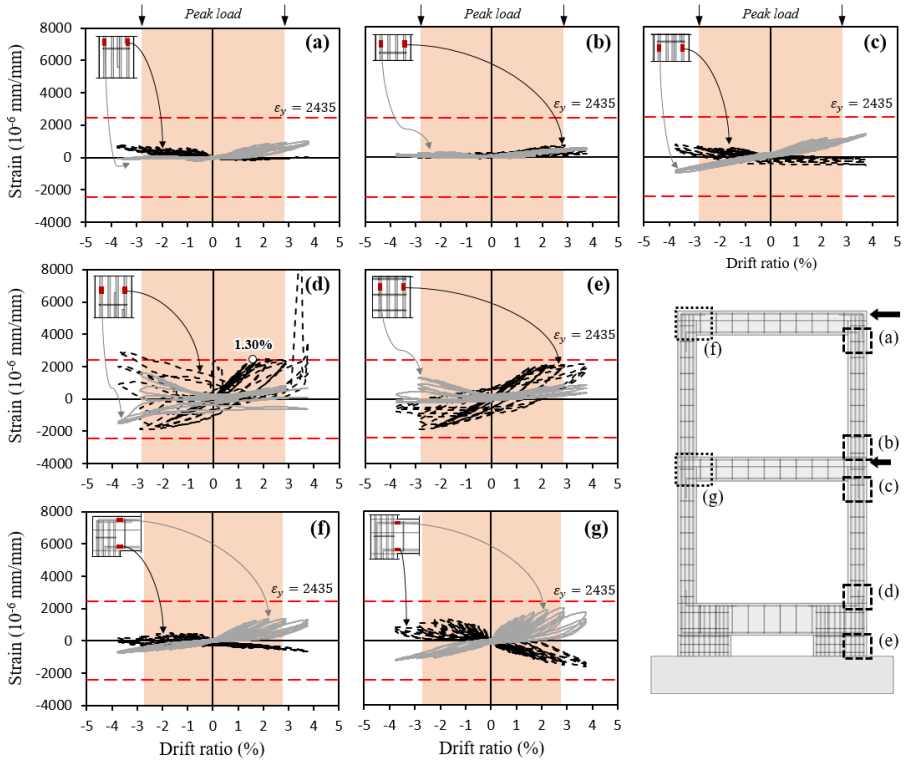

Figure 4-55 Strains of longitudinal bars in specimen **EX-1**

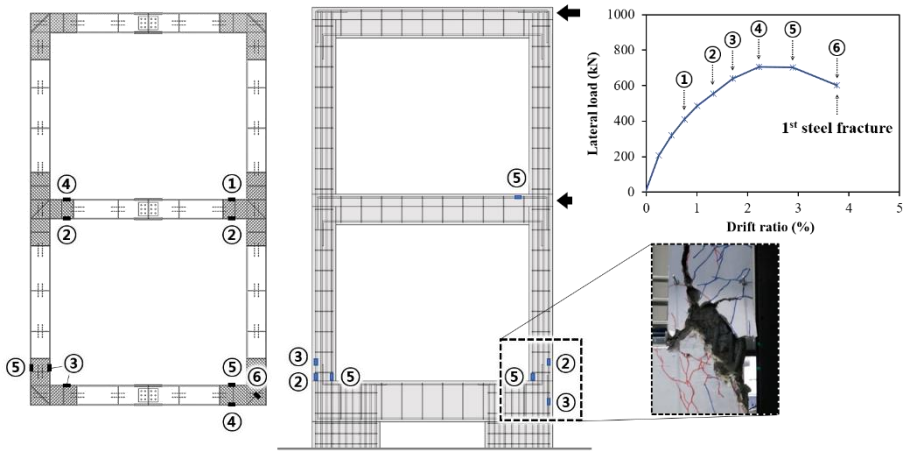

Figure 4-56 Sequence of plastic hinge mechanism in specimen **EX-1**

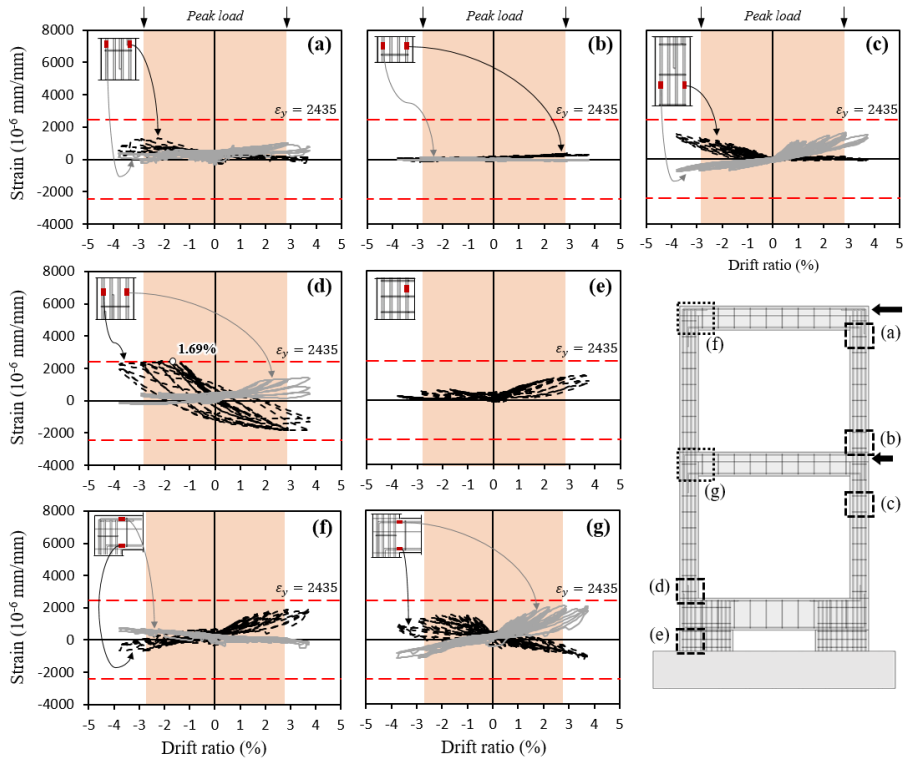

Figure 4-57 Strains of longitudinal bars in specimen **EX-2**

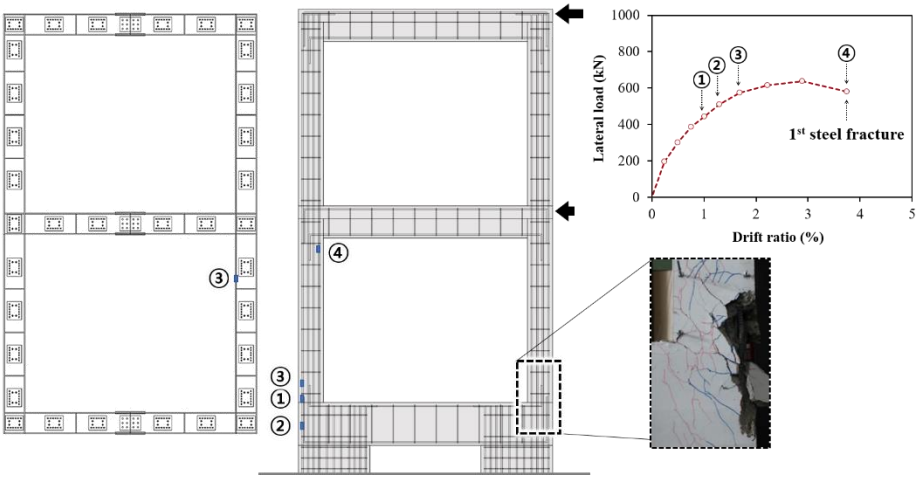

Figure 4-58 Sequence of plastic hinge mechanism in specimen **EX-2**

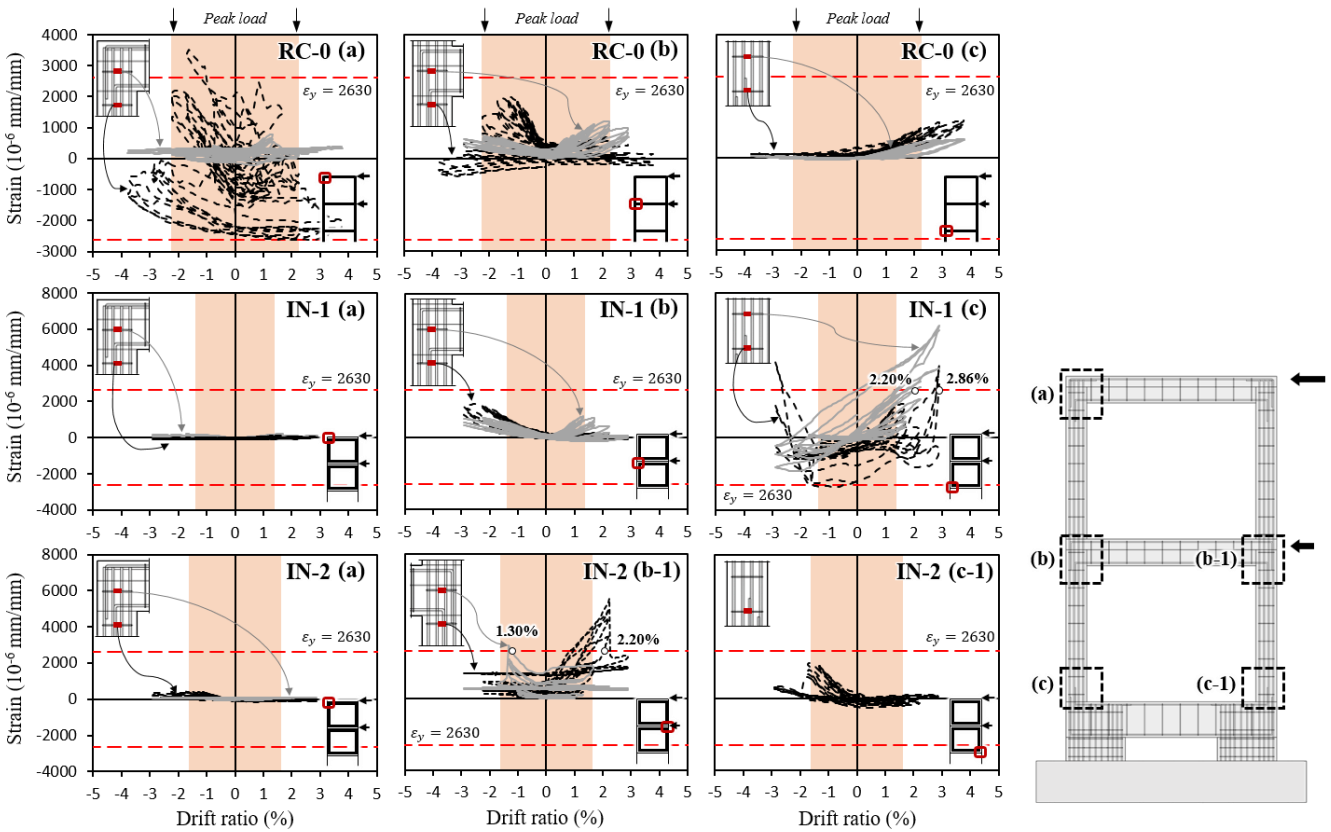

Figure 4-59 Strains of column shear reinforcement in specimen **RC-0**, **IN-1**, **IN-2** (Continued)

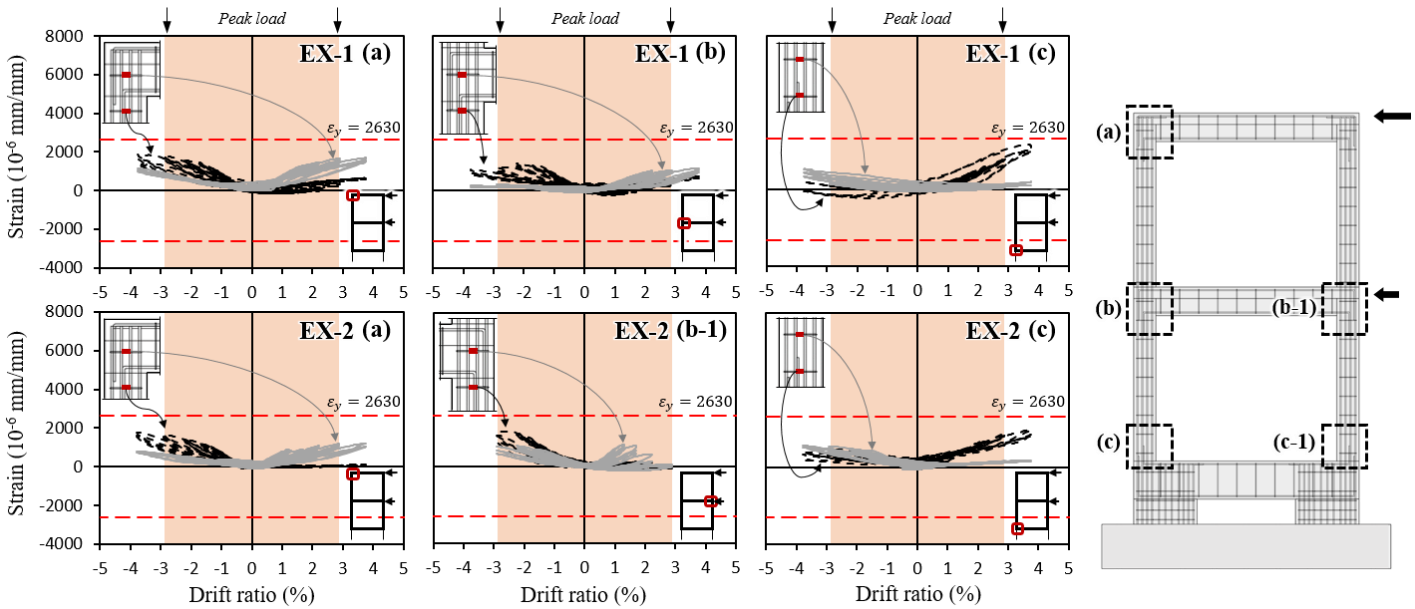

Figure 4-60 Strains of column shear reinforcement in specimen **EX-1**, **EX-2**

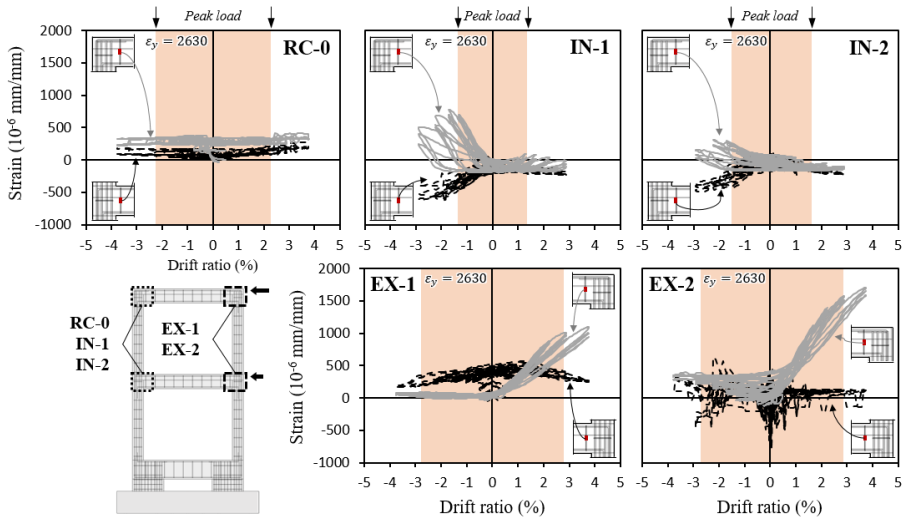

Figure 4-61 Strains of beam shear reinforcement

4.4.4 Deformation contributions of steel

The strains measured from steel flanges and panel zone in the 1st-story are important to verify how much retrofitted steel frame has contributed to improving seismic performance of existing frame. The strains measured from panel zone, flange of column and flange of beam in the 1st-story were examined (Figure 4-62 ~ Figure 4-65).

In specimen **IN-1** and **IN-2**, all panel zone in the 1st-story yielded before the RC column as shown in Figure 4-52 and Figure 4-54 and showed larger values than any other members. This results indicate that steel frame sufficiently resisted the seismic load before the existing RC frame was destroyed. After the maximum strength, fracture of steel beam flange first occurred at the heat-affected region of weld joint between the beam and column flanges without additional steel yielding.

In specimen **EX-1**, the flanges of steel beam in the 2nd-story yielded before the RC column as shown in Figure 4-56. The plastic hinges of steel beams in the 1st-story and 2nd -story occurred before the maximum strength. After the maximum strength and yielding of RC column in the 1st-story, concrete cover spalling occurred by crushing at the bottom of columns which resulted the strength degradation of frame. Specimen **EX-2** also showed similar failure mode to specimen **EX-1** considering the poor strain gauge conditions of **EX-2**.

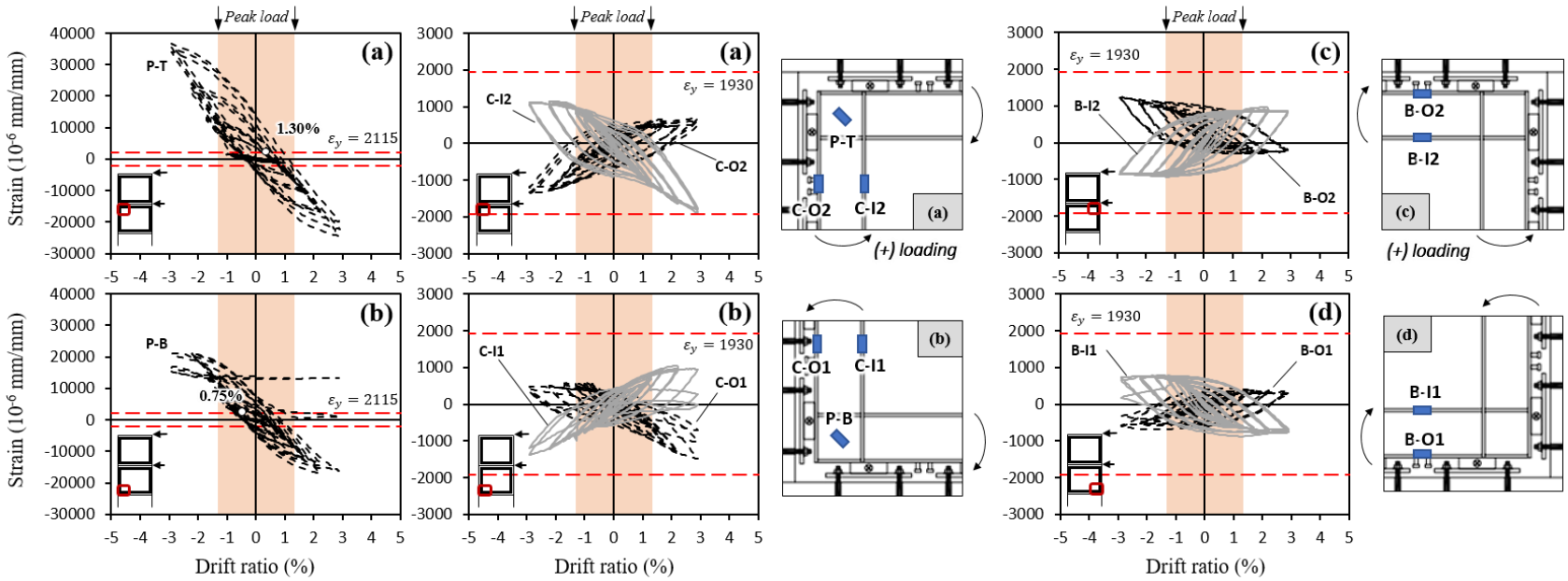

Figure 4-62 Strains of steel frame at the 1st-story in specimen IN-1

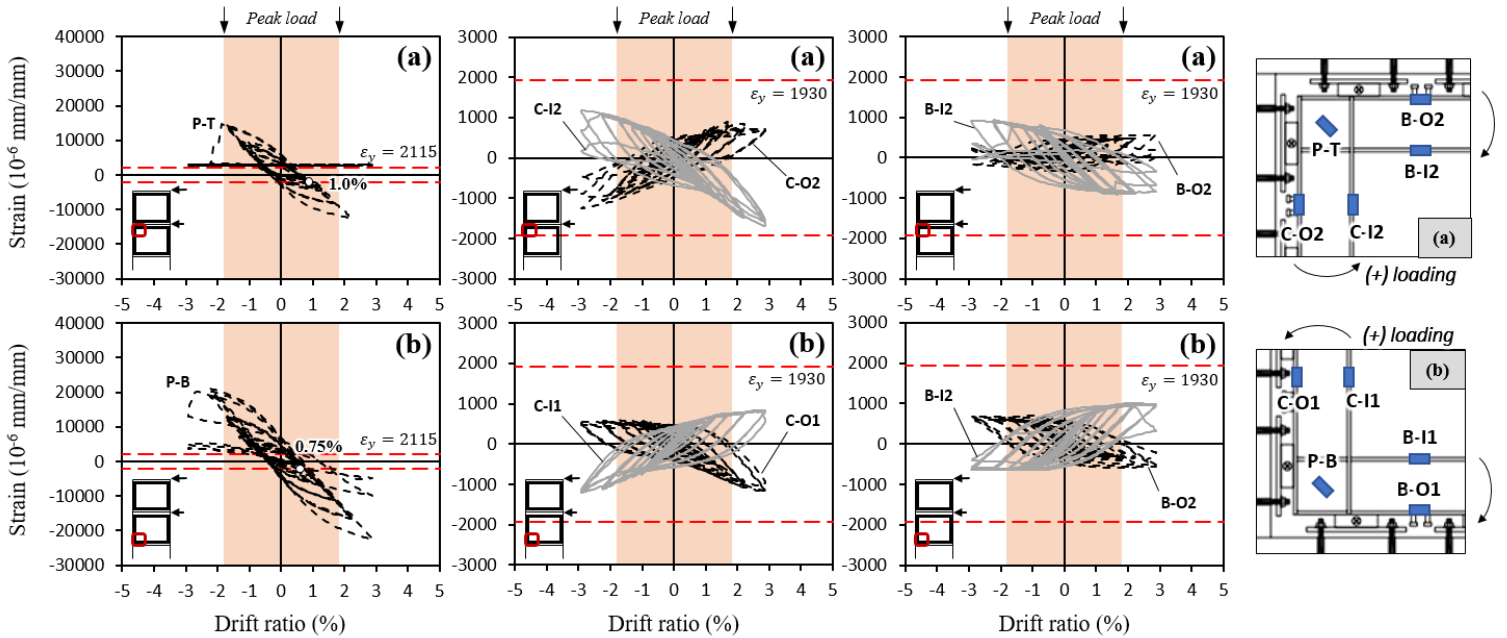

Figure 4-63 Strains of steel frame at the 1st-story in specimen IN-2

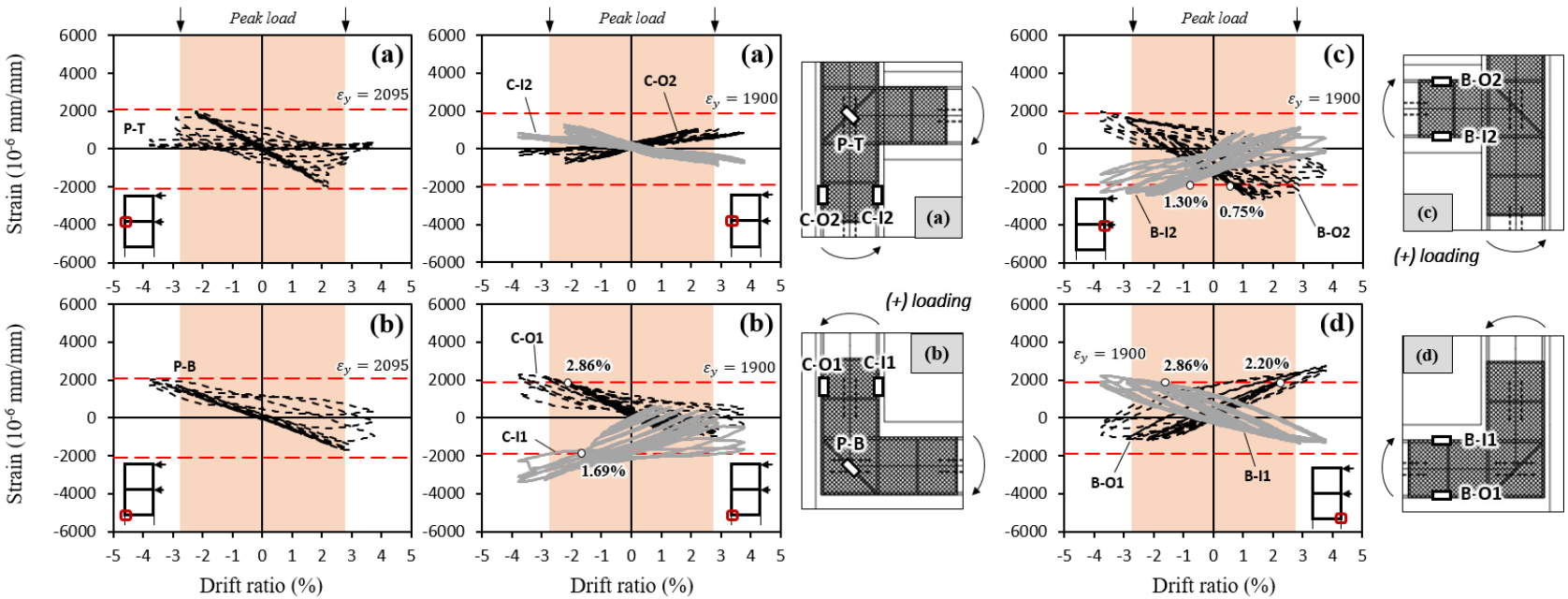

Figure 4-64 Strains of steel frame at the 1st-story in specimen **EX-1**

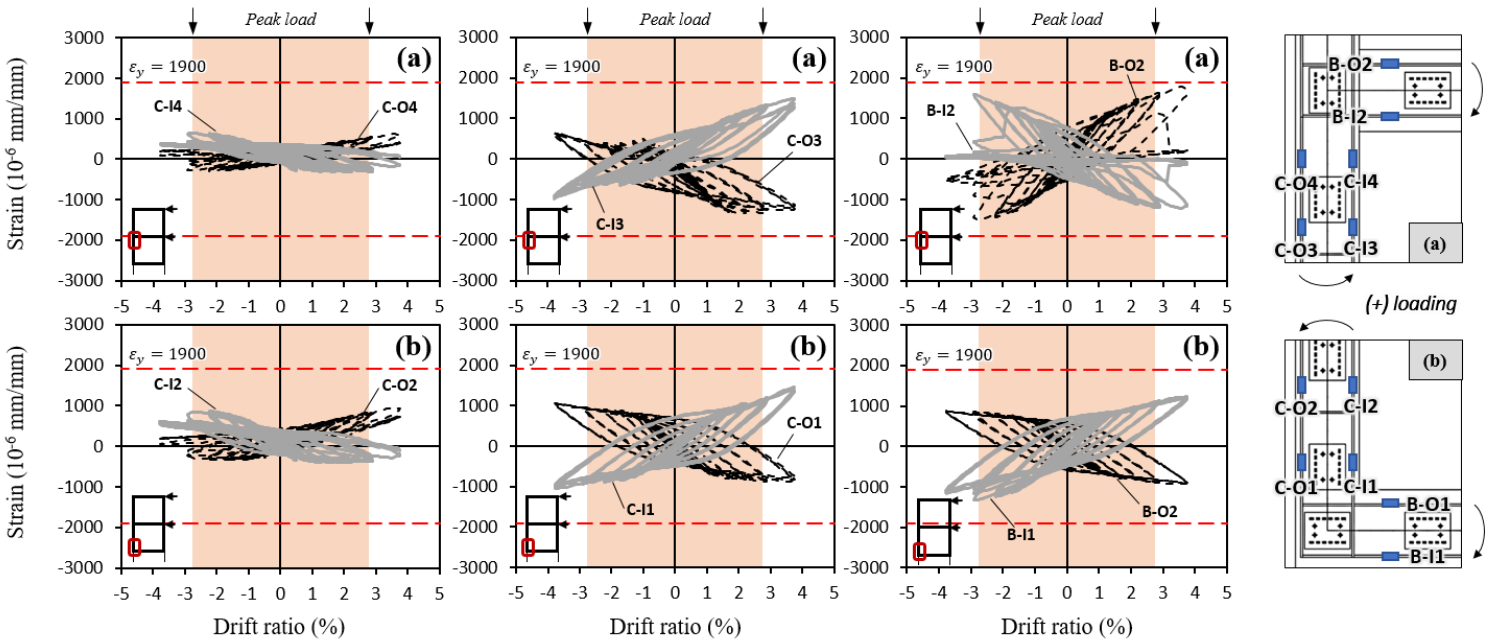

Figure 4-65 Strains of steel frame at the 1st-story in specimen **EX-2**

4.4.5 Strain distributions of RC column and steel column

In case of internal-retrofitting specimen, strains measured at the same height of the first-floor RC column and steel column were compared. Figure 4-66 and Figure 4-67 shows the strains of top and bottom section in 1st-story column. In case of specimen IN-1, 721 kN peak load at 1.3% drift ratio, the top and bottom of the first-floor column received bending moment in opposite directions. As shown in Figure 4-66, at the top of the column, the top flange(S1) and the inner longitudinal bar(C2) were subjected to compressive force while the bottom flange(S2) and outer longitudinal bar(C1) were subjected to tensile force. Specimen IN-2 also showed similar behavior in the first-floor column.

Unlike an external-retrofitting specimens that is attached in parallel and moved with existing RC frame, the columns of RC and internal steel frame are not integrated perfectly and behave separately This indicates that the shear stiffness of the connections connecting the steel to the RC frame is not large enough to enable the steel and RC frame to be moved into a single integrated composite member.

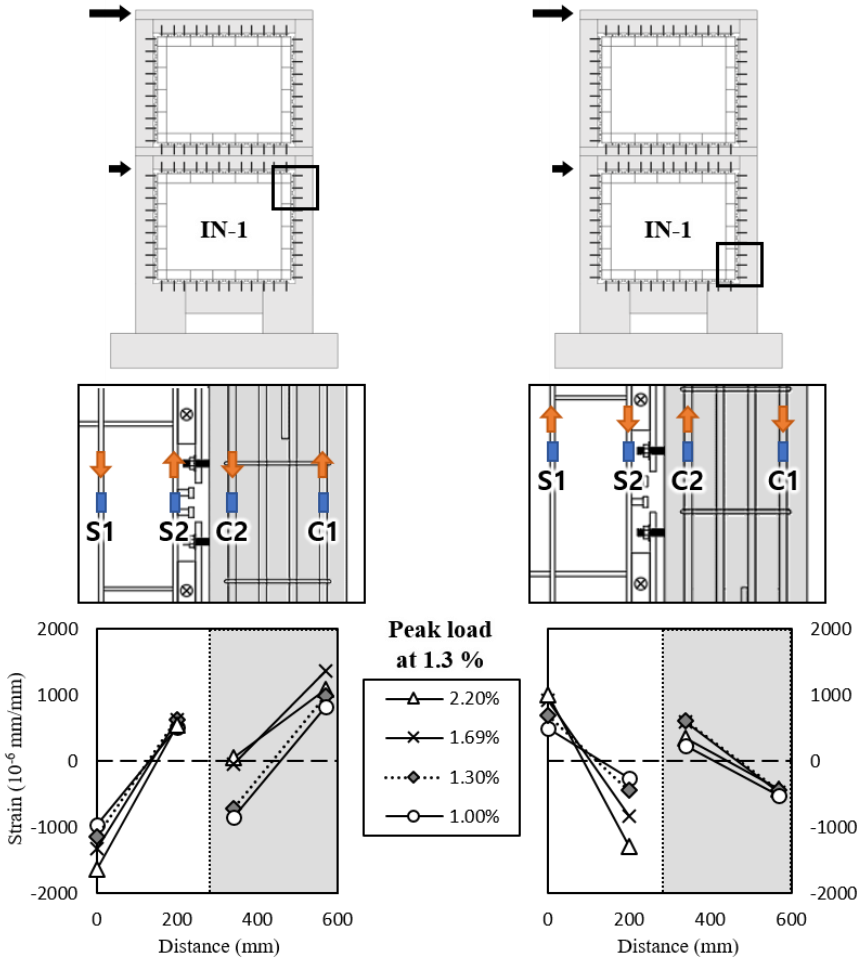

Figure 4-66 Strain distributions of steel flanges and vertical bars in the 1st-story column of specimen **IN-1**

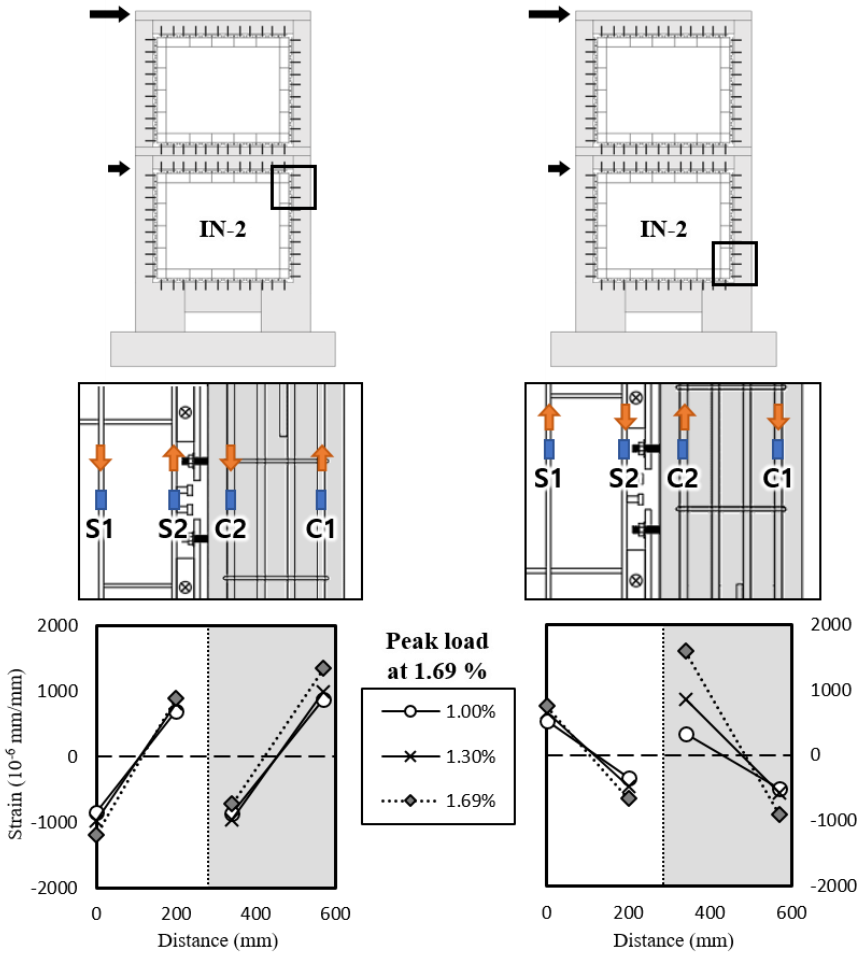

Figure 4-67 Strain distributions of steel flanges and vertical bars in the 1st-story column of specimen **IN-2**

4.5 Discussion

1) RC moment frame specimen (**RC-0**) without retrofit failed due to shear failure in the beam-column joints. The retrofitted specimens with internal steel frame(**IN-1** and **IN-2**), failed due to shear mechanism of the 1st-story columns and with external steel frame(**EX-1** and **EX-2**), failed due to flexural mechanism of the of the 1st-story columns.

2) The load-carrying capacity of **IN-1** and **IN-2** was more than 3.1 times greater than that of **RC-0**. The drift ratios corresponding to the peak loads were smaller in the retrofitted specimens (2.2%, 1.3%, and 1.69% in **RC-0**, **IN-1**, and **IN-2**, respectively).

3) The load-carrying capacity of **EX-1** and **EX-2** was more than 2.9 times greater than that of **RC-0**. The drift ratios corresponding to the peak loads were bigger in the retrofitted specimens (2.2%, 2.86%, and 2.86% in **RC-0**, **EX-1**, and **EX-2**, respectively).

4) The load-carrying capacity of **RC-0** gradually decreased until 3.71% drift ratio. In the case of **IN-1** and **IN-2**, the specimens were severely damaged at 2.86%. In the case of **EX-1** and **EX-2**, the specimens were severely damaged at 3.71%. In terms of the energy dissipation, the retrofitted specimens were superior to the non-seismic RC specimen.

Chapter 5. Structural Analysis of RC Frame Retrofitted with Steel Moment Frame

5.1 Linear Analysis for Frame Specimens

5.1.1 Overview of line element model

For the linear structural analysis of retrofitted RC frame, a line element model was proposed considering the connection with RC moment frame and retrofitted steel moment frame. Figure 5-1 shows the overview of proposed frame model for both linear and nonlinear analysis. The numerical model was composed of the existing RC elements, retrofitting steel elements, and connection elements. In the internal-retrofitting frame(Figure 5-1 (a)), the steel members were equally divided into 4 elements and the RC members were divided into 6 elements. The external-retrofitting frame(Figure 5-1(b)) members were not divided. Connection elements connect the RC and steel elements.

5.1.2 Modeling of connection element

The steel frame are not directly connected but indirectly connected by the concrete and anchors. Thus, the force transfer between stories should be limited by the concrete members and anchors. The model of connection element is shown in Figure 5-1 (c)~(e) and Table 5-1. The connection element of external-retrofitting frame transfers compression, tension and shear, while the connection element of internal-retrofitting frame transfers only compression and shear excluding tension. The reason for ignoring the tensile strength of the

connection element in internal-retrofitting frame is that the reinforced steel frame is constructed non-continuously inside the existing RC frame, so that the tensile forces between the second and first floors are transferred through the RC members.

Because the connection cannot be deformed to the maximum deformation when it was constructed on the frame, it is considered safe to model the connection element as a linearly elastic spring. The axial stiffness(compression) of the connection element was defined based on the elastic modulus of mortar and the mortar-RC contact area. The shear stiffness of the connection element was simplified based on the connection shear test in Chapter 2. Table 5-1 shows the yield stiffness per one connection module of specimen which was defined as $k_{shear} = V_y/\delta_y$ as shown in Figure 5-1 (d). The connection module of internal-retrofitting(**IN-1** and **IN-2**) and external-retrofitting(**EX-1** and **EX-2**) specimens contain two and four anchors, respectively. Each connection elements of **IN-1**, **IN-2**, **EX-1** and **EX-2** was defined 204 kN/mm, 215 kN/mm, 301kN/mm and 361 kN/mm.

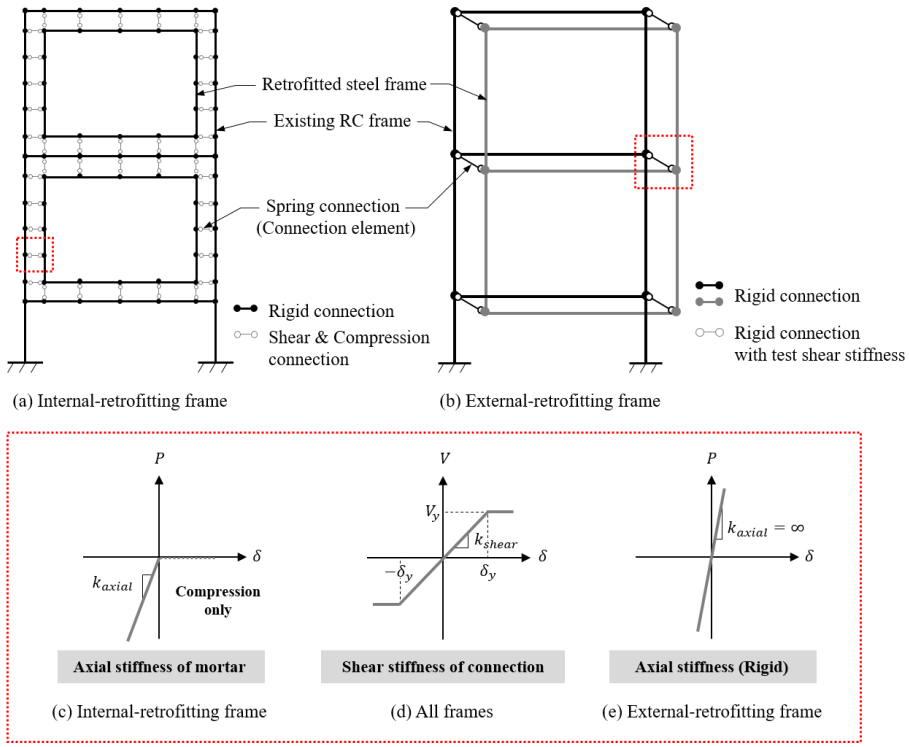

Figure 5-1 Proposed line element models for frame analysis

Table 5-1 Stiffness of connection element for frame specimens

Connection stiffness (kN/mm)	Type 1[3]		Type 2[4]	
	IN-1	**EX-1**	**IN-2**	**EX-2**
k_{axial}[1]	40900	Rigid	34000	Rigid
k_{shear}[2]	204	301	215	361

1) Compression stiffness of mortar = $(A_{bear}/n) \times E_m/l_{conn}$

, where A_{bear} is connected area btween mortar and concrete, n is the number of connection elements, E_m, elastic modulus of mortar, $8500\sqrt[3]{f_{cu}}$ where $f_{cu} = f_{ck} + \Delta f$ (KCI 2012), and l_{conn} is the length of connection element.

2) Yield stiffness per a connection module, the secant stiffness, connecting the origin and the prepeak point of $0.75V_u(= V_y)$ from the shear test in Chapter2.

3) R-connection method. 4) W-connection method.

5.1.3 Demand and capacity strength of frame specimen

Using the proposed line element model, the demand and capacity strength of each member at the maximum strength of the frame system was calculated. The linear analysis was performed by MIDAS Gen, the program used for structural analysis, considering the peak load of each specimen.

Table 5-2 summarizes member flexural and joint shear capacities calculated based on the actual material strengths. The flexural capacity of steel beam and column was nominal bending strength due to shear failure of beam-column joint. The capacity of RC column was evaluated based on properties at peak load of each specimen. Considering axial and moment forces on the column elements, the nominal capacity of RC column V_{nc} is calculated as follows (KCI 2017).

$$V_{nc} = V_c + V_s \tag{5-1}$$

$$V_{c1} = \left(0.16\sqrt{f_{ck}} + 17.6\rho_w \frac{V_u d}{M_u} \right) b_w d \le V_{c2} \tag{5-2}$$

$$M_m = M_u - N_u \frac{(4h - d)}{8} \tag{5-3}$$

$$V_{c2} = 0.29\sqrt{f_{ck}} b_w d \sqrt{1 + \frac{N_u}{3.5A_g}} \tag{5-4}$$

$$V_{c3} = \frac{1}{6}\left(1 + \frac{N_u}{3.5A_g} \right) \sqrt{f_{ck}} b_w d \tag{5-5}$$

$$V_s = \frac{A_v f_{yt} d}{s} \tag{5-6}$$

where V_c and V_s are shear contributions from concrete and transverse rebars, respectively. The effect of flexural moment is addressed by Equation 5-2; $V_c = V_{c1}$. The additional effect of axial compression N_u (positive for compression) is considered by calculating M_m (Equation 5-3) and substituting $M_u = M_m$ in Equation 5-2. It is noted that V_{c1} cannot exceed V_{c2} (Equation 5-4), and $V_c = V_{c2}$ is assumed for negative M_m. In the case of axial tension, V_c is calculated as V_{c3} (Equation 5-5).

The shear strength of RC beam-column joints was calculated as follows (ACI 2002)

$$V_{jc} = 0.083\gamma\sqrt{f_c'}b_j h_c \qquad 5\text{-}7$$

where γ = 12 and 8 for beam-column joints in the 2nd and 3rd floors, respectively, b_j [= (b_b+b_c)/2] indicates the joint effective width, and h_c is the column depth. In the case of **RC-0**, the joint shear capacities were V_{jc} = 620 and 413 kN, respectively in the 2nd and 3rd floors.

Based on the demand and capacity strength, the calculated strength ratio of each specimen were summarized in Table 5-2. To evaluate the design strength by elastic analysis, the maximum strength of specimen was divided into the maximum strength ratio of each specimen, respectively. The design strength of ordinary moment frame, internal and external retrofitting frame obtained from the maximum strength ratio were 134 kN, 359 kN, 376 kN ,respectively.

Table 5-2 Member capacities and demands from linear analysis of specimens

Specimen	RC frame														Steel frame							
	1F Column						2F Beam				Joint				1F Column				2F Beam			
	Capacity[1]			Demand[2]			Capacity		Demand		Capacity		Demand		Capacity		Demand		Capacity		Demand	
											2F	3F	2F	3F								
	M_{nc} (kN·m)	P_{nc}[5] (kN)	V_{nc} (kN)	M_{uc} (kN·m)	P_{uc} (kN)	V_{uc} (kN)	M_{nb} (kN·m)	V_{nb} (kN)	M_{ub} (kN·m)	V_{ub} (kN)	V_{jc} (kN)	V_{jc} (kN)	V_{ju} (kN)	V_{ju} (kN)	M_{nc} (kN·m)	V_{jc} (kN)	M_{nc} (kN·m)	V_{ju} (kN)	M_{nc} (kN·m)	V_{jc} (kN)	M_{nc} (kN·m)	V_{ju} (kN)
RC-0	167	141	141	231	196	141	107 -260	175	186 -186	116	620	413	536	371	-	-	-	-	-	-	-	-
IN-1	104	667	68	206	1300	68	107 -262	175	215 -211	278	627	418	955	481	120	516	91	147	120	516	84	133
IN-2	112	607	68	230	1275	68	107 -270	180	233 -220	280	660	440	925	568	120	516	93	142	120	516	85	126
EX-1	169	125	121	425	315	121	107 -272	180	281 -285	181	667	444	684	504	239	673	245	125	239	673	319	200
EX-2	169	122	125	389	280	125	107 -264	177	257 -261	166	636	424	693	452	239	673	226	115	239	673	292	184

1) Evaluated based on properties at peak load of each specimen

2) Evaluated based on numerical model at peak load of each specimen

3) Capacity of tension side columns

4) Demand of tension side columns

Table 5-3 Summary of strength ratio of frame member

Specimen	RC frame							Steel frame				Combined member[1)]				Connection
	1F Column			2F Beam		2F Joint	3F Joint	1F column		2F beam		1F column		2F beam		1F frame
	M_u/M_n	P_u/P_n	V_u/V_n	M_u/M_n	V_u/V_n	V_u/V_n	V_u/V_n	M_u/M_n	V_u/V_n	M_u/M_n	V_u/V_n	$M_u/M_{n,com}$	$V_u/V_{n,com}$	$M_u/M_{n,com}$	$V_u/V_{n,com}$	V_u/V_n
RC-0	1.39	1.38	0.83	(+) 1.74 (-) 0.72	0.66	0.86	0.90	-	-	-	-	-	-	-	-	-
IN-1	1.95	1.98	3.29	(+) 2.01 (-) 0.81	1.58	1.52	1.15	0.76	0.28	0.70	0.26	-	0.78	-	0.59	0.92
IN-2	2.10	2.05	3.35	(+) 2.18 (-) 0.81	1.56	1.40	1.29	0.78	0.28	0.71	0.24	-	0.78	-	0.58	0.88
EX-1	2.51	2.52	1.91	(+) 2.63 (-) 1.05	1.0	1.03	1.14	1.03	0.19	1.33	0.30	1.38	0.50	1.73	0.49	0.14
EX-2	2.30	2.30	1.69	(+) 2.40 (-) 0.99	0.94	1.09	1.07	0.95	0.17	1.22	0.27	1.24	0.45	1.59	0.45	0.13

1) Combined strength ratio = sum of RC and steel demand / sum of RC and steel capacity

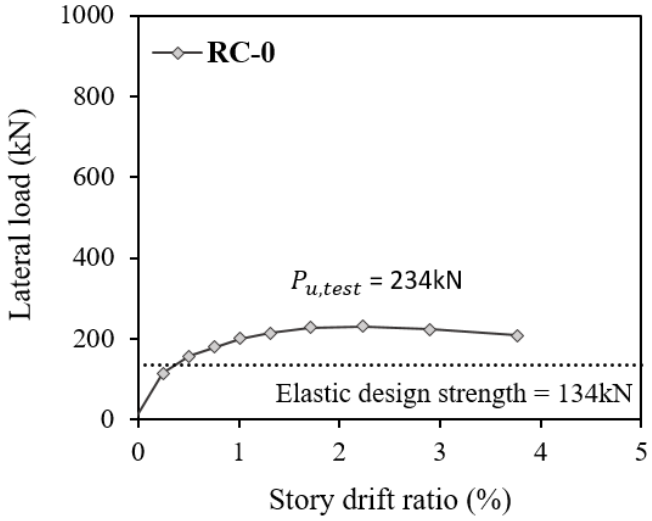

Figure 5-2 Design strength of frame specimens (**RC-0**)

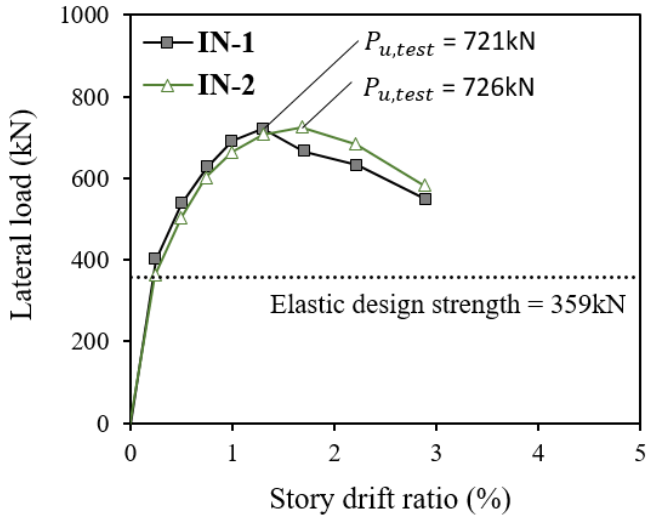

Figure 5-3 Design strength of frame specimens (**IN-1**, **IN-2**)

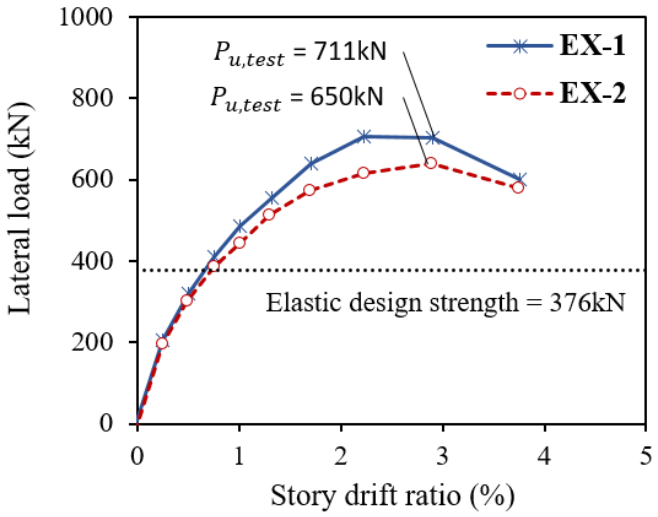

Figure 5-4 Design strength of frame specimens (**EX-1**, **EX-2**)

5.1.4 Elastic design process for steel retrofitted frame

The overstrength ratio was calculated based on the demand strength from linear analysis of the retrofitted frame and the strength capacity of each member. The overstrength factor is an important factor used in seismic design through elastic analysis with response modification coefficient. Figure 5-5 and Equation 5-9 shows the definitions and relationship of response modification coefficient (R), overstrength factor (Ω_o) and system ductility (μ), respectively, where V_D is the design strength of frame and V_E is the elastic strength of frame.

$$V_D = \frac{V_E}{\mu\Omega} = \frac{V_E}{R} \quad 5\text{-}8$$

$$R = \mu \times \Omega_o \quad 5\text{-}9$$

KBC 2016 defines the R coefficient value of ordinary reinforced concrete moment frames as 3. Thus, it is possible to obtain the ductility of ordinary RC moment frames according to R=3 from the Equation 5-9 for ductility and overstrength factor. For a seismic resistance structure system retrofitted with steel frame to perform its seismic resistance performance without the early destruction of the existing frame, the maximum story drift of the frame must be determined by the deformation capability of the ordinary RC moment frame. Therefore, the allowable displacement of the internal and external retrofitting frame systems during the elastic design is the same as that of the maximum displacement of the ordinary RC moment frame. Table 5-4 shows the response modification factors calculated by applying the same maximum story drift ratio

to internal and external retrofitting specimens. The internal-retrofitting frames showed higher initial stiffness than the external-retrofitting frames so that they presented higher value of ductility factor and response modification coefficient than the external-retrofitting frames, despite the small value of overstrength factor.

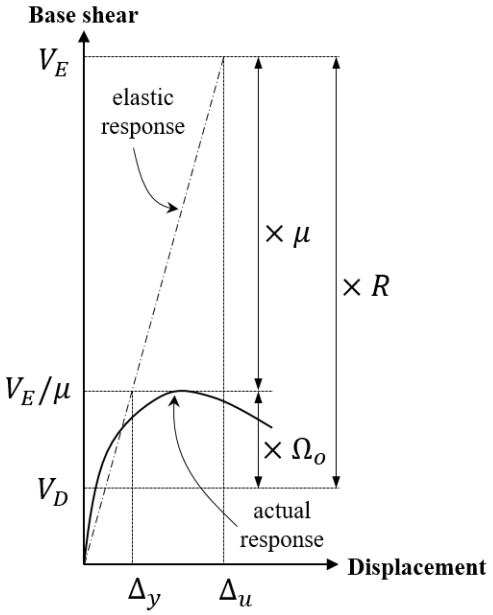

Figure 5-5 Definitions of overstrength and response modification factor

Table 5-4 Design coefficients for frame retrofitted with steel frame

Specimen	System overstrength factor (**Ω**)	System ductility (μ)[1)]	Response modification coefficient (R)	Ultimate story drift ratio[3)] $\Delta_{u,RC}$ (%)
RC-0	1.7	1.7	3[2)]	1.70
IN-1	2.0	2.6	5.1	
IN-2	2.2	2.2	4.8	
EX-1	2.5	1.0	2.6	
EX-2	2.3	1.1	2.6	

1) Ductility = $\Delta_{u,RC}/\Delta_y$, where Δ_y is the yield drift ratio defined in Table 4-4

2) Response modification coefficient, R factor, defined in KBC 2016

3) Ultimate story drift ratio defined as the maximum drift ratio of ordinary reinforced concrete moment frame(**RC-0**) calculated by R=3 defined in KBC 2016

5.2 Nonlinear Analysis for Frame Specimens

For verification and evaluation of the test results, nonlinear numerical analysis using line elements was performed. Such nonlinear model is important to perform nonlinear static analysis of overall frame, which have become more popular for the seismic evaluation. Thus, for practical applications, the use of line elements was encouraged rather than continuum finite element analysis. The analysis was performed by MIDAS Gen (2015)

The behavior of plastic hinges on each member to perform nonlinear static analysis of the frame model was referred to Seismic Performance Evaluation and Reinforcement Manual of School Facilities(2019). The plastic hinge behavior of each member is shown in Figure 5-6.

Table 5-5 shows the results of nonlinear static analysis. In case of non-retrofitted frame, the maximum strength and story drift ratio were 211 kN and 2.20%, respectively. The numerical model of internal-retrofitting presented 688 kN of maximum strength with 0.67% of story drift ratio and presented half of deformation capacity due to the early shear failure of tension column in the 1st-story. That can be explained that the compressive forces of the connection elements were transfered to the RC column by concentrated shear force instead of redistributed forces. In case of external-retrofitting frame, the maximum strength and story drift ratio were 551 kN and 1.66 %, respectively.

The results of pushover analysis were plotted in Figure 5-7 ~Figure 5-9. The initial stiffness of frame quite similar to experiment results except the internal-

retrofitting frame. The external-retrofitted frame maintained 80% of maximum strength up to 3.71% where the experiment finished and the load was decreased due to the bending failure of steel beam on the second floor.

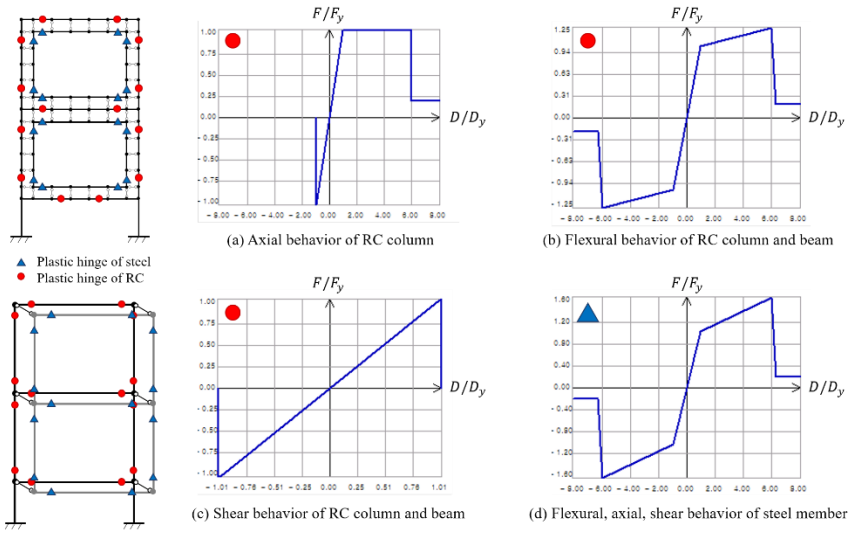

Figure 5-6 Properties of plastic hinges and assumed hinge location

Table 5-5 Summary of 2-story RC frame behavior

Frame type			Peak load (P_u, kN)	Drift ratio at peak load (%)	Failure mode[1)]
Ordinary moment frame	Specimen	**RC-0**	234	2.20	JS
	Numerical model		210	1.94	CF
Internal-retrofitting frame	Specimen	**IN-1**	721	1.30	CS
		IN-2	726	1.30	CS
	Numerical model		688	0.67	CS
External-retrofitting frame	Specimen	**EX-1**	711	2.86	CC
		EX-2	650	2.86	CC
	Numerical model		551	1.66	CF

1) JS : Joint shear failure before beam and column flexural yielding, CF : 1F Column flexural failure, CS : 1F Column shear failure due to anchors, CC : 1F Column failure due to crushing

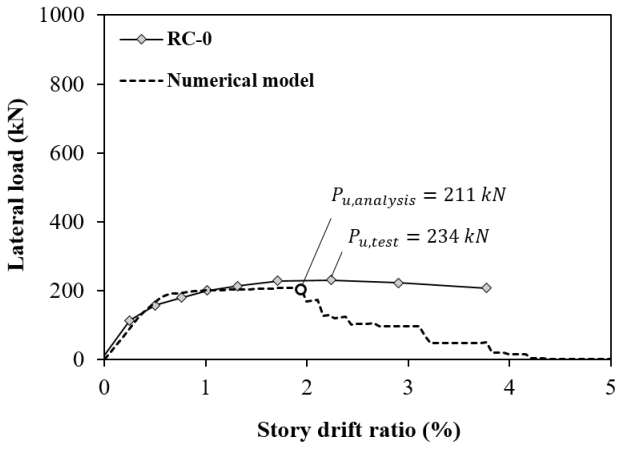

Figure 5-7 Comparison of numerical result and test result (**RC-0**)

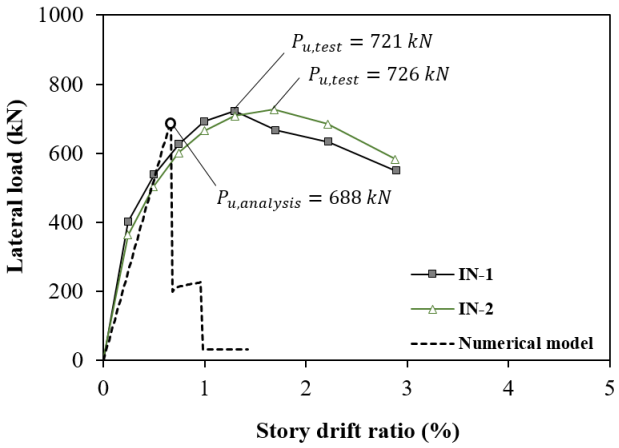

Figure 5-8 Comparison of numerical result and test result (**IN-1**, **IN-2**)

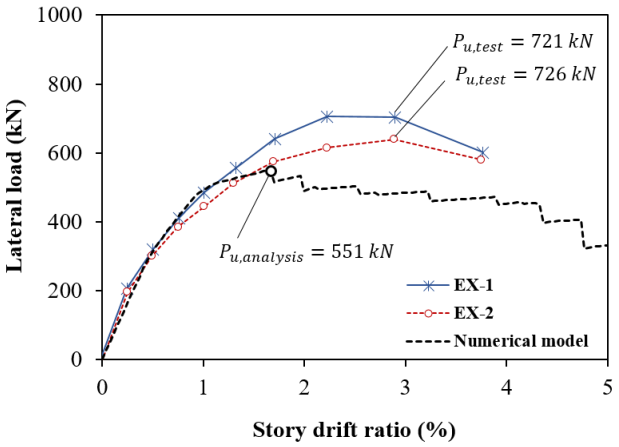

Figure 5-9 Comparison of numerical result and test result (**EX-1, EX-2**)

5.3 Discussion

On the basis of experimental and numerical results, design considerations for internal and external steel frame-retrofitting of non-seismic RC school buildings are recommended as follows:

1) Existing RC school buildings are prone to the shear failure of exterior beam-column joints with poor anchorage detail of beam rebars as well as insufficient shear reinforcements. Although the load-carrying capacity was maintained beyond 3% drift ratio, the energy dissipation capacity was deficient.

2) The retrofit scheme using unbraced internal steel frame is effective in enhancing stiffness, strength, and energy dissipation of non-seismic RC buildings. However, the primary failure mode tends to be the column shear mechanism in tension side. It is recommended in practice that the story drift ratio of retrofitted frames be limited within 1% to prevent the early failure of existing members. The actual shear resistance of RC columns can be far greater than the code prediction due to the unified action with the retrofitting steel and connection.

3) Based on the deformation capacity of non-retrofitted RC frame, response modification coefficient, R, of internal and external retrofitting system was calculated. The values of R factor can be used in elastic seismic retrofitting design in practice.

4) In nonlinear static analysis, the maximum strength of internal-retrofitting frames can be reasonably predicted by addressing the connection stiffness.

However, the poor deformation capacity compared to that of the actual frame needs to be revised by developing the line element model.

References

[1] ACI Committee 374 (2005). *Acceptance Criteria for Moment Frames Based on Structural Testing and Commentary*, American Concrete Institute, Detroit.

[2] ACI Committee 318 (2014). *Building Code Requirements for Structural Concrete (ACI 318-14) and Commentary*, American Concrete Institute. Farmington Hills, MI.

[3] ACI Committee 352 (2002). *Recommendations for Design of Beam-Column Connections in Monolithic Reinforced Concrete Structures.* American Concrete Institute. Farmington Hills, MI.

[4] AISC Committee 360 (2016). *Specification for Structural Steel Buildings*, American Institute of Steel Construction, East Randolph, IL.

[5] AIK (Architectural Institute of Korea) (2016). *Korean building code,* KBC 2016, Seoul, Korea.

[6] KCI (Korea Concrete Institute) (2017). *Korea structural concrete design code*, KCI 2017, Seoul, Korea.

[7] 교육부. (2019). *학교시설 내진성능평가 및 보강 매뉴얼.*

[8] 문교부. (1980). *80년도 학교 교사 표준설계도*

[9] 윤수용, 박지훈. (2014). “내진보강용 후설치 앵커의 전

단성능에 관한 실험적 연구.” *대한건축학회 논문집-구조계*, 30(9), 41-51

[10] 윤수용, 박지훈. (2015). “내진보강용 후설치 앵커의 인장성능에 관한 실험적 연구.” *대한건축학회 논문집-구조계*, 31(3), 27-36

[11] Ozcelik, R., Akpınar, U., and Binici, B. (2011). "Seismic retrofit of deficient RC structures with internal steel frames." *Advances in Structural Engineering*, 14(6), 1205-1222.

[12] Ueki, R., Imai, K., Tomatsuri, H., and Kuramoto, H. (2010). "Influence of indirect joint on retrofitting effect by external steel frames." *Journal of Structural and Construction Engineering (Transactions of AIJ)*, 75(654), 1501-1508 (in Japanese).

[13] Mitsuyoshi, I. et al. (2009). “Experimental study on seismic retrofitting steel brace of existing RC school buildings with low-strength concrete.”

초 록

끼움강재골조 및 외부강재골조로 보강된 철근콘크리트 골조의 내진 성능

이 해 빈

서울대학교 건축학과 대학원

국내 지진발생 가능성에 대한 인식이 증가함에 따라 비내진상세를 가진 기존 철근 콘크리트 구조체의 내진보강설계에 대한 관심도 증대되고 있다. 특히 비내진상세를 가진 학교 건물에 대한 다양한 내진보강공법이 개발되어 왔으나, 오래된 학교 건물의 경우 기존 구조체가 비내진상세를 가지는 것 뿐만 아니라 콘크리트 강도, 시공 품질 등에서 매우 열악하여 이에 맞는 적절한 보강법을 찾기란 매우 어렵다.

최근 이러한 학교 건물에 대하여 기존 구조체의 강도와 강성을 증가시켜 내진성능을 확보하는 강도증가공법이 많이 사용되고 있으며, 특히 장방향으로 취약한 학교 건물의 특성을 고려해 기존 골조 면외에 강재 골조를 설치하는 외부강재골조 공법과 면내에 액자 형태의 철골프레임을 설치하는 끼움강재골조 공법이 많이

사용되고 있다. 그러나 끼움강재골조는 기존 골조의 기둥이 연속적으로 보강되지 않으므로 기존의 하중 전달경로와 분포를 변화시키고 구조물에 작용하는 전체 하중을 증가시키므로 기존 골조의 파괴가 선행되어 의도한 보강 효과를 얻을 수 없는 경우가 많다. 따라서 본 연구에서는 정적반복횡가력 실험을 통하여 기존 철근콘크리트 골조에 외부강재골조 보강법과 끼움강재골조 보강법을 적용한 보강 골조에 대한 내진성능을 평가하고, 실험결과와 탄성 해석에 따른 예상 강도 및 파괴모드의 적합성을 검토하였다. 또한 보강강재골조를 기존 구조체에 접합시키는 접합 공법의 구조 성능에 대한 연구가 선행되었다.

제안된 외부강재골조와 끼움강재골조로 보강된 골조의 내진성능을 평가하기 위하여, 실물대와 유사한 2층-1경간 골조에 대하여 반복횡가력실험을 수행하였다. 실험결과 무보강 골조는 보 주근의 부적절한 정착 상세로 인하여 2-3층 보-기둥 접합부에서 전단파괴가 발생하였다. 끼움강재골조로 보강된 골조는 1층 기둥의 휨 항복 이후 기둥 중앙의 전단파괴로 하중이 감소하였고, 무보강 골조 대비 강도가 3배 이상 증가하였다. 연성 능력은 무보강 골조에 비해 다소 감소하였으나 보강 강재의 항복으로 인해 우수한 에너지소산을 보였다. 외부강재골조로 보강된 골조는 1층 기둥 단부의 휨 압괴로 최대 하중에 도달하였으며, 피복 탈락 후 기둥 주근의 좌굴로 하중이 감소하였다. 끼움강재골조로 보강된 실험체에 비하여 변형 능력이 우수했던 반면, 에너지소산은 작았다.

초 록

실무에서의 보강 설계를 위해 선재로 이루어진 해석모델이 제안되었으며 해석결과는 실험결과와 비교되었다. 해석모델의 연결재는 내부보강의 경우 전단과 압축 거동이, 외부보강의 경우 인장, 압축, 전단 거동이 고려되었다. 해석결과 무보강 골조의 경우 2층 보의 휨 파괴를 나타냈지만, 실험체 보 주근의 부적절한 정착 상세로 인해 실제 파괴모드와 일치하지 않았다. 내부보강골조의 경우는 1층 인장 기둥의 전단파괴를 나타냈으며 실험결과와 부합하였다. 외부보강골조 역시 실험결과와 마찬가지로 1층 RC기둥의 압축파괴를 보였다.

본 학위 논문에서는 비내진상세를 가지는 철근콘크리트 골조에 적용되는 강재 골조 보강법에 따른 내진성능을 검증하기 위해 기존 콘크리트-보강 강재 접합부와 2층-1경간 골조에 대한 실험을 수행하였다. 또한 실험결과를 바탕으로 보강골조에 대한 해석모델을 제안하였고, 탄성 해석 결과와 실험결과를 비교하여 제안된 모델에 대한 설계의 적절성을 확인하고 강재보강골조 시스템에 대한 설계 방안을 제시하였다.

주요어 : 내진보강; 학교건물; 끼움강재골조; 외부강재골조; 연결부; 탄성해석; 반응수정계수; 푸쉬오버

학 번 : 2017-23408